DIAGENETIC AUREOLES INDUCED BY HYDROCARBON MIGRATION IN THE PERMIAN REDBEDS OF SOUTH-CENTRAL OKLAHOMA

By

JANET LORRAINE CAIRNS

Bachelor of Science

Oklahoma State University

Stillwater, Oklahoma

1983

Submitted to the Faculty of the
Graduate College of the
Oklahoma State University
in partial fulfillment of
the requirements for
the Degree of
MASTER OF SCIENCE
July, 1985

DIAGENETIC AUREOLES INDUCED BY HYDROCARBON MIGRATION IN THE PERMIAN REDBEDS OF SOUTH-CENTRAL OKLAHOMA

Thesis Approved:

Zuhair al-Shaieb
Thesis Adviser

Gary J. Stewart

D C Kent

Norman N. Kluchman
Dean of the Graduate College

PREFACE

Hydrocarbon-induced diagenetic aureoles form in the redbeds over oil fields in southwestern and south-central Oklahoma that are controlled by anticlinal features. Formation of the alterations in the Velma, Carter-Knox, and Healdton oil fields was related to seepage of hydrocarbons.

I wish to extend my sincere gratitude to the people who were instrumental in this thesis project. First, I would like to thank my friends in the geology department for their encouragement. In particular, I would like to give a special thanks to my advisor, Dr. Zuhair Al-Shaieb, for his continuous guidance and concern. I would like to thank my other committee members, Dr. Doug Kent, and Dr. Gary Stewart for their constructive remarks in this research.

In addition, I would like to express my appreciation to my parents for their ever present support throughout my schooling. I am also thankful to Johnny, Beth, and Shayne Johnson for providing bread, water, and bed during my field work.

Special thanks are due to the University Center of Energy Research and EXXON Production and Research Company for their financial support of the HIDA research.

TABLE OF CONTENTS

Chapter		Page
I.	INTRODUCTION	1
	Location and History	5
	Methodology	8
II.	GEOLOGIC SETTING	11
	Regional Tectonic Setting	11
	Stratigraphic Setting	17
	Depositional Environment	21
III.	SURFACE AND SUBSURFACE CHARACTERISTICS	28
	Velma Oil Field	31
	Healdton Oil Field	39
	Carter-Knox Oil Field	44
	Well-Log Characteristics	44
IV.	PETROLOGY AND DIAGENESIS OF THE HIDA STRATA	49
	Detrital Constituents	49
	Diagenetic Constituents	51
	Porosity Development	66
	Paragenesis of the Diagenetic Events	70
V.	GEOCHEMICAL MECHANISMS IN THE FORMATION	77
	Carbon System	79
	Iron System	84
	Sulfur System	88
	Authigenic Clays	94
	Mechanisms of Formation	95
VI.	ISOTOPE GEOCHEMISTY	103
	Basic Isotope Theory	103
	Carbon Isotopes	105
	Theory	105
	Results and Interpretation	108
	Oxygen Isotopes	113
	Theory	113
	Results and Interpretation	116

Chapter Page

Sulfur Isotopes.....120
Theory.....120
Results and Interpretations.....121

VII. SUMMARY AND CONCLUSIONS.....127

BIBLIOGRAPHY.....131

APPENDIX.....141

LIST OF TABLES

Table | Page

I. Isotope Data on carbonates, sulfides, oil, and water samples.....110

LIST OF FIGURES

Figure Page

1. Photograph typifying coloration changes in HIDA....2
2. Index map of the study area....6
3. Oklahoma Geologic Provinces....12
4. Major fault trends of Southern Oklahoma....16
5. Stratigraphic column of the study area....18
6. Paleolatitudes and paleoclimates of North America during the Permian System....23
7. Stratigraphic column and equivalent depositional environments, south-central Oklahoma....25
8. Outcrop photograph of resistive carbonate-cemented sandstone (zone 1)....29
9. Outcrop photographs of bleached sandstone (zone 2)....30
10. Outcrop photograph of the dramatic color change....32
11. Outcrop photograph of nodular pyrites in the bleached sandstone (zone 3)....33
12. Outcrop photograph of a pyrite nodule....33
13. Outcrop photographs of oxidized pyrite (zone 3)....34
14. Topographic map of Velma 35
15. Cross section of the Velma anticline 36
16. Velma: surface map of diagenetic zones....37
17. Velma: subsurface limits of pyritization....39
18. Cross section of the Healdton anticline....40

Figure Page

19. Healdton: surface map of diagenetic zones.....41

20. Healdton: subsurface limits of pyritization.....42

21. Cross section of the Carter-Knox anticline.....44

22. Carter-Knox: surface map of diagenetic zones.....45

23. Carter-Knox: subsurface limits of pyritization.....46

24. (a) Resistivity log signature outside the HIDA limit. (b) Resistivity log signature inside the HIDA limit.....48

25. QFR Diagram.....50

26. Photomicrograph of general lithology.....52

27. Photomicrograph of unaltered redbed.....54

28. SEM photomicrographs of hematite 55

29. SEM photomicrographs of rhodocrosite.....56

30. SEM photomicrograph of Fe-Mn dolomite.....57

31. EDXA spectrum of the Fe-Mn dolomite.....57

32. Photomicrographs of iron-rich dolomite.....58

33. Photomicrograph of poikilotopic texture.....59

34. Photomicrograph of pseudomorphsis replacement of kaolinite by carbonate.....61

35. Graph of quartz and and carbonate percentages determined from thin section.....62

36. Photomicrograph showing the extent of pyritization in the sandstones.....63

37. Photomicrograph of pyrite cement.....63

38. Photomicrograph of pyrite, marcasite, and pyrrhotite.....64

39. Photomicrograph of kaolinite.....65

40. SEM photomicrograph of partially dissolved kaolinite.....65

Figure Page

41. SEM photomicrographs of smectite-illite mixed layered clay.....67

42. Photomicrograph of smectite-illite mixed layered clay.....68

43. Photomicrograph showing a quartz overgrowth and hematite dust rim.....69

44. Photomicrograph of chalcedony.....69

45. Photomicrographs of dissolution of hematite in the dolomite rhombs.....71

46. Graph of porosity and carbonate percentages determined from thin section.....72

47. Paragenetic sequence.....73

48. Photomicrograph shows the carbonate displacement of pyrite.....75

49. Photomicrograph of dolomite rhombs enclosing oxidized pyrite, hematite.....75

50. Anomalous API gravity values of crude oil for the Healdton field.....80

51. Graph of mangangese versus iron concentration.....82

52. Eh-pH stability diagram of common manganese minerals.....83

53. Eh-pH stability diagram for the aqueous ferric-ferrous system.....86

54. Eh-pH stability diagram of iron minerals.....87

55. Eh-pH stability diagram for aqueous sulfur species.....89

56. Eh-pH stability diagram combining the iron, sulfur, and carbonate systems.....90

57. Stability field diagrams of iron minerals.....92

58. Photomicrograph of pyrrhotite blades.....93

59. Stability diagram for kaolinite.....96

Figure Page

60. Outcrop photograph showing alteration along the crossbedding.....97

61. Illustration of the stages of carbonate and sulfide mineralization.....98

62. Outcrop photographs showing the mineralization of carbonate.....99

63. Outcrop photographs showing concretions of carbonate.....100

64. Illustration of the cross sectional view of the HIDA diagenetic model.....102

65. Illustration of the extent of the fractionation...106

66. δC^{13} isotopes for the Cement field.....108

67. Model for the hydrocarbon contribution of the Cement data.....108

68. Frequency distribution of δC^{13} values for the Velma, Healdton, and Carter-Knox fields.....112

69. Model for the hydrocarbon contribution of the Velma, Healdton, and Carter-Knox fields.....114

70. Frequency distribution of δO^{18} isotopes for the Velma, Healdton, and Carter-knox fields: (a) oxygen isotopes of water, (b) oxygen isotopes of carbonate 117

71. Graph of δC^{13} and δO^{18} values for the various fields.....118

72. Isotopic separation of δO^{18} isotopes for calcite and water as a function of temperature.....119

73. Frequency distribution of δS^{34} isotopes for the Velma, Healdton, and Carter-Knox fields.....122

74. Cummulative frequency of the δS^{34} values for the pyrite and H_2S gas associated with petroleum.....123

75. Frequency distribution of δS^{34} isotopes for the Healdton field.....125

CHAPTER I

INTRODUCTION

Oil and gas are substantial natural resources for the State of Oklahoma. Exploration and production in Southwestern Oklahoma has been extensive since the 1900s with the discovery of the Granite field in 1901 and the Wheeler field in 1905 (Gouin, 1956).

Present methods of continental petroleum exploration focus on subsurface mapping while the utilization of diagenesis and geochemistry are given little consideration. One question that must be addressed is the value of geochemical and diagenetic criteria in relation to petroleum exploration. If these criteria could delineate the subsurface structure in which hydrocarbons have been or are now present, then continental exploration might experience reduced research costs along with increased productivity. Therefore, the applicability of geochemical and diagenetic uses in exploration should be evaluated.

Many oil and gas accumulations in southern Oklahoma lie within anticlinal structures that are covered by a blanket of Permian redbeds. Distinct changes in coloration (Figure 1) and cementation occur in the redbeds along these northwest-southeast trending lines of production. The

Figure 1.--Photograph typifying coloration changes in HIDA.

coloration patterns were first recorded by Reeves (1921) in his investigation of the Cement oil field in Caddo County. He observed that the normal reddish-brown color of the Permian Whitehorse Sandstone had altered to pink, yellow, and white on the flanks of the Cement anticline. He also reported a change in the cementation of both the Whitehorse Sandstone and the Cloud Chief gypsum over the crest of the structure. The origin of the alteration was unclear to Reeves. Harlton (1960) recorded similar alteration patterns in the Carter-Knox, Velma, and Eola anticlines.

The first comprehensive study on the redbed alteration was published by Donovan (1974). He conducted extensive chemical analyses of surface outcrops in the Cement anticlinal area. His conclusions were that the altered redbeds, bleached zones on the crest of the structure, were related to underlying hydrocarbon reservoirs.

Olmstead (1975), in an evaluation of uranium potential, recorded uranium concentrations associated with the altered Permian redbeds where they overlie hydrocarbon productive zones. He suggested that the same geochemical mechanisms responsible for the bleaching at Cement, were also influential in the uranium mineralization along the crest of the anticline.

Ferguson (1977) mapped the diagenetic pyrite distributions in the subsurface for the Chickasha, Eola, and Velma oil fields. Ferguson concluded that the spatial distribution of pyrite in the shallow subsurface delineated

hydrocarbon productive areas.

Donovan and Dalziel (1977) identified signs of hydrocarbon seepage in the Permian redbeds. They suggested three mechanisms of seepage that operate over the oil and gas fields. δO^{18} and δC^{13} isotopic data was used to support their ideas.

Surface alteration zones of the Cement-Chickasha area and the Velma field were extensively mapped by Allen (1980) and Donovan et al. (1981), respectively. Allen furthered Olmstead's studies of the uranium potential of the area. In addition to mapping the surface zones, Donovan et al. used isotopic analysis of carbonate samples gathered from Velma to demonstrate the relationship of the alterations and the hydrocarbon productive areas.

Lilburn (1981) conducted an extensive isotopic and geochemical study on the Cement-Chickasha area. This study consisted of the examination of well cuttings, the construction of diagenetic cross sections, and the isotopic analysis of diagenetic carbonates and pyrites for isotope studies. He showed that the diagenetic imprints are strongly related to hydrocarbon migration.

Past studies have shown that the alterations of redbeds in southern Oklahoma are related seepage of hydrocarbon from underlying oil and gas reservoirs. Diagenetic events are controlled by the rock composition and the chemistry of migrating pore fluids. The purpose of this study was to test the proposition that a positive correla-

tion exists between diagenesis of the redbeds within the project area and seepage of hydrocarbons.

Location and History

The project area (Figure 2) includes several petroleum fields in southwestern south-central Oklahoma that are overlain by Permian redbeds (T4N to T5S and R3W to R6W). Fields included are the Healdton field in Carter County, and Velma in Stephens County, and the Carter-Knox field in Grady County. In addition, observations were made in the Loco, Palacine, Fox, Hewitt fields that are near to the immediate study area.

Healdton

The Healdton field is located in the northwestern part of Carter County, Oklahoma (T3S to T4S and R3W to R4W). This oil field is one of the earliest discovered in southern Oklahoma. The first well drilled by the Red River Oil Co. in August, 1913, was stationed on Wirt Franklin's farm in the NE. 1/4 sec. 8, T.4S., R.3W. Initial production of the foremost gusher was 25 barrels per day. Red River Co. drilled a subsequent well which produced 300 barrels a day. Excitement aroused over the findings at Healdton. In 1914, Magnolia Pipe Line Co. extended a line from Bowie, Texas to the Healdton field. By this time, production was so prominent that the line was unable to handle all of the production, and operators stored the oil

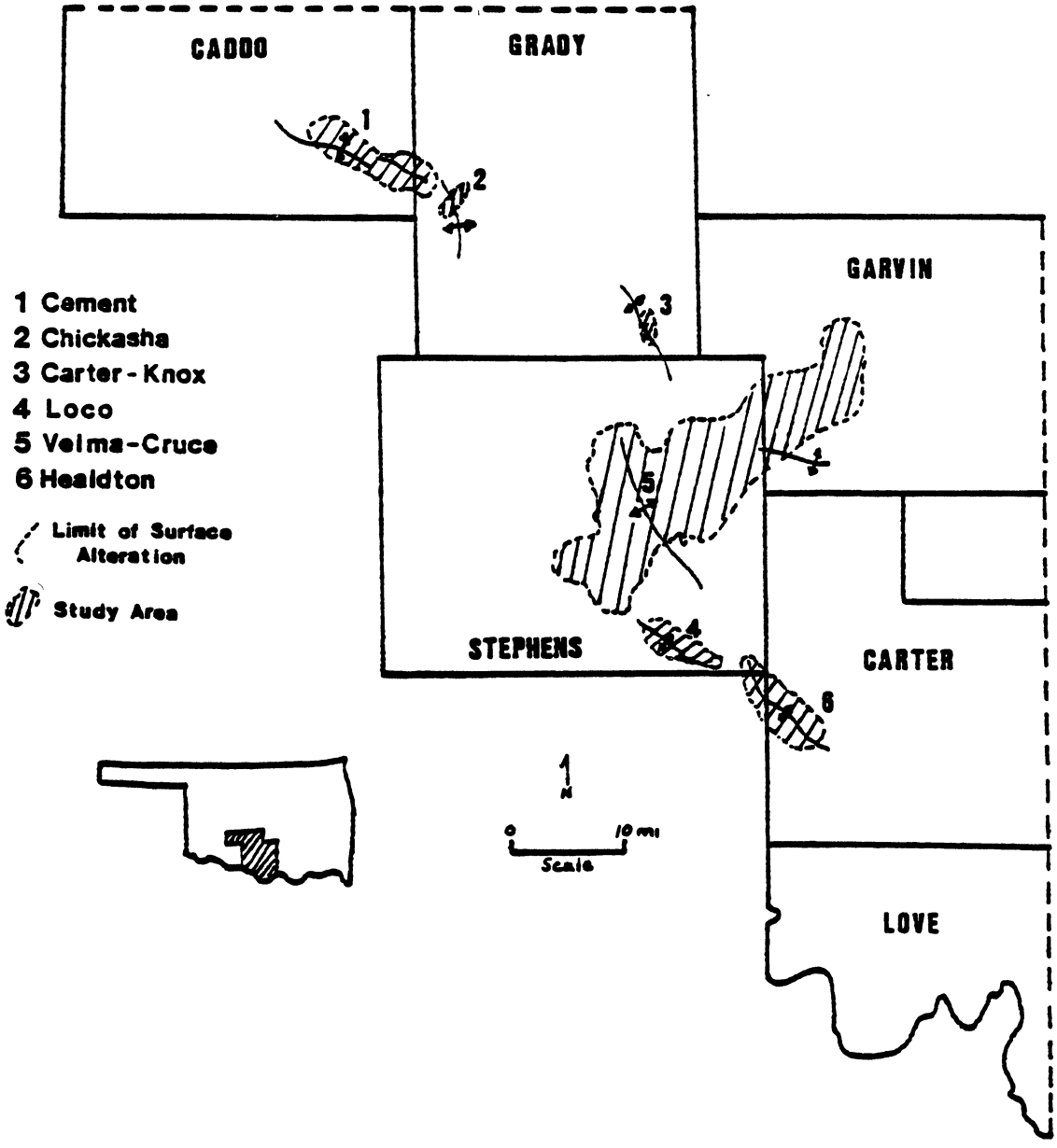

Figure 2.--Index map of the study area.

in storage tanks (Wegemann and Heald, 1915). Future development of the field resulted in oil production from four Hoxbar sandstone horizons of Pennsylvanian age--the Healdton sandstones. Between 1955 and 1970, approximately 2,600 wells were drilled. These covered a production area of more than 7,100 acres. In 1960, production from the Ordovician Arbuckle dolomites was discovered. The younger and older reservoirs appear to have different origin and migration histories (Latham, 1970).

Velma

The Velma field is located in the east half of T.1S., R.5W., Stephens County, Oklahoma. In July, 1917, the Texas Company completed the discovery well located in the SW 1/4 sec. 36, T.1S., R.5W. Production was from the Permian for 10 barrels per day. Development of the field was very slow until after the installation of a pipeline outlet in 1920. During the first fifteen years of production, an estimated 5,000,000 barrels of oil were produced from the shallow Permian sands. In 1925, more than twenty test wells were drilled into the Pennsylvanian but were either dry or unprofitable. In May, 1941, deep production of the Simpson sandstone was initiated by Skelly Oil Company. Subsequent discoveries in other horizons such as the Hoxbar, Deese, and Springer were also developed (Rutledge, 1956).

Carter-Knox

The Carter-Knox field is located in southeastern Grady County and northeastern Stephens County. The first well was drilled by Clyde Griswold in 1916 for the Santa Fe Railway Company in NE 1/4 sec. 2, T.2N., R.5W. Griswold's well was a dry hole. First production was discovered in NE 1/4 section 28, T.3N., R.5W. in shallow Permian sandstone. This well was completed in 1923 for 10 barrels of oil per day. In February, 1947, Springer gas production was discovered and completed for a production potential of 48,708,000 cubic feet of dry gas per day. Springer sandstone oil production was discovered in April, 1947, with an initial production of 808 barrels per day. In 1956, gas was discovered in both the Bromide and the Oil Creek sandstones (Reedy and Sykes, 1959).

Methodology

Permian redbeds in these fields exhibit similar surface characteristics such as discoloration and varying degrees of carbonitization and pyritization. Relationships can be seen between the alteration of the redbeds and hydrocarbon seepage. The term HIDA (Hydrocarbon-Induced Diagenetic Aureole) is proposed to include the segments of host rocks having undergone alteration as the result of the hydrocarbon seepage.

Although the Velma and Carter-Knox fields were studied and mapped, emphasis has been placed on the

Healdton field. Field mapping, sample collection, sample analysis, and sample description of the altered redbeds within the project area were conducted. The field mapping consisted of observing the surface exposures of the area to determine the degree of alteration. Four diagenetic facies, alteration zones, were defined based on criteria determined primarily by petrographic and lithologic analysis. The following criteria describe the four facies:

1. Extensively carbonate cemented sandstone
2. Altered (buff to yellow) redbed with minimal carbonate cement
3. Altered redbed with pyrite
4. Original, unaltered redbed.

Sample analysis and sample description consisted of the identification of constitutents using the scanning electron microscope (SEM) coupled with the energy dispersive x-ray analyzer, x-ray diffraction, and thin section analysis using the petrographic microscope.

Cuttings from thirty-four wells were examined to determine the extent of pyrite and carbonate mineralization.

The geochemical study consisted of analysis of selected sulfide, carbonate, water, and oil samples to determine their isotopic ratios of sulfur, carbon, and oxygen. Isotope data were used to determine the relationship of the diagenetic constituents to the underlying oil and gas reservoirs. The energy dispersive x-ray analyzer

and scanning electron microscope were used to determine chemical identities.

CHAPTER II

GEOLOGIC SETTING

Regional Tectonic Setting

Southern Oklahoma geology was formed by complex tectonism which resulted in the construction of an extensive structural belt that reaches from the Ouachita Mountains to the North Texas Panhandle. The structural belt of southern Oklahoma is characterizes by faults and folds that developed during various stages of the evolution of the aulacogen. The major structural features associated with the aulacogen formation are illustrated in Figure 3.

Three major structural provinces in southern Oklahoma were formed during the tectonic cycle. The provinces are named by their associated uplifts. These are the Wichita province, the Arbuckle province, and the Ouachita province. Evolution of these complex structural features probably began in the early Cambrian time, continued through the Paleozoic, and closed following the Permian (Webster, 1980).

The Wichita province includes the Wichita Mountains, the Hollis or Hardeman basin, and the Anadarko basin. While, southeast of the Wichita province is the Arbuckle province which includes the Arbuckle uplift, the Ardmore

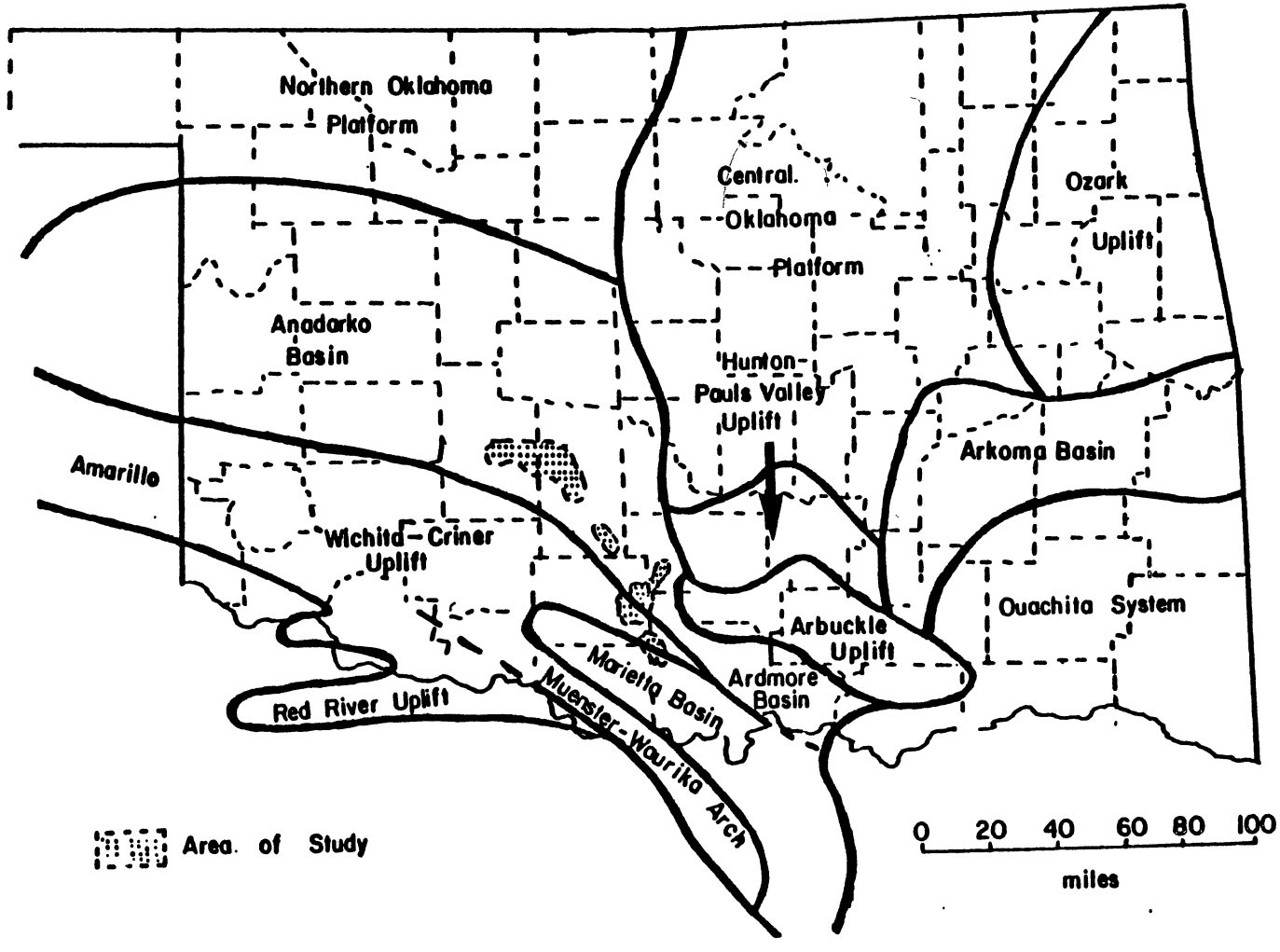

Figure 3.--Oklahoma Geologic Provinces (Al-Shaieb, Shelton, and others, 1977).

basin, the Criner arch, the Marietta basin, and the Muenster arch. These structural features extent southeastward where they are concealed by the overthrusts of the Ouachita province. The easternmost structural province, the Ouachita province, comprises the Arkoma basin and the thrust-faulted and folded Paleozoic rocks of the Ouachita Mountains.

The Wichita-Criner or the Amarillo-Wichita uplift trends northwest-southeast; this structural feature is believed to be the axis of the Southern Oklahoma Aulacogen (Pruatt, 1975). Plutonic and extrusive igneous rocks of possible Precambrian and Early to Middle Cambrian age outcrop in the Wichita Mountains area and disappear into the North Texas Panhandle subsurface.

The north flank of the uplift is bound by a 10-20 km wide complex fault zone consisting predominantly of high angle reverse faults. This fault system separates the uplift from the northerly Anadarko basin (Webster, 1980). The basin is the deepest persistent Paleozoic sedimentary basin on the North American Craton (Ham and other, 1964) containing up to 38,000 feet of Paleozoic sediments (Ham, 1969). Southeastward, the Anadarko Basin merges into the Ardmore basin. The Ardmore basin sediment thickness is approximately 34,000 feet of Paleozoic sedimentary rocks where the basin disappears beneath the Ouachita Thrust Belt (Ham, 1969). To the north of the Ardmore basin, the Arbuckle Mountains parallel the axis of the Ardmore basin.

The Arbuckle province is structurally more complex than the western Wichita province (Hicks, 1971). Both the Precambrian granite and the Cambrian rhyolite are exposed in the northern Arbuckle uplift. To the south of the Ardmore basin is the Criner arch, a faulted anticline that extends the Wichita fault zone trend. Southward, the shallower Marietta basin continues the Amarillo-Wichita uplift trend as the old axis of the aulacogen (Pruatt, 1975).

The Wichita orogeny, from Morrowan through Desmoinesian time, was characterized by the rise of the Wichita-Criner horst block. Extensive vertical displacement, approximately 30,000 feet, occurred along the frontal zone. As a result of the displacement a series of southerly dipping high angle to nearly vertical reverse faults developed along the northern edge of the uplift. Also occurring with the uplift was the development of large anticlines and fault structures in the Anadarko basin and the rise of the Criner arch accompanied by the development of the echelon folds in the Ardmore and Marietta basins.

The Arbuckle orogeny in the Virgilian was delineated by the uplifting of the Arbuckle Mountains. Folding of the Ardmore basin and the reverse faulting along the Criner arch and Arbuckle uplift regions occurred during the Arbuckle orogeny (Webster, 1980). Faults trending at acute angles to the main structural orientations are indicative of a leftlateral wrench fault system suggested by Pruatt

(1975).

Simultaneous to the two orogenies was the formation of the Ouachita Thrust Belt. This belt of faulted and folded sediments is believed to be the result of continental collision between the North American and South American continents (Webster, 1980).

In Late Pennsylvanian time, the tectonism was greatly subdued; however, minor folding of the Permian sediments occurred over the Pennsylvanian structures (Ferguson, 1977). Subsidence of the Anadarko and Ardmore basins continued through the Permian. Postorogenic Permian sediments are predominantly red clastics and evaporites that were deposited in broad epicontinental seas. This marked the last period of significant deposition in the region. The area has been tectonically inactive since the close of the Paleozoic (Webster, 1980).

The structural complexity of southern Oklahoma has provided areas of significant hydrocarbon accumulation. Through several periods of tectonism and rapid environmental changes of deposition, a wide variety of trapping mechanisms were formed to allow the development of extensive oil and gas reservoirs. Anticlinal, faulted, and stratigraphic traps occur within the area (Webster, 1980). The anticlinal structures are aligned along a northwest-southeast trend and show similar characteristics. The folds are generally asymmetric bound by high angle reverse faults. Figure 4 shows the locations of the major faults

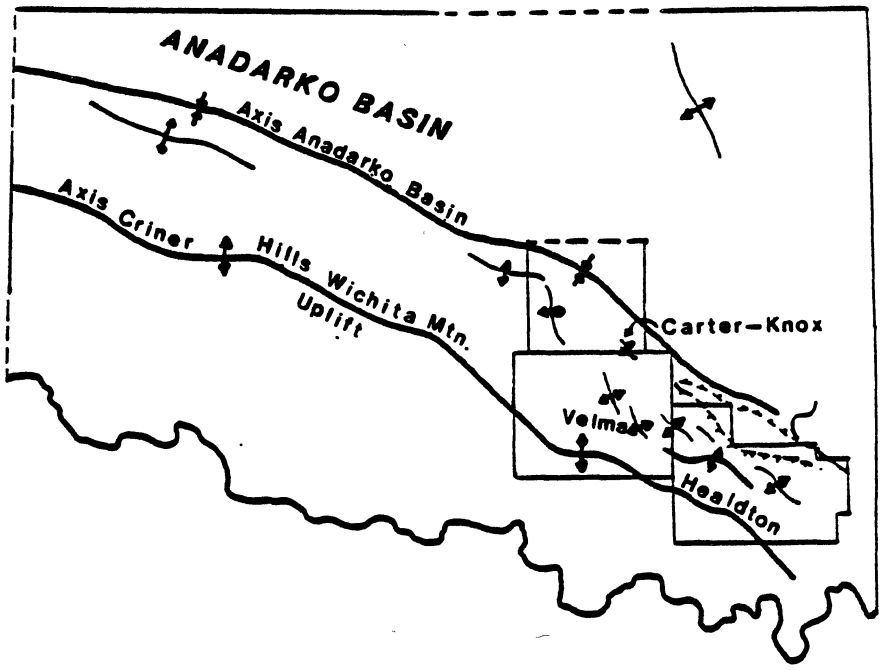

Figure 4.--Major fault trends of Southern Oklahoma (Rutledge, 1956).

in southern Oklahoma. The fields included in the study area are structurally controlled, anticlinal traps that lie in zone of complex faulting.

Stratigraphic Setting

The stratigraphic column of the Permian System (Figure 5) utilized in this discussion is after Miser (1954). Although the rocks encountered in the subsurface range in age from Cambrian through Permian, the alteration of strata is confined to rocks of Permian age. These rocks range in age from Wolfcampian through the Guadalupian Cloud Chief Formation.

Surface Stratigraphy

The surficial lithology of the Healdton, Velma, and Carter-Knox fields is Permian in age. The Pontotoc Group overlies the Healdton topography (Latham, 1970). Strata of the Sumner Group outcrop on the Velma anticline (Rutledge, 1956; Gouin, 1956). Carter-Knox has surface outcrops of the Chickasha-Duncan formation (Reedy and Sykes, 1959).

Subsurface Stratigraphy

The Permian subsurface stratigraphy section in south-western and south-central Oklahoma is described in the order in which it is penetrated by drilling

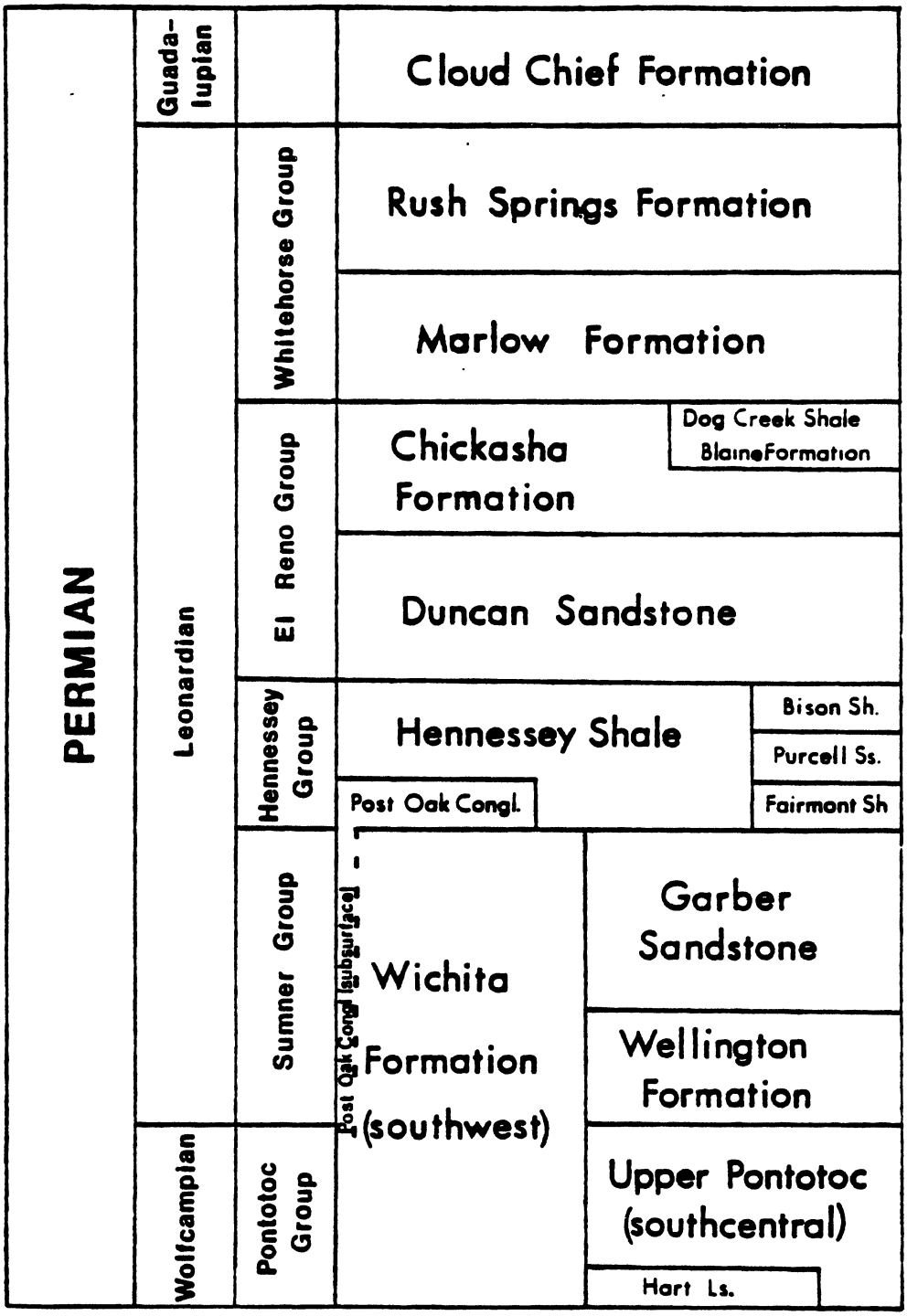

Figure 5.--Stratigraphic column of the study area.

Guadalupian Series

Cloud Chief Formation. The Cloud Chief Formation consists of irregular, impure gypsum beds interbedded with red shales . This formation caps topographic highs in the Chickasha and Cement areas (Fay, 1969).

Leonardian Series

Whitehorse Group. The Whitehorse Group is composed mainly of fine-grained sandstones and siltstones with occasional appearances of thin dolomite and gypsum beds.

(a) Rush Springs Formation. This formation is a light brown to reddish-brown, even to highly cross-bedded, friable, silty sandstone. The sandstone is generally fine-grained with moderate amounts of hematite and clay minerals as cements. The formation is prominent in northern Stephens County but thins towards the northwest (Davis, 1955).

(b) Marlow Formation. The Marlow Formation outcrops in Grady County (Davis, 1955). The formation consists mainly of reddish-brown, even-bedded, fine-grained silty sandstones and shales. Satin-spar gypsum is distributed randomly throughout the formation. The Verden Sandstone Member, a lenticular, medium to coarse sandstone, is characterized by thick, highly cross-bedded beds. Two thin dolomite beds, separated by a red sandstone and shale unit, can be observed in the upper portion of the formation.

El Reno Group. The El Reno Group was used to map the surface structure in the Carter-Knox field.

(a) Chickasha Formation. In the Carter-Knox area, the Chickasha sandstone comprises 160 feet of lenticular sandstones with shales, siltstones, and mudstones purple-maroon in color.

(b) Duncan Sandstone. The Duncan sandstone in the Carter-Knox area attains a maximum thickness of 180 feet. The sandstone consists of cross-bedded maroon sandstone and clay shales.

Hennessey Group. The Hennessey Group is a thick sequence consisting mainly of varied colored shales. This shale zone, averaging 400 feet thick, consists of red shale and mottled red and green shale with thin lenses of cross-bedded, friable, greenish-gray silty sandstone.

Sumner Group. This group is composed of the Wichita Formation in the southwest and the Garber and Wellington in the south-central. The Sumner Group outcrops in the Velma area.

(a) Garber Sandstone. The sandstone formation averages 320 feet in thickness. It is a massive, fine to medium grained, slightly calcareous, arkosic sandstone. The sandstone is commonly red. The basal Garber sandstone is a massive, bituminous gray sandstone.

(b) Wellington Formation. This formation consists of 750 feet of alternating sandstone and shales. The shales

are predominantly red with some green coloration. The sandstones are fine to medium grained and slightly calcareous.

Wolfcampian Series

The Wolfcampian Series is comprised of the Wichita Formation to the southwest and the Upper Pontotoc Formation in the south-central. The lowest most unit of the Pontotoc Group in the south-central area is the Hart Limestone.

Pontotoc Group (Upper Portion). These rocks outcrop in the Healdton area and unconformably overlie the Pennsylvanian Hoxbar Formation. The Pontotoc strata consists predominantly of red to varicolored shales and sandy shales with thick conglomeratic sandstones. The thickness over the Healdton structure ranges from 500 feet over the axis to 2000 feet on the flanks (Ferguson, 1977).

Depositional Environments

Deposition of redbed strata was common in central and western North America throughout Permian time. Redbeds are colored by finely dispersed ferric oxides, usually in the form of hematite (Turner, 1980). Theories on the genesis of the redbeds and the mechanisms of their formation are often disputed. The presence of hematite is often considered a paleoclimatic indicator of a hot, dry, semi-arid or arid environment (Walker, 1967). Redbeds most definite-

ly signify an oxygenated atmosphere but they may occur in both arid and tropical climates (Turner, 1980; Habicht, 1979). However, climatic conditions in areas of redbed deposition are reflected in the flora and fauna. All known redbed floras indicate warm-temperate, subtropical, or even tropical environments (Van Houten, 1964). In addition to paleontological indicators, there may also be lithological evidence suggested by Walker (1974):

(a) a desert-evaporite redbed in which redbeds are associated with eolian sands, desert fluvial sediments and evaporites formed in playa lakes and inland sabkhas,

(b) a moist climate-redbed in which redbeds are interbedded and interfingered with coal-bearing strata. Although these are climatically different, they both occur in a similar latitude within 30 degrees of the equator. For this reason, the hypothesis that redbed formation may indicate low paleolatitudes has been suggested by Turner (1980). The paleolatitude is an important factor in climatic dependent deposition. Figure 6 illustrates the paleolatitudes and paleoclimates of North America during Permian time. Oklahoma was positioned approximately 10-13 degrees from the equator during the Permian (Habicht, 1979). Flora such as the first conifers, cycads, and ferns, and fauna like the first reptiles found in the Permian redbeds indicate that the climate increased in aridity throughout deposition.

Permian strata in Southern Oklahoma record evidence

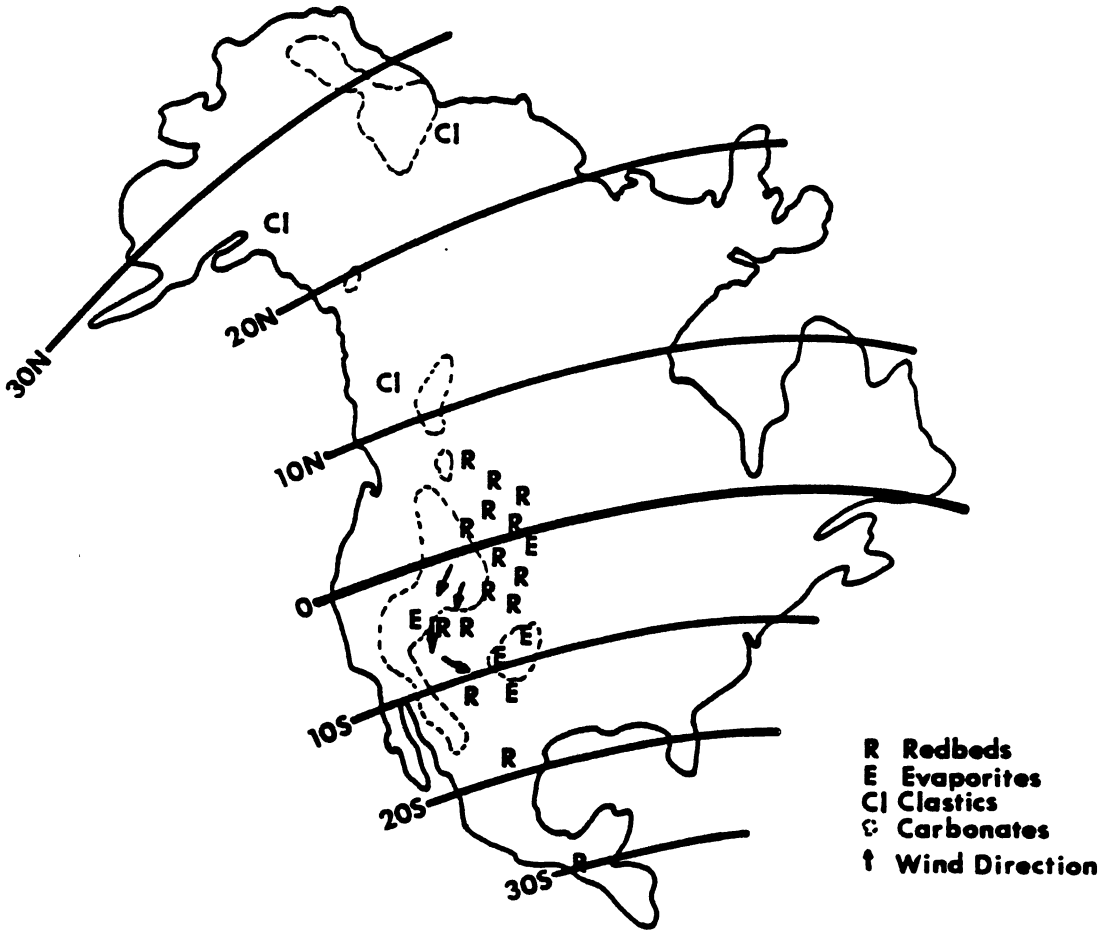

Figure 6.--Paleolatitudes and paleoclimates of North America during the Permian System (Habicht, 1979).

suggesting that the environments of deposition progressed from fluvio-deltaic to normal marine to marginal marine to restricted marine (Rascoe and Adler, 1983; Flood, 1969; MacLachlan, 1967; Figure 7). The Wolfcampian sediments are products of a transgressive phase which deposited red alluvial plain shales, channel sandstones, and limestones accumulated in a nearshore marine environment. A subsequent regressive phase resulted in the deposition of similar lithologies in reverse order. The Leonardian Series is composed of cyclic red beds (siltstones, shales, and fine-grained sandstones) and evaporites. This redbed-evaporite sequence is indicative of an arid climate in semi-continental and restricted marine environments associated with the later stages of marine regression (Rascoe and Adler, 1983; Walker, 1967).

Lower Permian lenticular sandstones in south-central Oklahoma have been interpretted as fluvial in origin while the siltstones and shales represent flood-plain and delta-flat deposits (Flood, 1969; Ferguson, 1977). The Wellington Formation, the Garber Sandstone, and the Hennessey Shale were interpretted by Davis (1955) to have been deposited in several types of marine-dominated environments such as deltaic, shallow marine, tidal flat, and supratidal. Paleocurrent indicators and the trend of the channel sandstones indicate a northwesterly flow of the streams. The current direction and trend imply a southeasterly source area. The Ouachita and Arbuckle uplifts

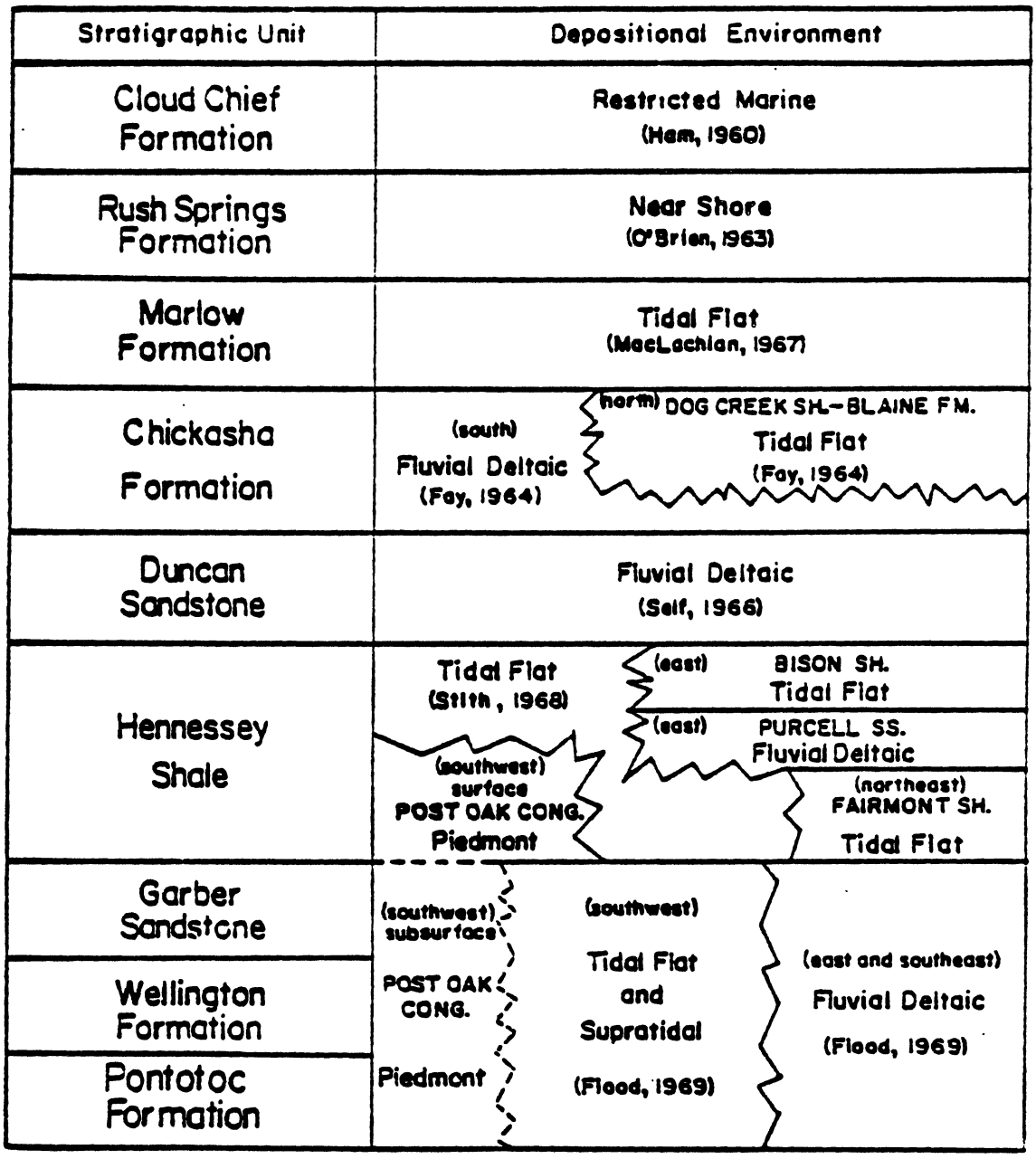

Figure 7.--Stratigraphic column and equivalent depositional environments, south-central Oklahoma (Olmsted, 1975).

were present in southeastern Oklahoma at the time of deposition. Because detritus from the Arbuckle Mountains appears only in the Wolfcampian age sediments, Flood (1969) concluded that the Arbuckle Mountains contribution of detritus was minimal following the Wolfcampian Series. Therefore, the Ouachita Uplift was the major source of sediment to south-central Oklahoma throughout the remaining Permian time (Flood 1969; Ferguson, 1977).

Fay (1964) described the Duncan and Chickasha Formations as sediments of a delta deposited on a northwesterly flowing river sourced from the Ouachita Mountains.

The Marlow Formation was deposited in a shallow transgressed sea. Fay's interpretation (1964) of the depositional environment was that of a gradation between deltaic and shallow-brackish marine; however, MacLachlan (1967) suggested a marine-mudflat environment.

The Rush Springs Sandstone was deposited in a shallow Permian sea (Davis, 1955). The sea level periodically fluctuated allowing eolian conditions. The sediment was reworked into dune sands (MacLachlan, 1967). Siltstones and and shales within the formation may represent coastal plain playa lakes or brackish backshore lagoons while the gypsum and dolomite present may represent coastal sabkha deposits (Allen, 1980).

The Cloud Chief Formation suggests an environment of

restricted marine where an arid climate and evaporitic conditions prevailed (Ham, 1960; Rascoe and Adler, 1983).

CHAPTER III

SURFACE AND SUBSURFACE CHARACTERISTICS OF THE VELMA, HEALDTON, AND CARTER-KNOX OIL FIELDS

Hydrocarbon seepage in southern Oklahoma has had an effect on the preservation of Permian structures in the various fields. Topographic expressions of these oil fields reflect not only their structural features but also, the diagenetic features of the rocks. Structural highs occur along the crest of the anticline and are preserved by the presence of resistive carbonate-cemented sandstones. The intensity of carbonate cement is directly related to the structure. Areas that are in close proximity to underlying faults show more extensive mineralization than those areas further from the faults.

Four distinct diagenetic zones are observed in the aureoles. Zone 1 represents extensively carbonate-cemented sandstone (Figure 8). This zone commonly occurs over the crest of the anticline and above prominent fault boundaries. Zone 2 (Figure 9) represents altered redbed sandstones (buff to yellow) with slight carbonate cementation. Formation of the buff colored sandstone, usually, occurs on the flanks of the structures as a grada-

Figure 8.--Outcrop photograph of resistive carbonate-cemented sandstone (zone 1).

Figure 9.--Outcrop photographs of bleached sandstone (zone 2).

tion between the carbonate-cemented sandstone and zone 4, the unaltered redbed sandstones. The coloration change in Figure 10 is dramatic. The contact between zone 2 and the unaltered redbeds defines the limit of the HIDA on the surface. Pyrite occurs as nodules (Figures 11, 12, and 13) and as dissemination in both the carbonate-cemented sandstone and the altered, bleached sandstone. Therefore, zone 3 defines the presence of pyrite in the altered sandstone.

Velma Oil Field

The topographic relief of the Velma anticline reflects the subsurface structure as well as the diagenetic carbonate-cemented sandstone (Figure 14). The composite structure of Velma is a faulted, asymmetrical anticline trending northwest-southeast. A horst block bounded by high-angle reverse faults defines the axis of the anticline (Figure 15). Surface exposures can aide in defining the structural axis and fault zones over areas of oil and gas production. The surface map of the diagenetic zones (Figure 16) indicates that the diagenetic limestone (Zone 1) trends along the subsurface fault patterns. Zone 2 occurs on the flanks of the structure while the redbeds are distal from the structure. The occurrence of pyrite, zone 3, is observed in both zone 1 and zone 2.

Unique occurrences of hematitic-rich sandstones are evident in the Velma field. These areas appear as elevated mounds. Thin section analysis revealed that these rocks

Figure 10.--Outcrop photograph of the dramatic color change.

Figure 11.--Outcrop photograph of nodular pyrites in the bleached sandstone (zone 3).

Figure 12.--Outcrop photograph of a pyrite nodule (1" dia.).

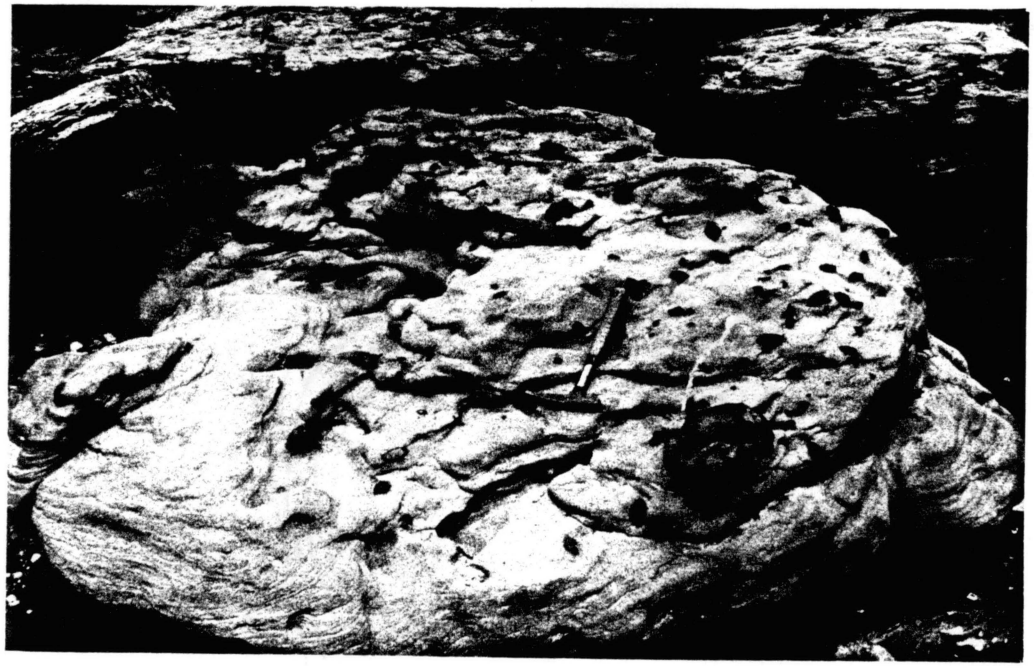

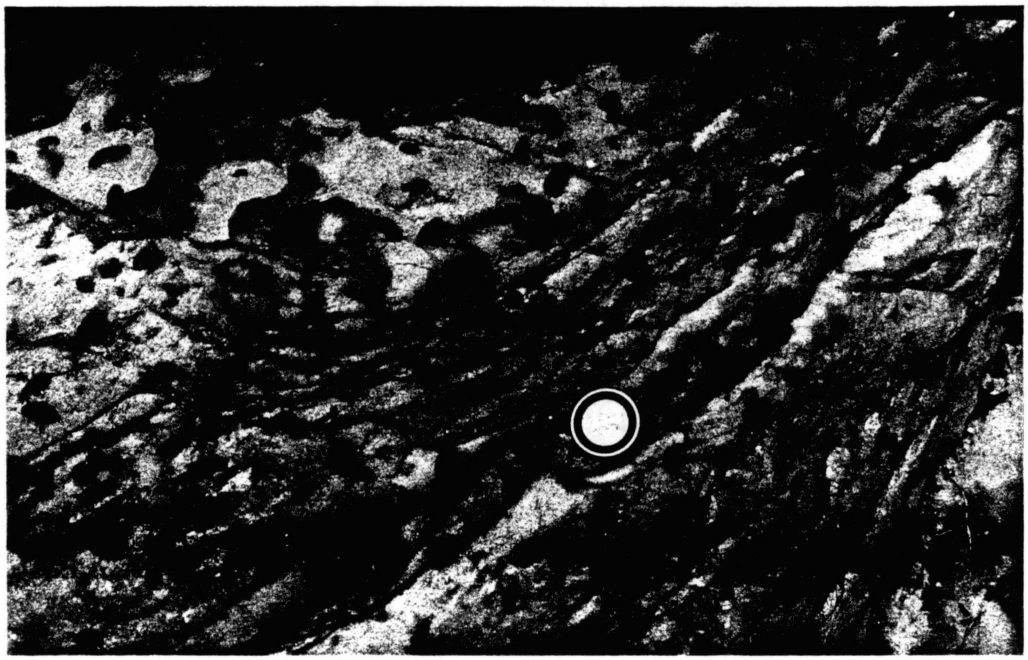

Figure 13.--Outcrop photographs of oxidized pyrite (zone 3).

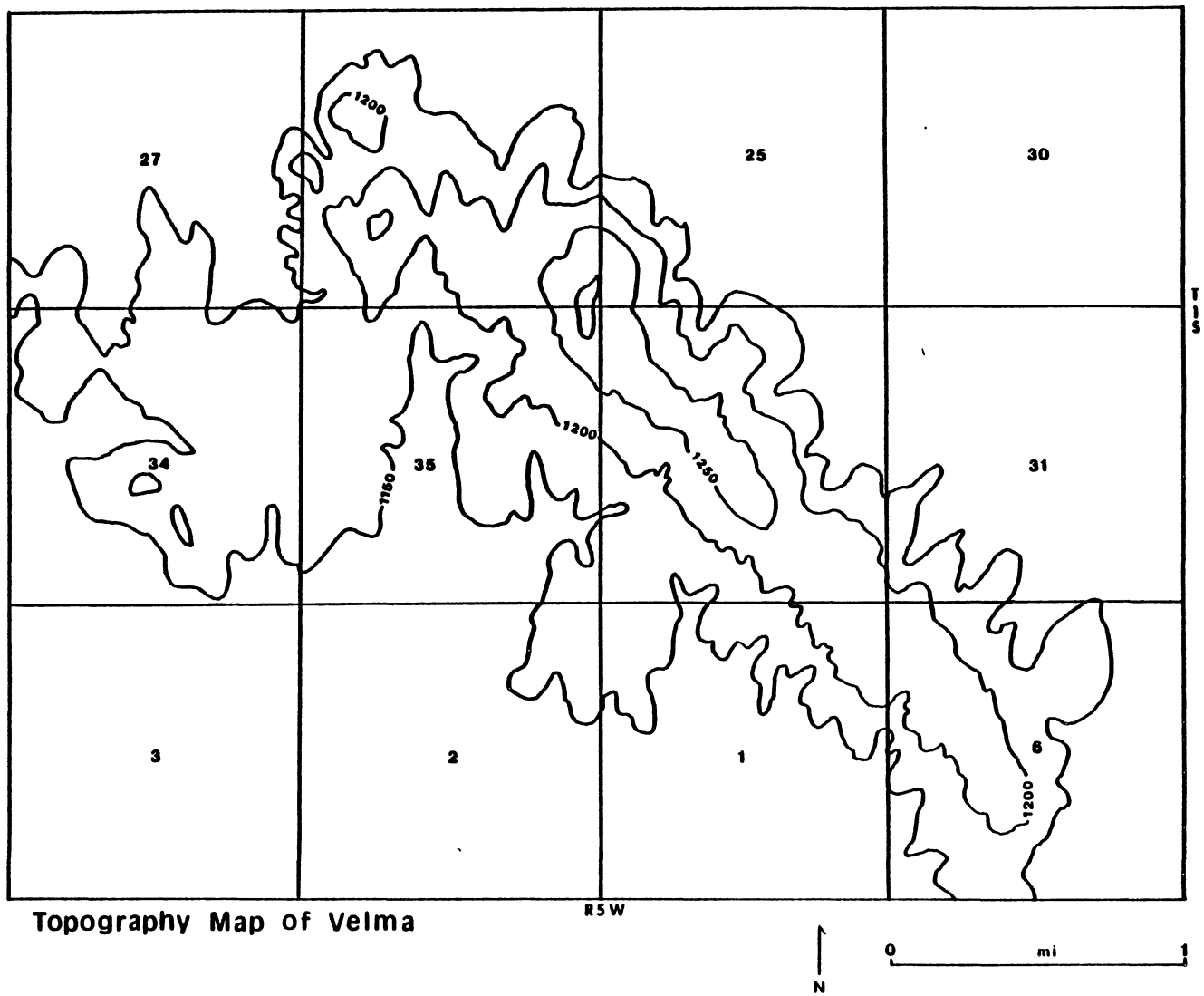

Figure 14.--Topographic map of Velma (U.S. Geol. Survey, 1974).

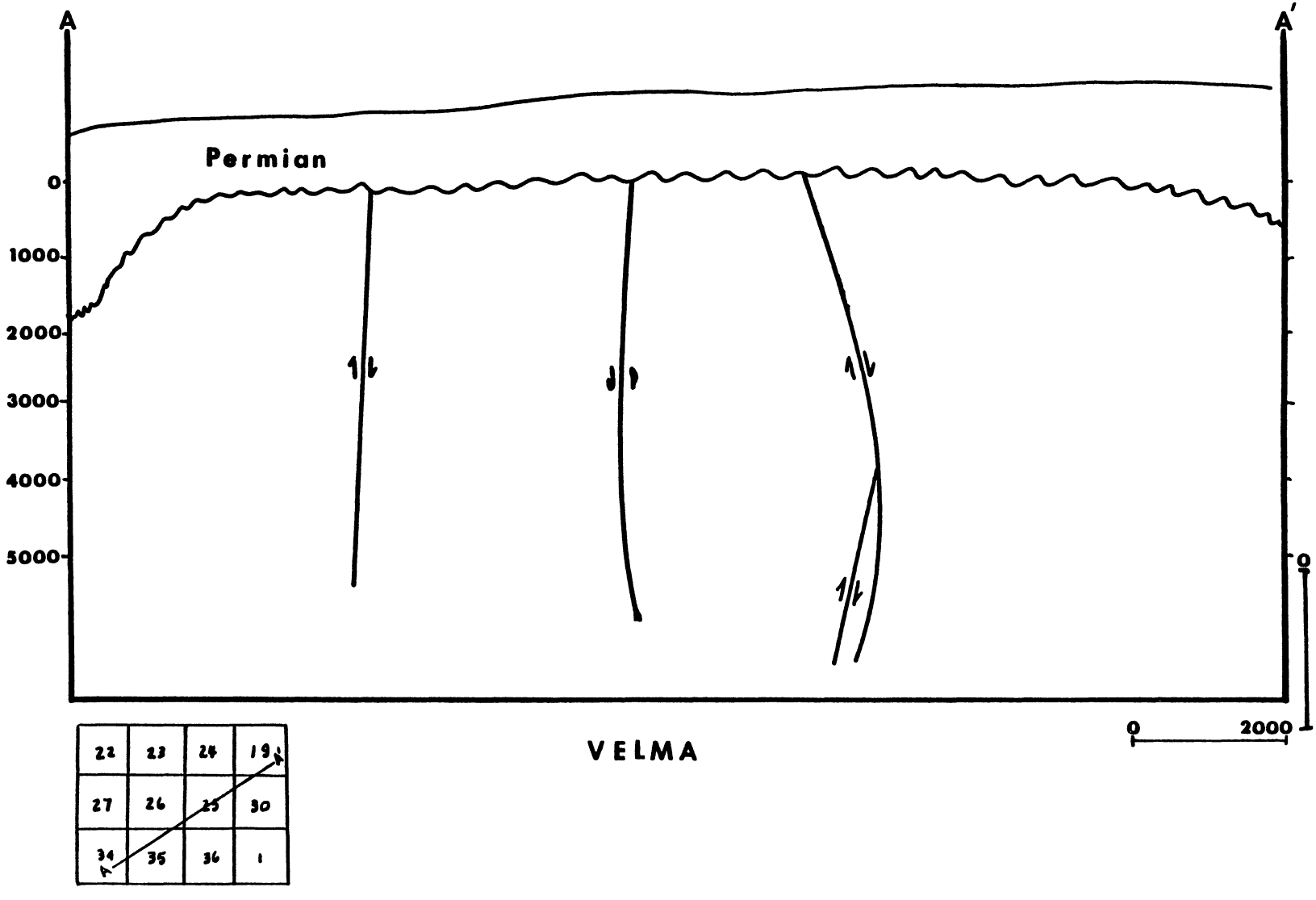

Figure 15.--Cross section of the Velma anticline (Rutledge, 1956).

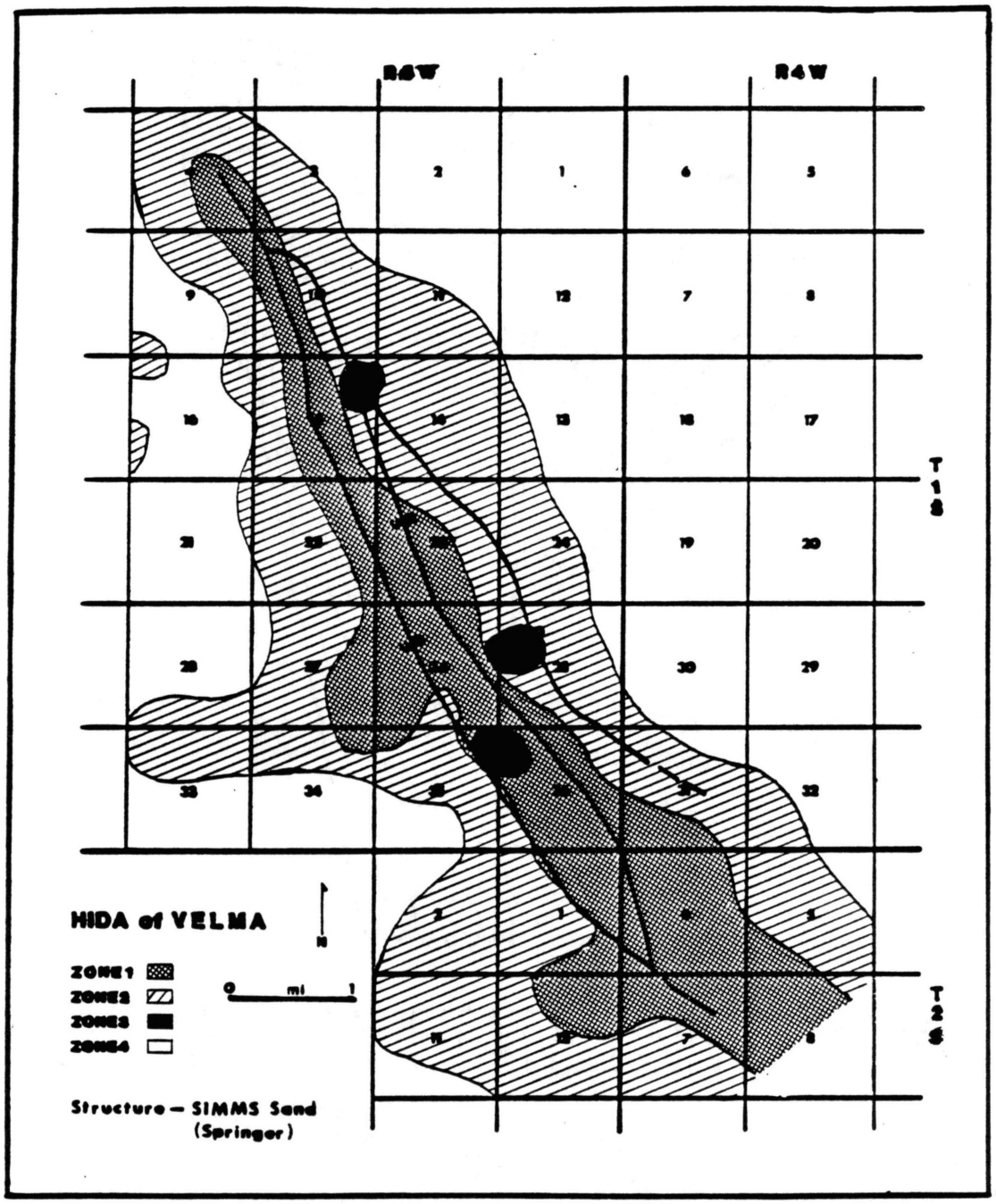

Figure 16.--Velma: surface map of diagenetic zones (structure after Rutledge, 1956).

are cemented by hematite as an oxidation product of pyrite. These surface exposures show the magnitude of the pyrite mineralization. The extent of pyritization can be mapped in the subsurface. Figure 17 (Ferguson, 1977) represents the extent of pyrite cement in the subsurface Permian sandstones of the Velma field. As shown in Figure 17, pyrite formation coincides with the production limits and fault boundaries.

Healdton Oil Field

The Healdton field was developed on a northwest-southeast trending anticlinal structure (Figure 18) that is part of the Wichita Mountains-Criner Hills anticlinorium. Topography of the Healdton field is characterized by gently rolling hills of the Pontotoc Group (Latham, 1970). The topographic relief of Healdton is more subdued than that of Velma due to lesser intensities of carbonate cementation as previously mentioned.

Although zone 1 is concentrated near the fault, the carbonate-cemented sandstone is prevalent over the axis of the anticlinal structure (Figure 19). The extent of the faults in the subsurface probably has a direct relationship to the degree of carbonate mineralization. Zone 2 occurs on the flanks of the anticline. Pyrite nodules were seen in the bleached sandstone. The subsurface pyrite trends along the anticlinal structure (Figure 20). In fact, the limits of the pyrite mineralization appear to be controlled

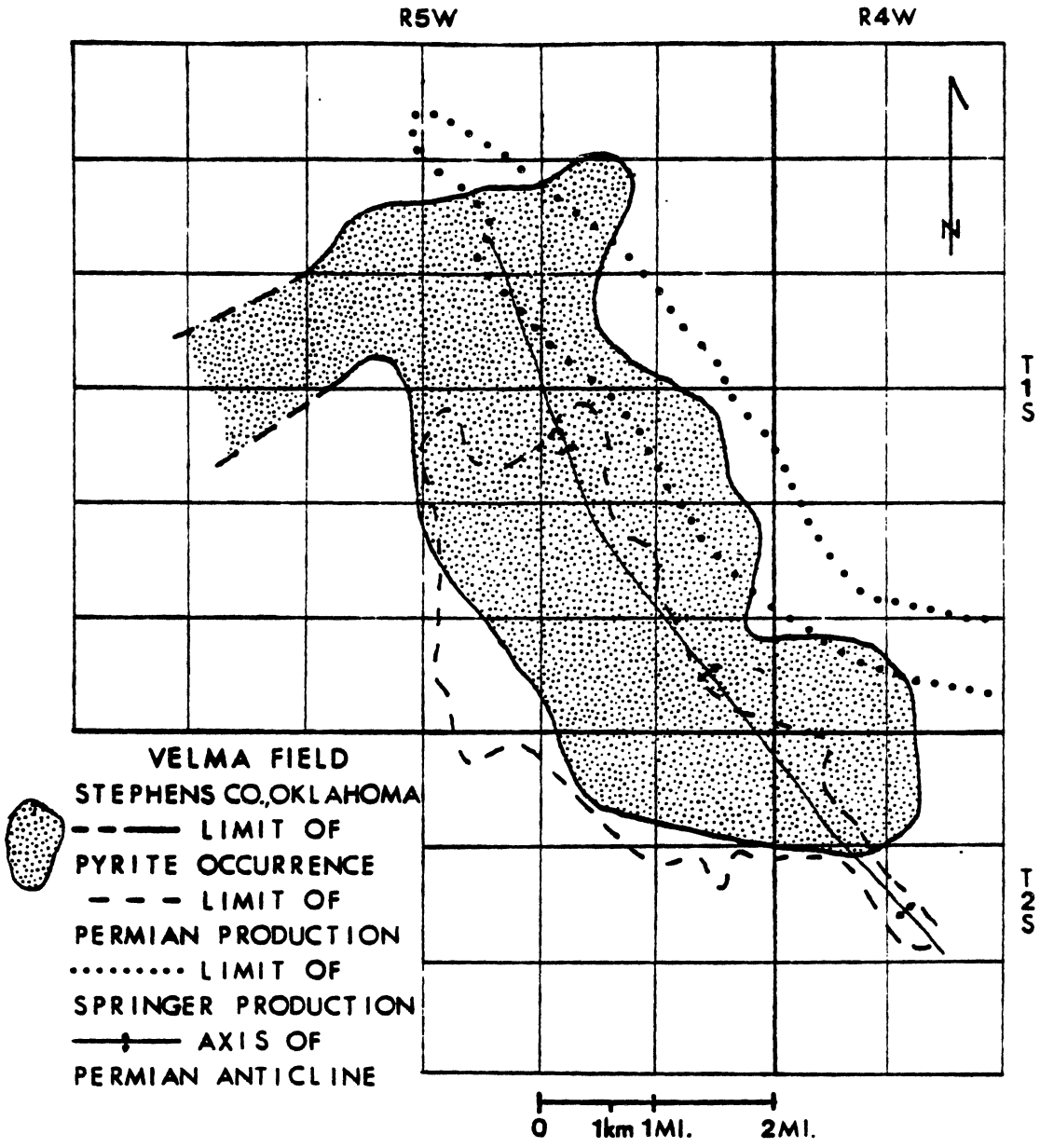

Figure 17.--Velma: subsurface limits of pyritization (Ferguson, 1977).

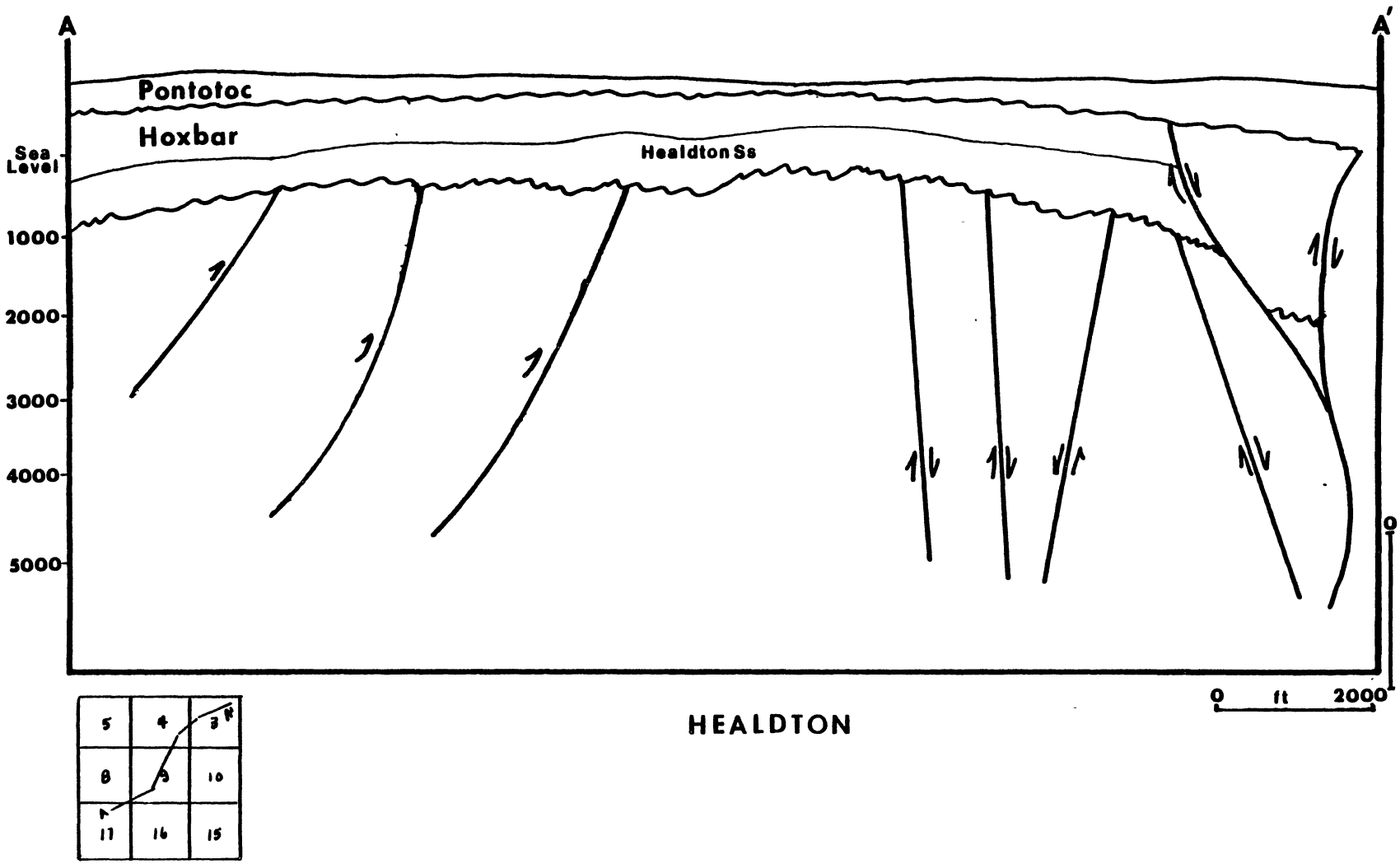

Figure 18.--Cross section of the Healdton anticline (Latham, 1970).

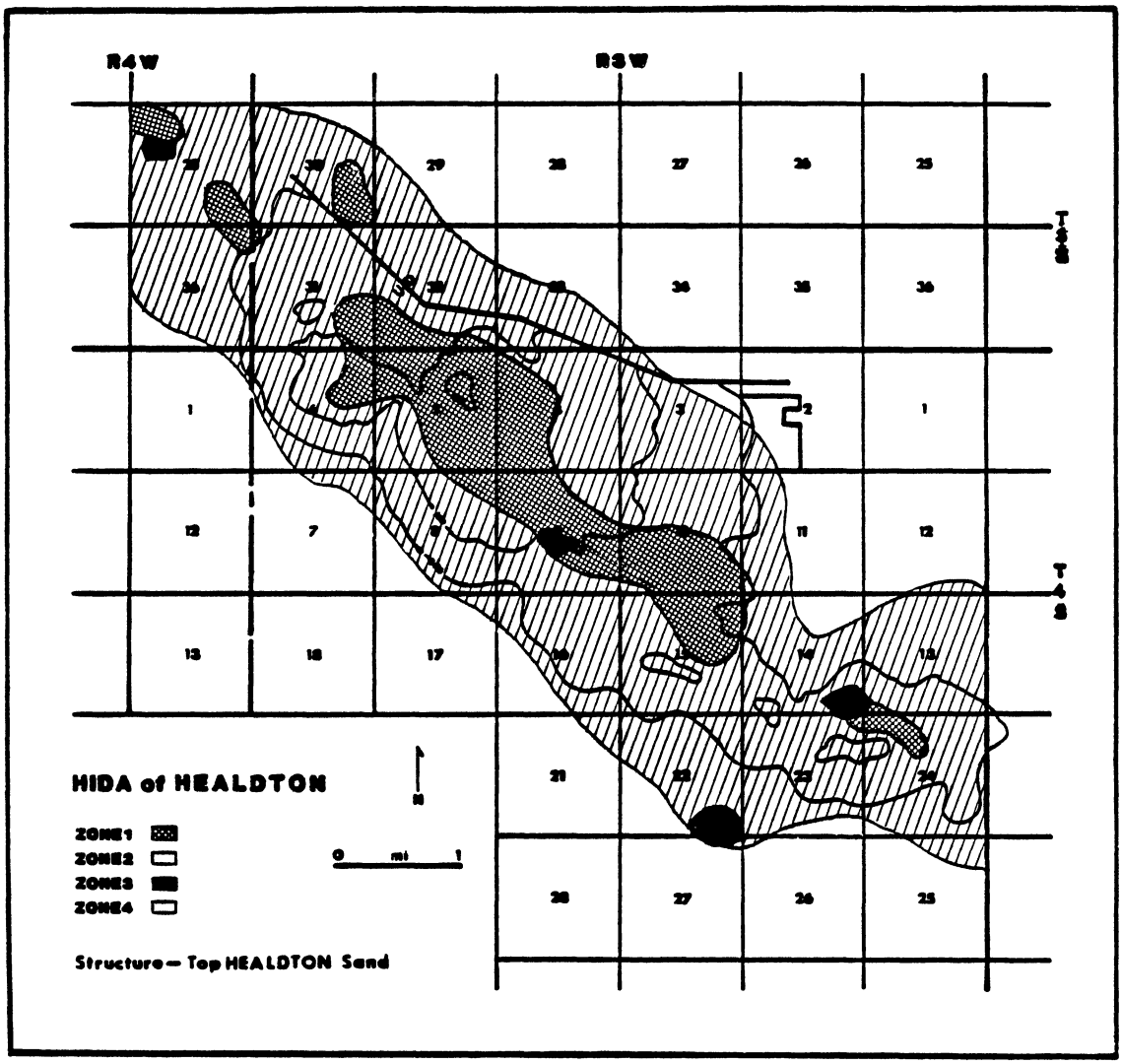

Figure 19.--Healdton: surface map of diagenetic zones (structure after Latham, 1970).

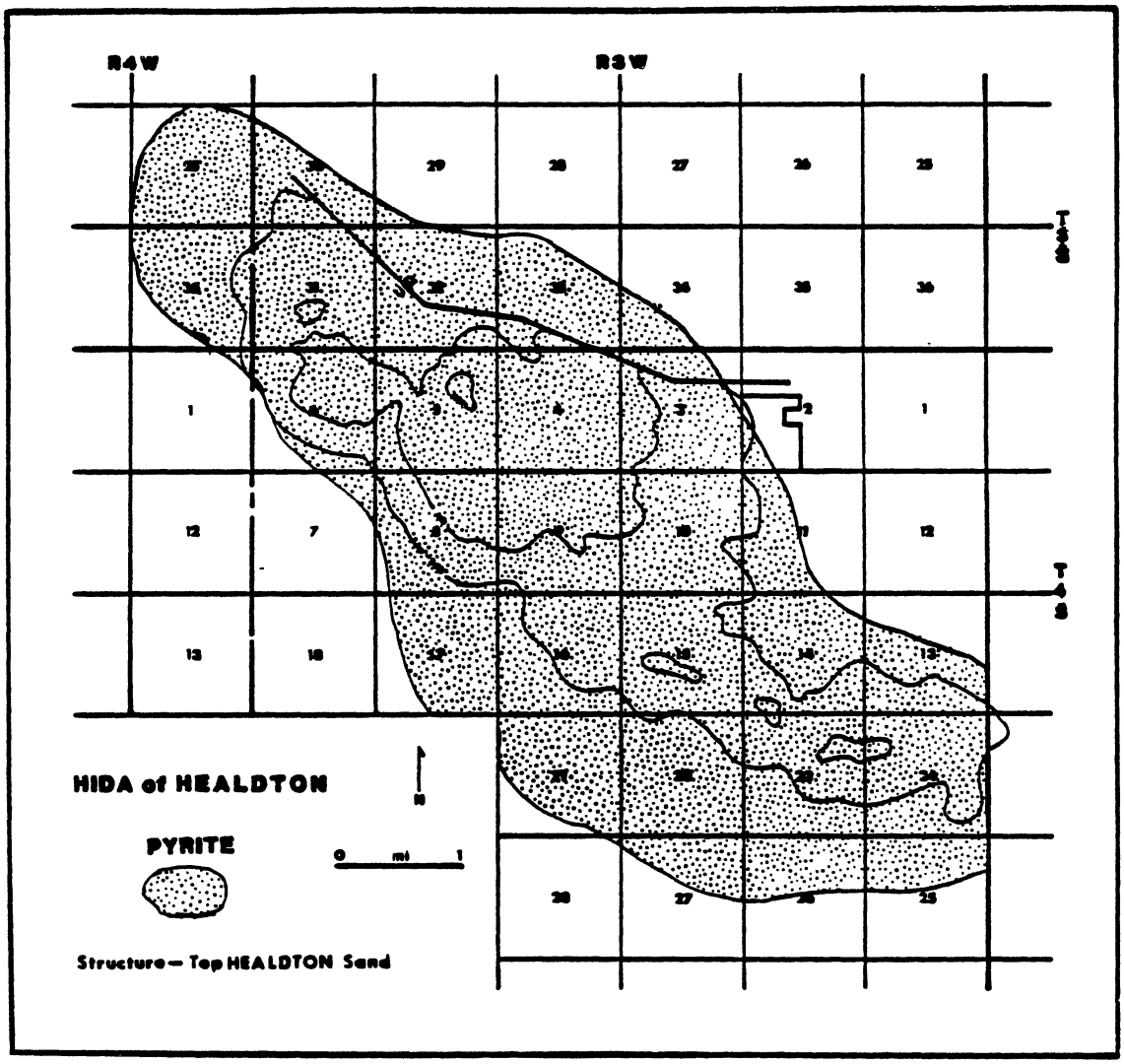

Figure 20.--Healdton: subsurface limits of pyritization (structure after Latham, 1970).

by the subsurface structure.

Carter-Knox Oil Field

The Carter-Knox topography is characterized by sandy hills formed by erosion of the outcropping Chickasha-Duncan sandstone. The structure of the field is characterized by two normal faults in the Permian that parallel deeper thrust faults in the Pennsylvanian. Figure 21 indicates that the movement in Carter-Knox was more vertical than horizontal. The surface alteration (Figure 22) trends in the same direction as the anticlinal structure. Carbonate mineralization coincides with the faults and the axis of the structure. The bleached sandstone is found on the outer edge of zone 1. Pyrite cement in the field is observed primarily in zone 1. Pyritization in the subsurface of Carter-Knox is extensive and occurs along the structural trends (Figure 23).

Well Log Characteristics

Diagenetic aureoles exhibit characteristic well log signatures. Both the resistivity curve and the spontaneous potential curve show signs of the diagenetic carbonate-cemented sandstones. The resistivity curve can be an aid in determining the limits of the HIDA. Because carbonate is nonconductive, the resistivity increases in carbonate-cemented sandstones. The carbonate mineralization reduces porosity and permeability. The spontaneous potential curve

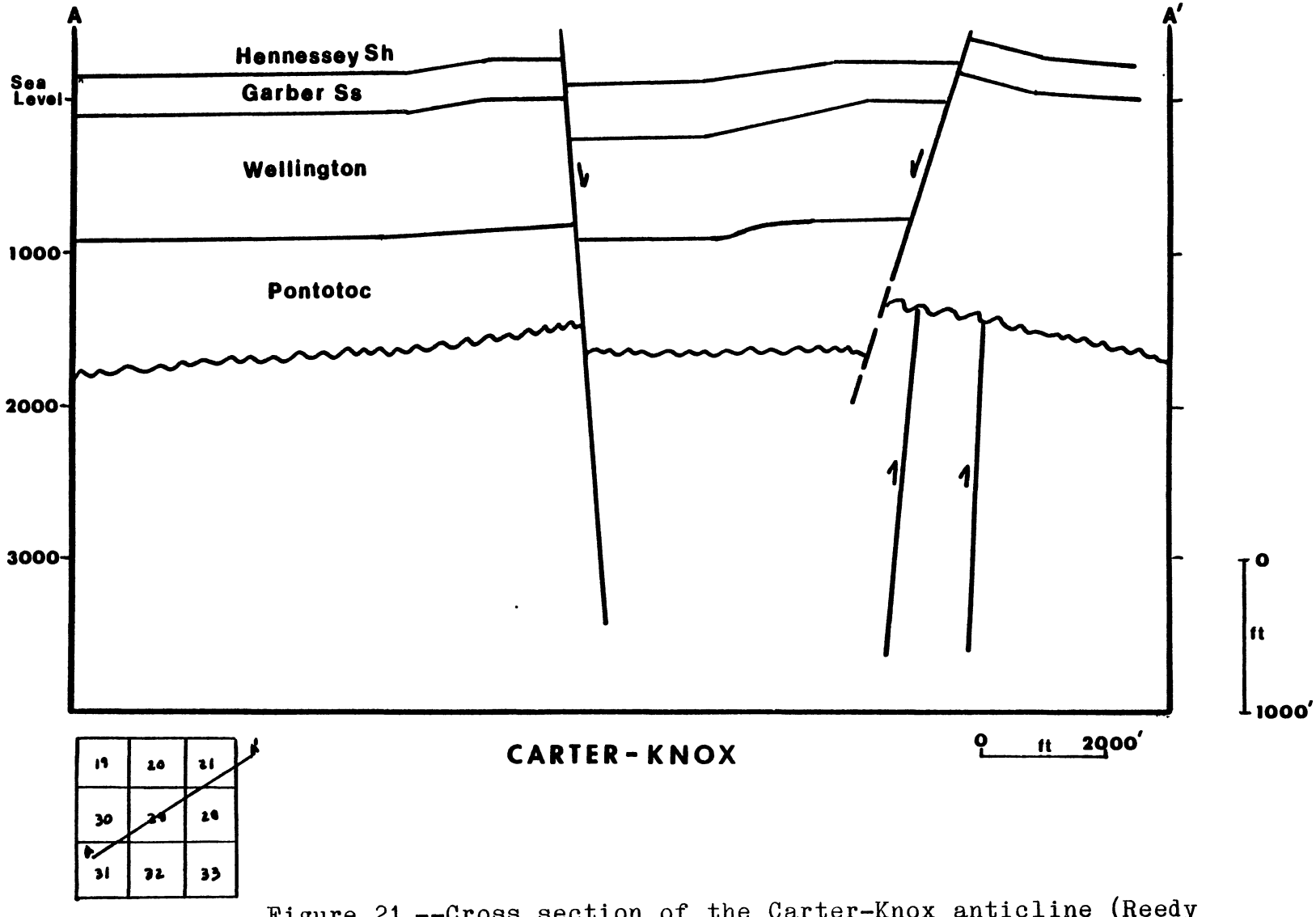

Figure 21.--Cross section of the Carter-Knox anticline (Reedy and Sykes, 1959).

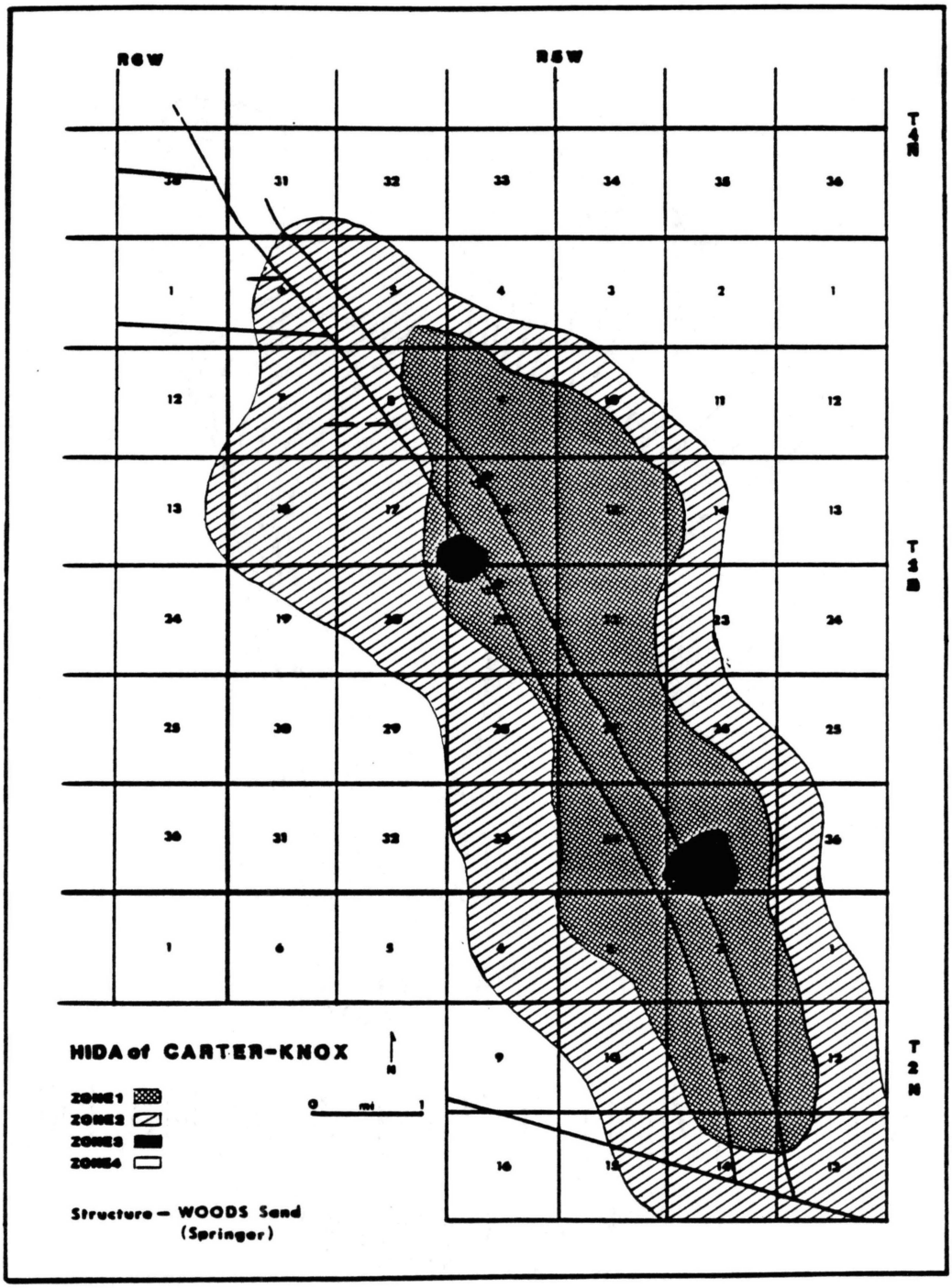

Figure 22.--Carter-Knox: surface map of diagenetic zones (structure after Reedy and Sykes, 1959).

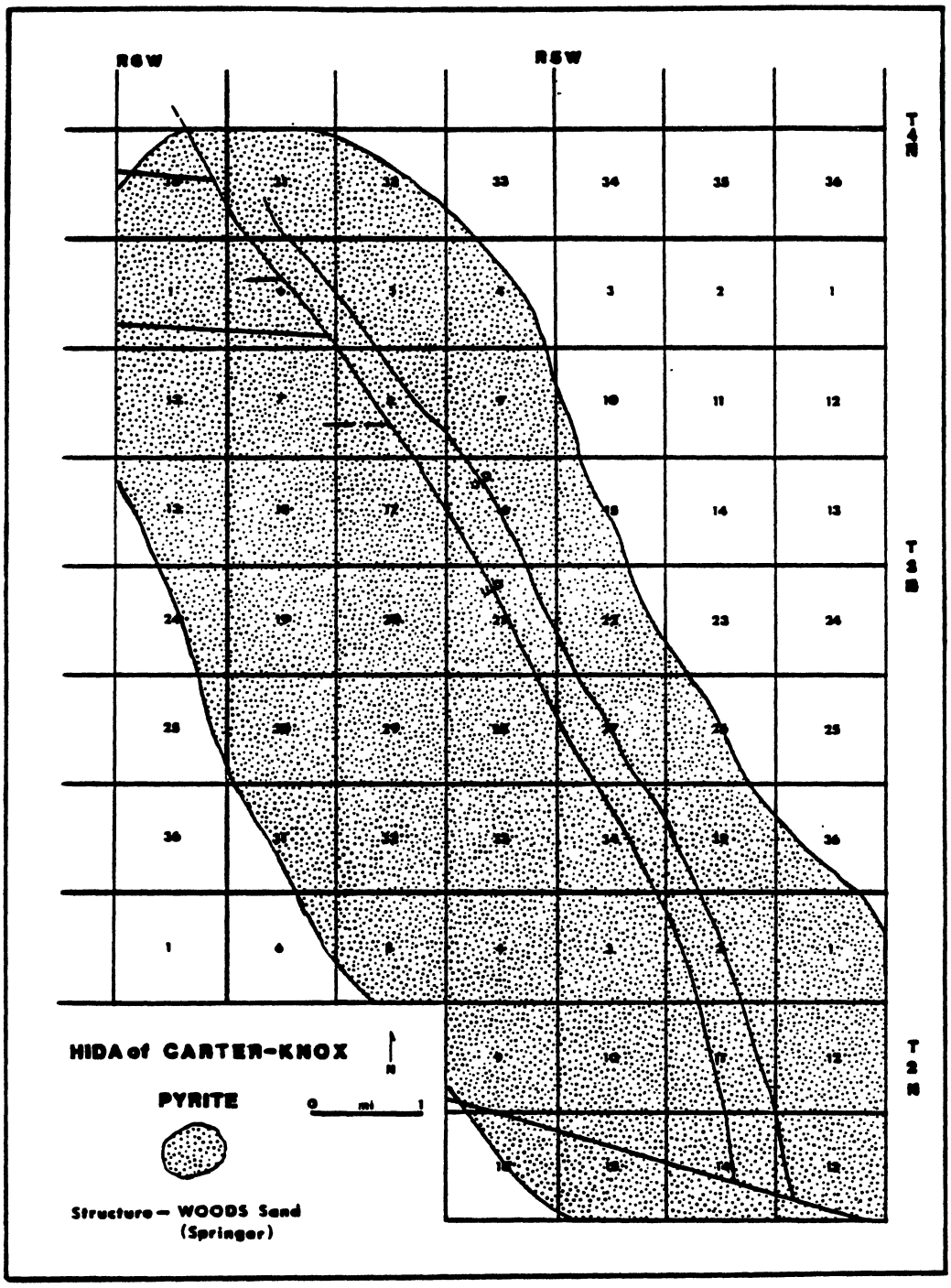

Figure 23.--Carter-Knox: subsurface limits of pyritization (structure after Reedy and Sykes, 1959).

suppresses in response to the mineralization. Composite logs were constructed for demonstration of the effects of diagenetic carbonate on these curves. Figure 24 represents the logs that show the typical behavior of the resistivity and SP curves both outside and inside the limits of the HIDA in the Healdton field. The Permian-Pennsylvanian contact of the well logs was determined by correlating to well logs used in a subsurface study by Wilkinson (1955). The logs in Appendix A show a general increase in carbonate concentration towards the axis of the structure and the subsurface fault planes. The effects of the diagenetic carbonate can be seen on the log signatures. Lilburn (1981) has shown this for the Cement field as well.

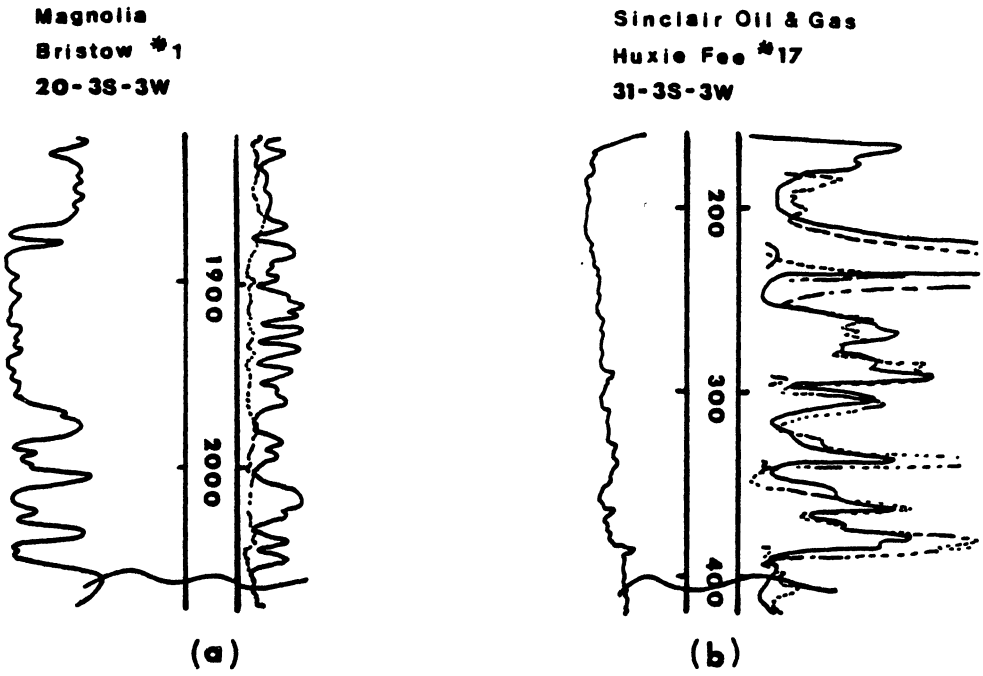

Figure 24.—(a) Resistivity log signature outside the HIDA limit. (b) Resistivity log signature inside the HIDA limit.

CHAPTER IV

PETROGRAPHY AND DIAGENESIS OF THE HIDA STRATA

The petrography and diagenesis of Permian rocks in the project area were investigated using a variety of techniques. Identification of the lithology and diagenetic constituents was based on thin section and x-ray diffraction analysis, SEM coupled with EDXA, and cathodoluminescence. The lithologies range from sandstones to siltstones to shales. In areas outside the aureole limit, the aforementioned lithologies are maroon to red to dark-orange in color. Within the HIDA limits, the sandstones and siltstones are buff to white to gray while the shales are usually green to gray in color. The majority of the sandstones classified as sublitharenites, although a few samples are litharenites and quartzarenites (Figure 25).

Detrital Constituents

Quartz, rock fragments and feldspars make up the basic detrital constituents of the sandstones. Of the three constituents, quartz is the most abundant averaging 53% of the total rock. Quartz grains consists of both monocrystalline and polycrystalline types. They typically are

Q-F-R DIAGRAM

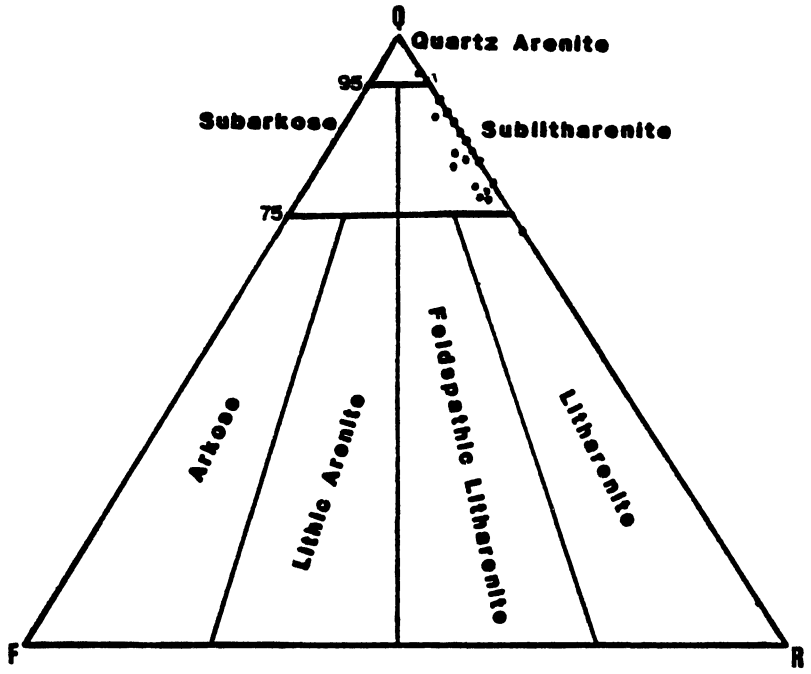

Figure 25.--QFR Diagram.

subangular to subrounded and range in grain size from very fine to medium grained sand. The quartz grains are etched in samples with extensive diagenetic mineralization.

Rock fragments are second in abundance averaging 10% with a grain size of fine sand. These include recrystallized metaquartzite and phyllite fragments with minor occurrences of chert fragments. Because rock fragments in the samples are metastable, they are easily dissolved and replaced by diagenetic cements.

Feldspars occur in minor quantities in the samples with maximum concentrations of 2% of the total rock composition. Plagioclase is the most prominent, but microcline and orthoclase are also present. Figure 26 shows this typical lithology.

Other detrital grains consist of minor occurrences of muscovite, biotite, and zircon. These constituents were only a trace of the original framework.

Diagenetic Constituents

Migrating pore fluids have a definite influence on the diagenesis in these sandstones. The chemistry of the fluids is the major determinant in the type of authigenic precipitants.

Diagenetic constituents of the redbeds include hematite cement, extensive carbonate and pyrite cements, authigenic clays, and silica cements.

The hematite cement gives the Permian strata their

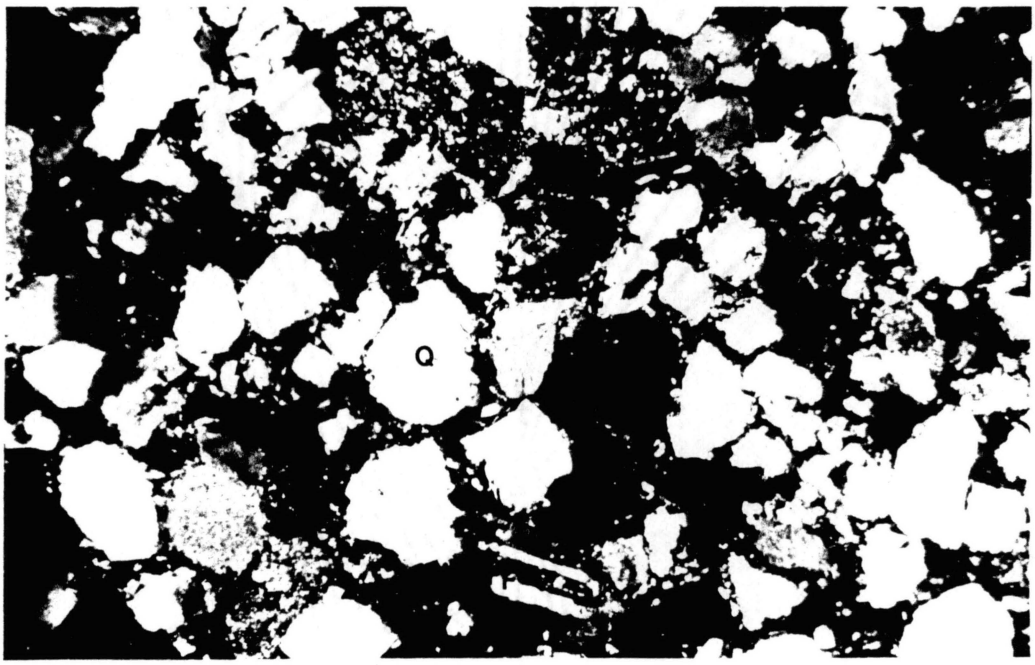

Figure 26.--Photomicrograph of general lithology (Q-quartz, F-feldspar, R-rock fragment, 100X, CN).

trademark (red coloration). Two stages of hematite mineralization were observed in the HIDA strata. The first stage formed shortly after the deposition where grains of the unaltered sandstones were coated by the hematite cement (Figure 27). The late stage of hematite mineralization is the result of oxidation of pyrite cement. This hematite occurs as authigenic platelet coatings (Figure 28).

Carbonates are the most important and widespread cement in the oil fields investigated. Calcite is the most abundant carbonate while varieties of ferroan and manganese-rich calcites and dolomites also occur in the altered strata. Rhodocrosite forms as nodules and rosettes having the botryoidal texture as seen in Figure 29. Ferroan-manganesian dolomite (Figure 30 and 31) was identified by SEM and x-ray analysis. Commonly, in hematite-rich samples, iron-rich dolomite is present (Figure 32). In these samples, hematite is often incorporated into the rhomb as impurities outlining overgrowths. Samples abundant in ferrous iron but poor in magnesium, usually form as ferroan calcite. In areas where the iron concentration is low, calcite is the dominant carbonate.

Quartz grains and their overgrowths and rock fragments show corrosion features and are partially dissolved in areas dominated by carbonate mineralization. Poikilotopic texture is very common and usually formed as carbonate cement replaced and displaced original grains (Figure 33). Pseudomorphous replacement of authigenic constituents

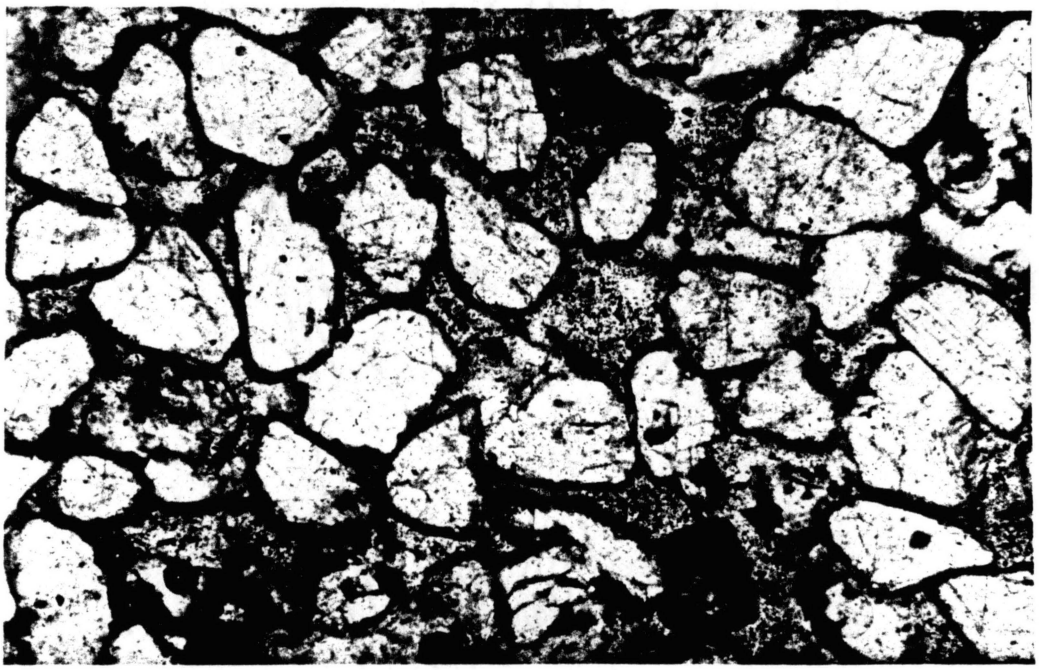

Figure 27.--Photomicrograph of unaltered redbed (200X, PP)

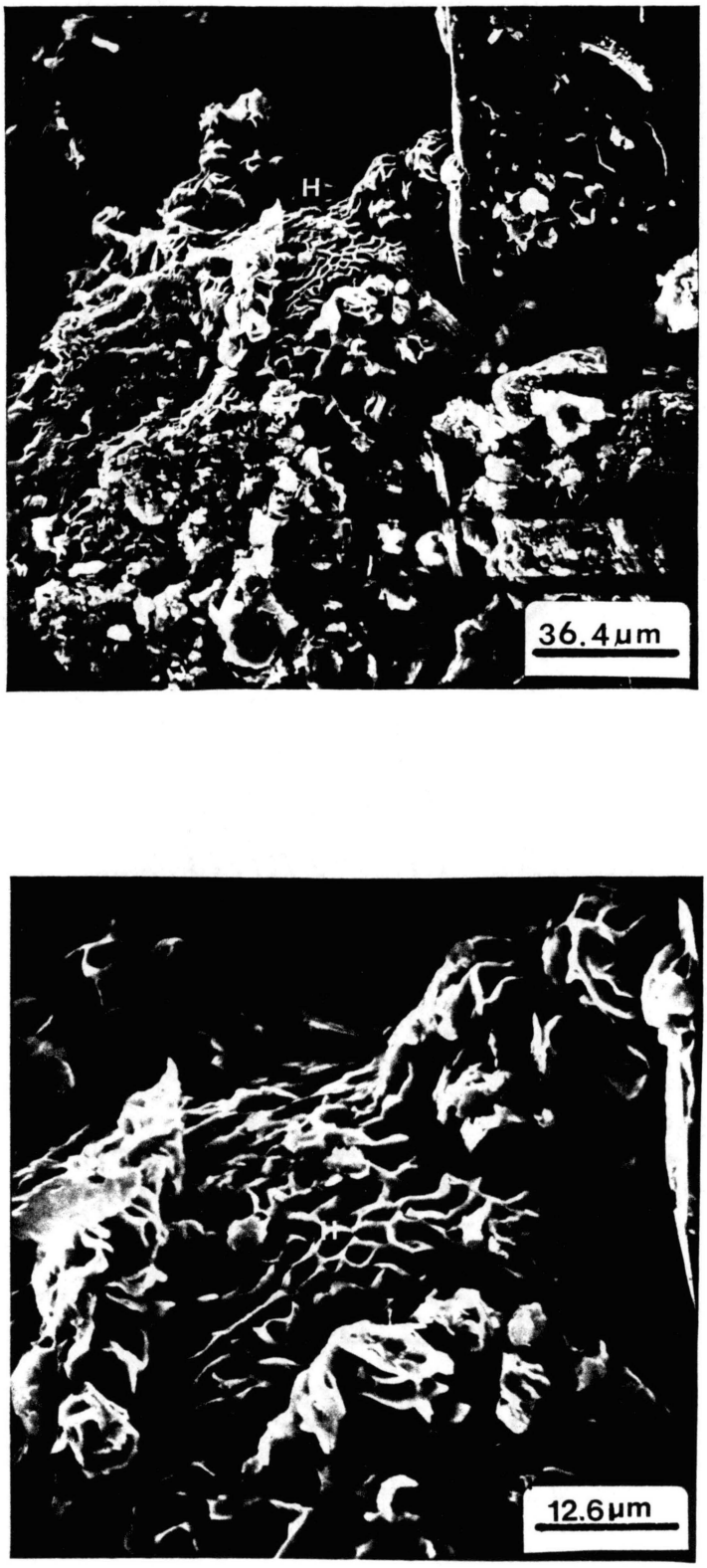

Figure 28.--SEM photomicrographs of hematite.

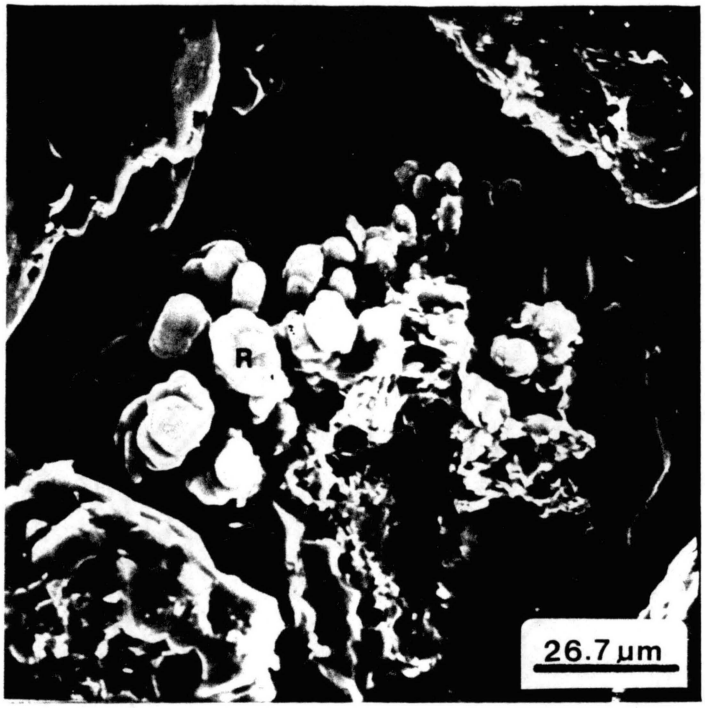

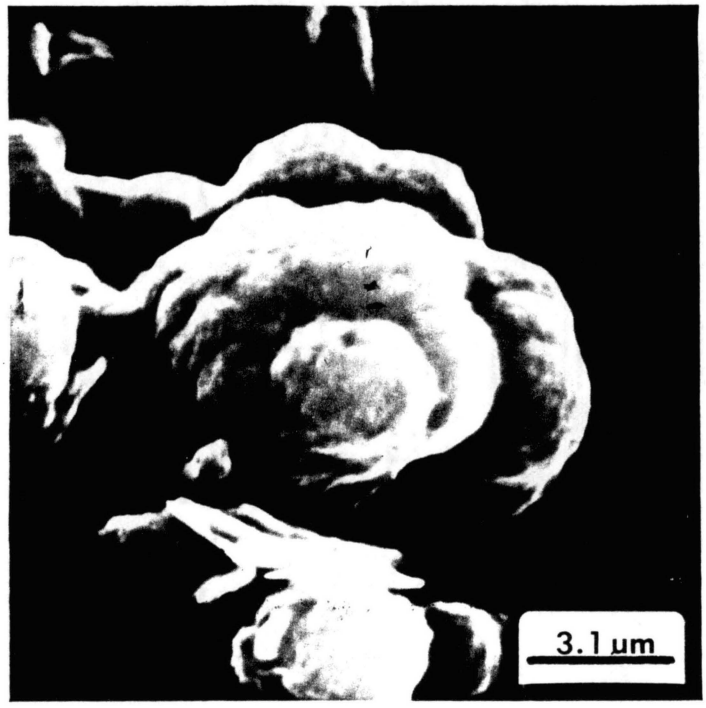

Figure 29.--SEM photomicrographs of rhodocrosite.

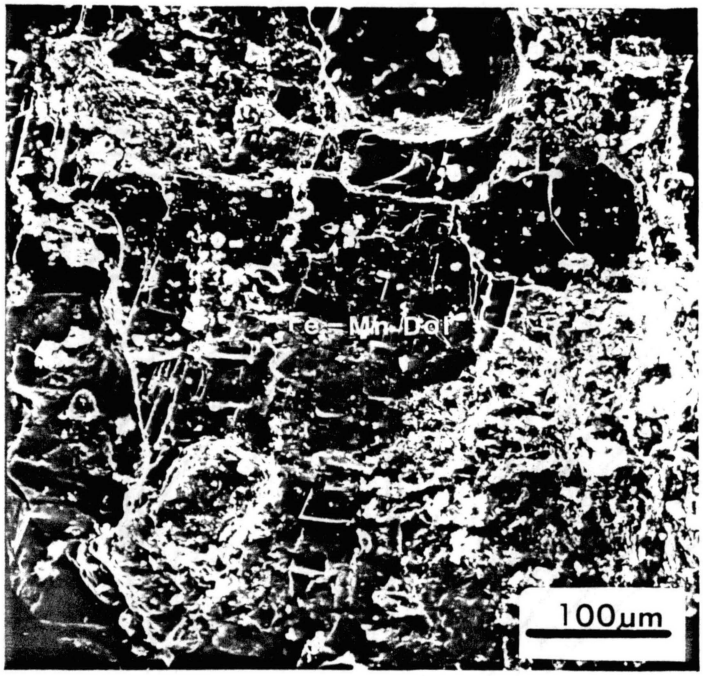

Figure 30.--SEM photomicrograph of Fe-Mn Dolomite.

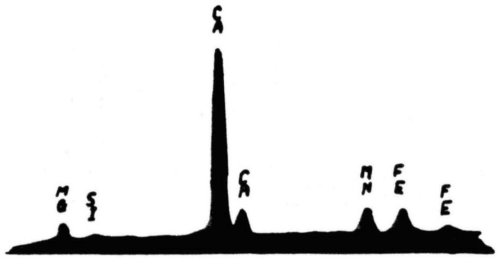

Figure 31.--EDXA spectrum of the Fe-Mn Dolomite.

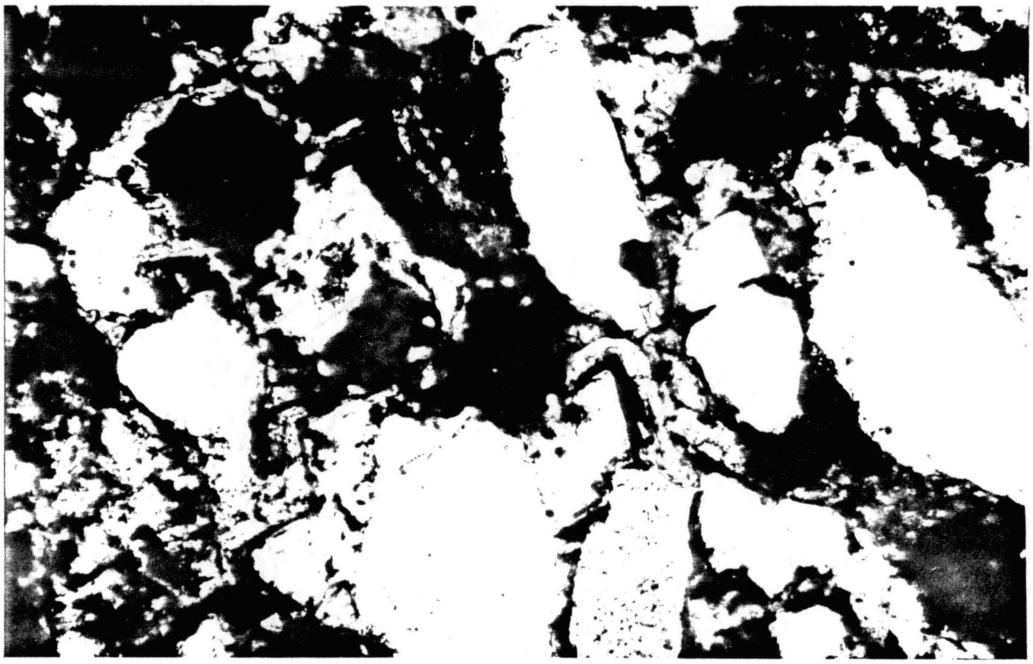

Figure 32.--Photomicrographs of iron-rich dolomites (200X, CN).

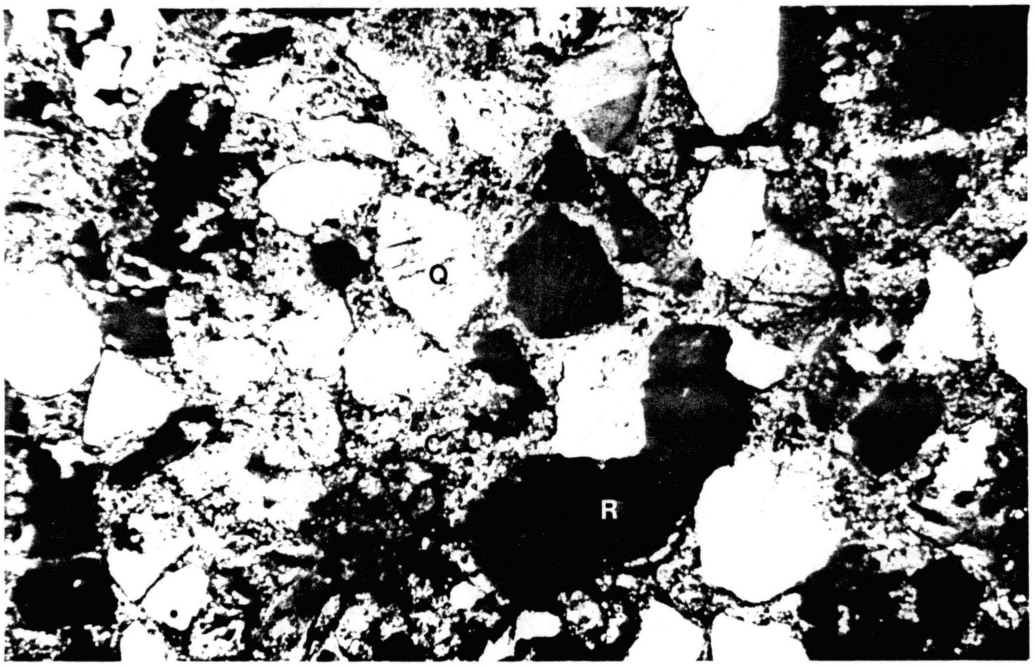

Figure 33.--Photomicrograph of poikilotopic texture (100X, CN)

such as kaolinite by calcite is very common (Figure 34). Diagenetic limestone is the final product when rock constituents are completely replaced. Figure 35 shows the relationship between carbonate cement and quartz. This graph shows clearly that an increase in carbonate cement results in a decrease in quartz content.

Pyrite cement (Figure 36) is abundant in the Permian strata that overlie the hydrocarbon productive areas. The sulfide occurs as a cement (Figure 37). Upon oxidation, pyrite changes to hematite. Reflective microscopy reveals remnants of pyrite in the hematite cement suggesting that the original cement was pyrite. In hand specimens, the weathered redbed samples are friable whereas the hematite altered from pyrite occurs as a resistive cement. Other sulfides such as galena, sphalerite, marcasite and pyrrhotite may be present with the pyrite (Figure 38).

Authigenic clays are present in both the altered and unaltered sandstones. The majority of the illite identified is probably associated with the redbeds and is most likely detrital; however, diagenetic illite is found outlining the pore spaces where hematite has dissolved. Kaolinite is the most common clay in these rocks. Two stages of kaolinite are associated with the samples. The early stage forms large booklets as long as .1mm (Figure 39). Figure 40 is an SEM photomicrograph of early kaolinite etched and partially dissolved. The later stage of kaolinite is a precipitate in pore spaces created by the

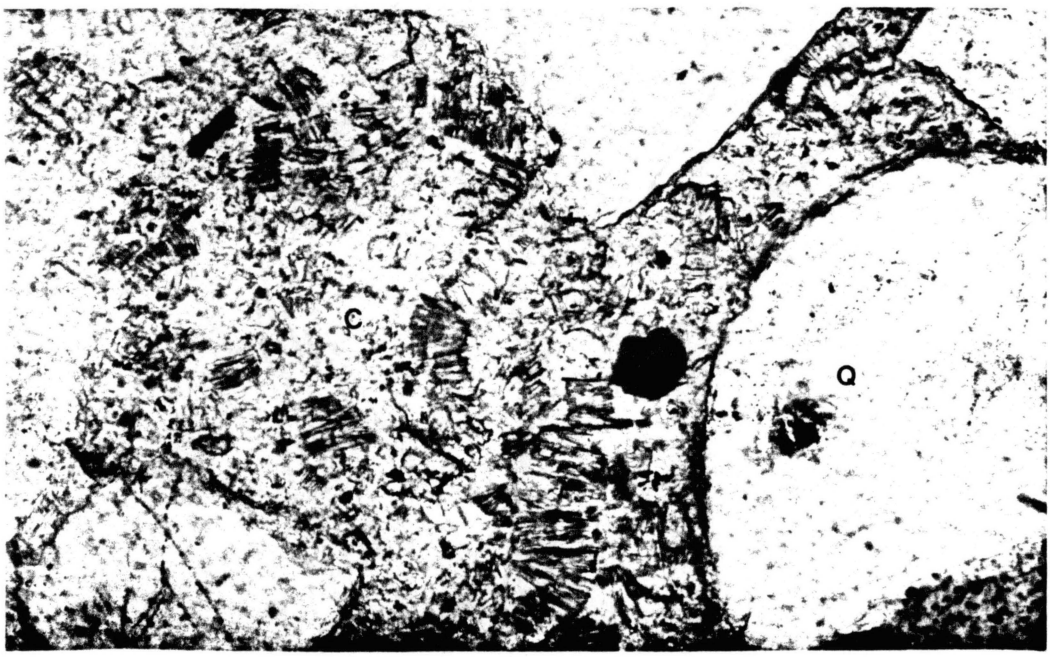

Figure 34.--Photomicrograph of pseudomorphsis replacement of kaolinite by carbonate (400X, PP).

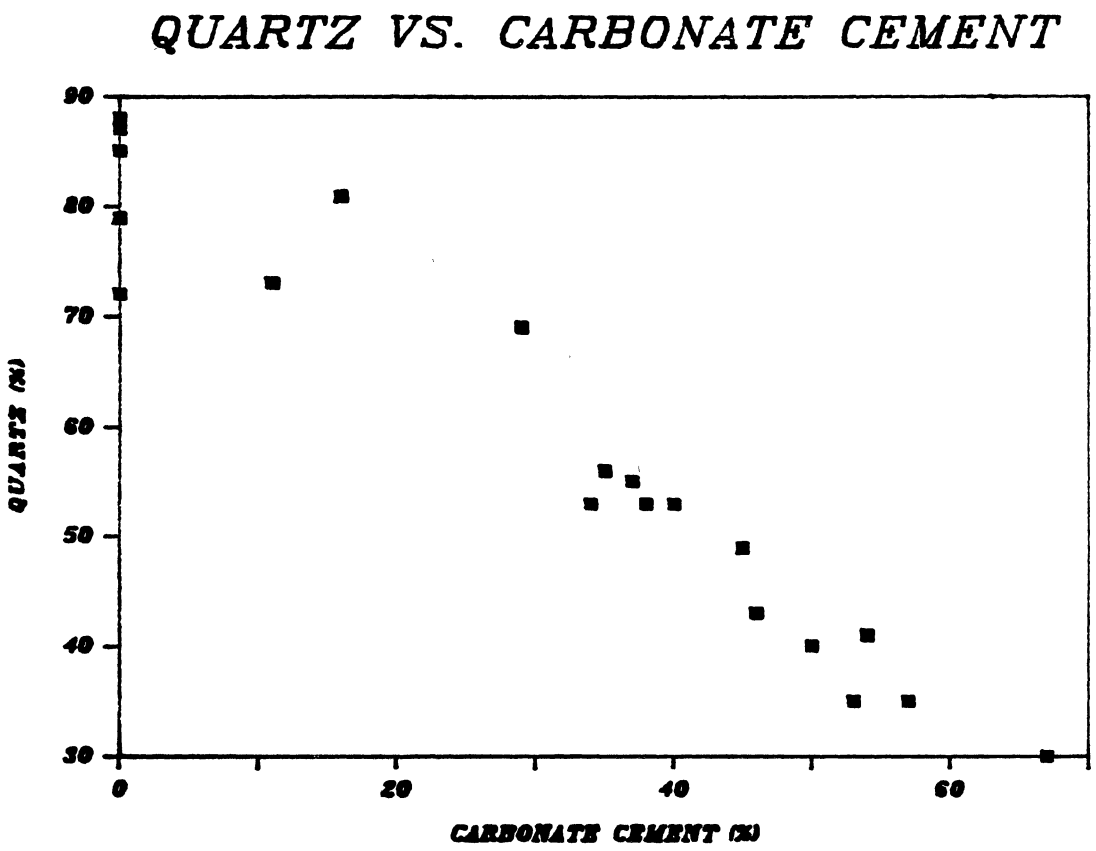

Figure 35.--Graph of quartz and and carbonate percentages determined from thin section.

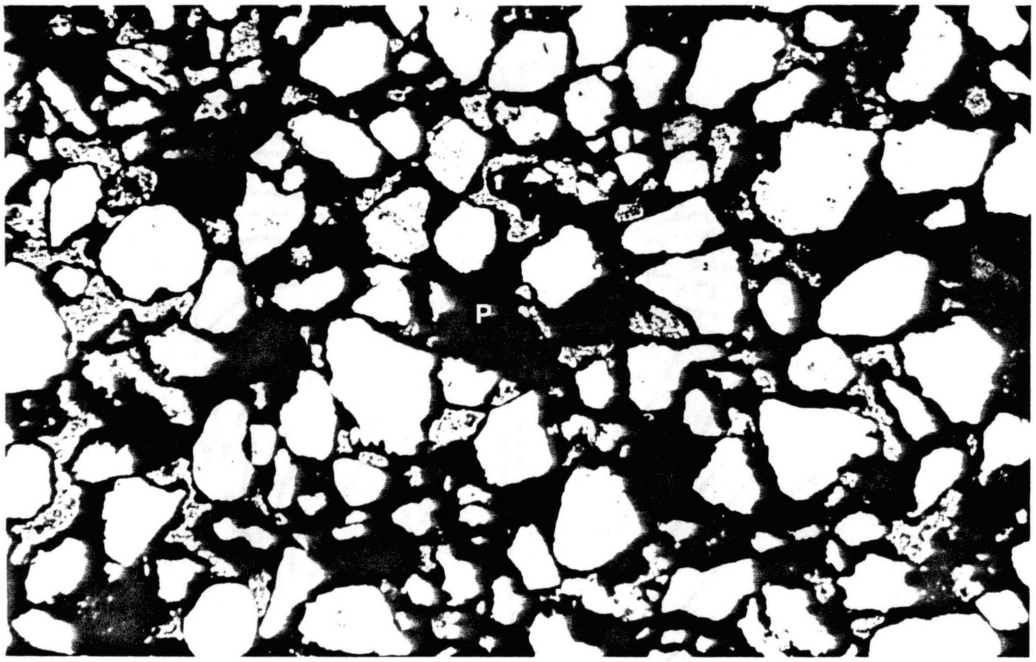

Figure 36.--Photomicrograph showing the extent of pyritization in the sandstones (100X, PP).

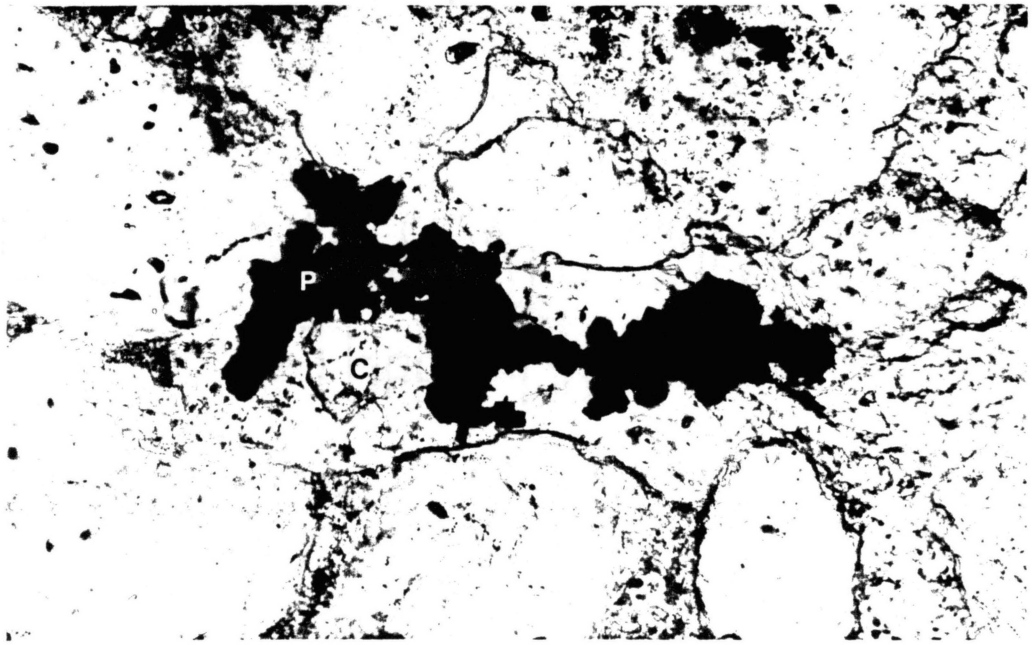

Figure 37.--Photomicrograph of pyrite cement in carbonate cement (400X, PP).

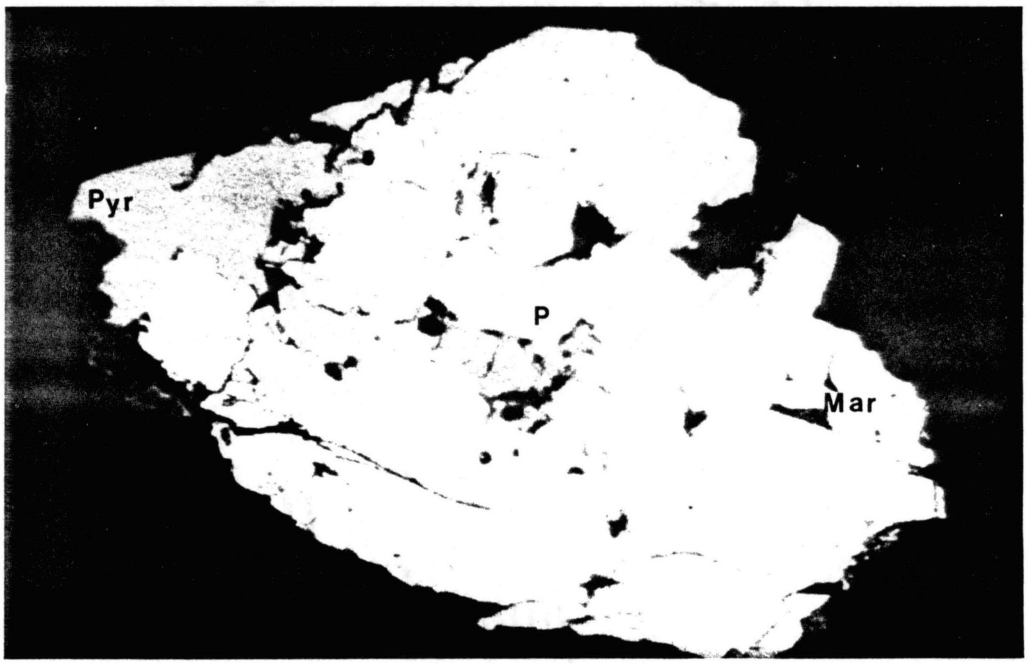

Figure 38.--Photomicrograph of pyrite, marcasite, and pyrrhotite (photo by Reynolds, 1985).

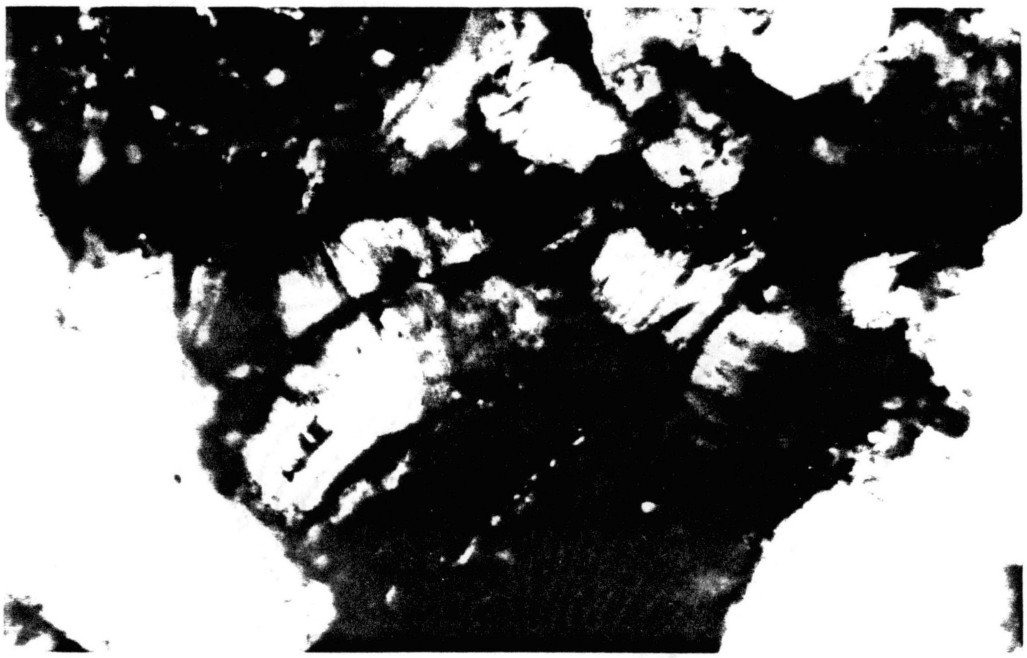

Figure 39.--Photomicrograph of kaolinite (400X, CN).

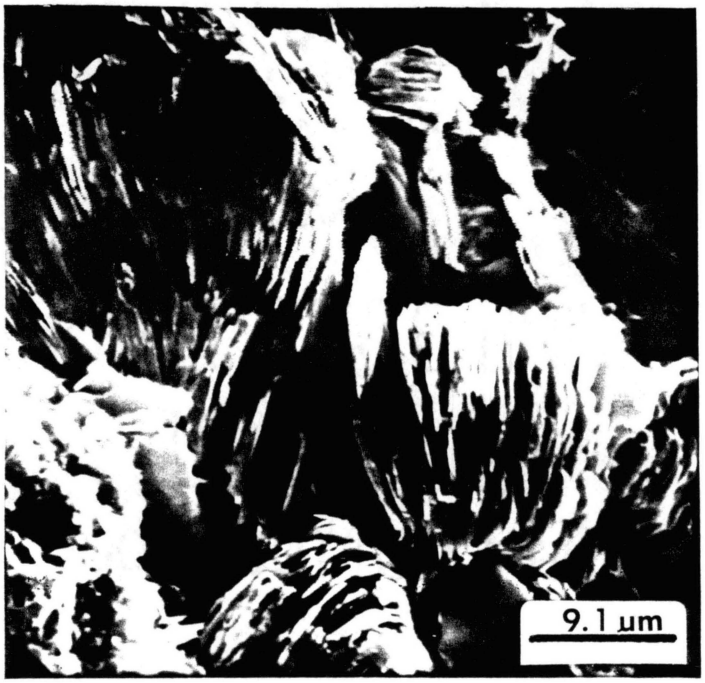

Figure 40.--SEM photomicrograph of partially dissolved kaolinite.

dissolution of carbonate. These booklets are much smaller than those of the earlier stage of kaolinite precipitation. Smectite-illite mixed layered clay was identified by SEM and x-ray analysis (Figure 41). Figure 42 is a photomicrograph showing smectite-illite mixed layered clay. Chlorite was found in a few samples in trace amounts.

Silica overgrowths, silica cement, and chalcedony are early diagenetic events associated with the redbeds. Figure 43 shows a quartz overgrowth separated from the detrital grain by a dust rim of hematite. Figure 44 represents early chalcedony with its characteristic radial morphology filling pore spaces.

Porosity Development

Several porosity types occur within the sandstones. Because primary porosity was destroyed by early hematite cement, the porosity is secondary, generated by the dissolution of authigenic cements and detrital constituents. Types of secondary porosity include intergranular, intracement, intragranular, and microporosity.

Intergranular porosity was produced by the dissolution of authigenic cements and detrital rock fragments. Likewise, intracement porosity was the result of the incomplete removal of the authigenic cements and the dissolution of detrital grains. Figure 36 shows an example of intracement porosity in the partial dissolution of pyrite cement. The partial dissolution of hematite and carbonate

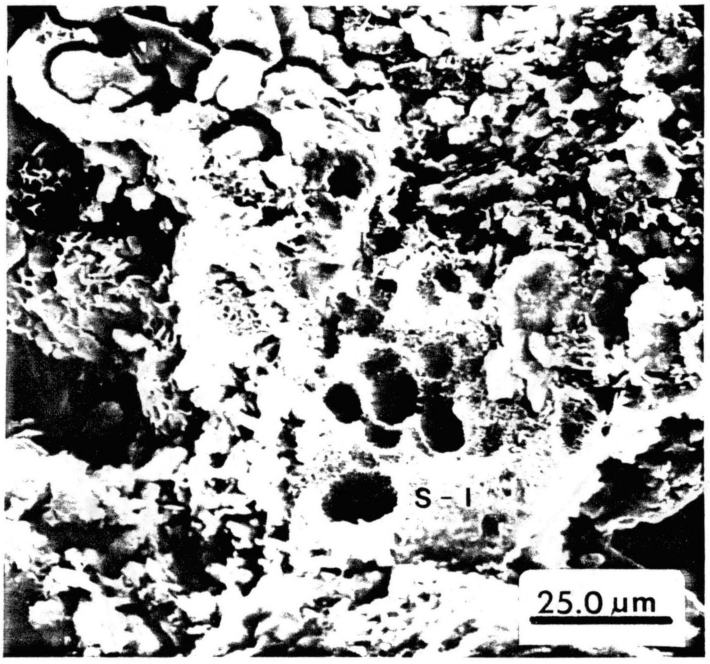

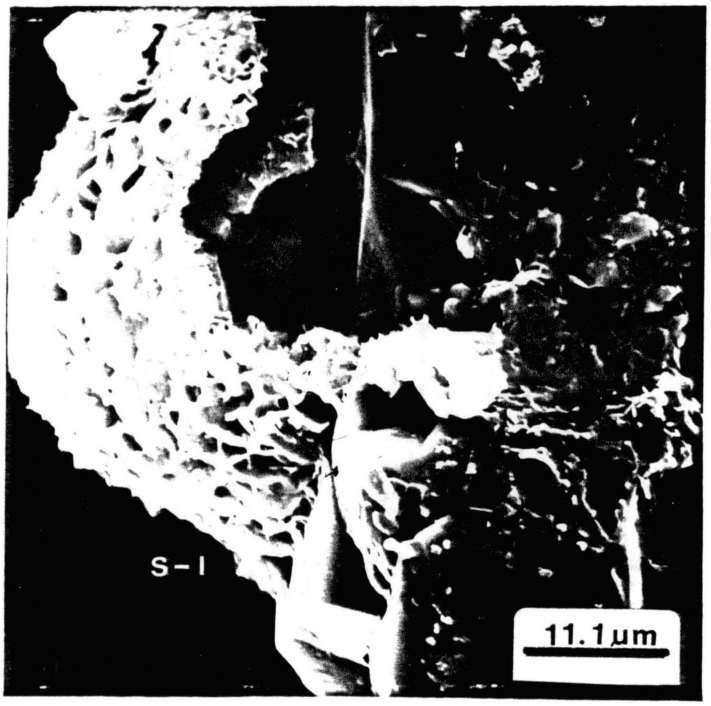

Figure 41.--SEM Photomicrographs of smectite-illite mixed layered clay.

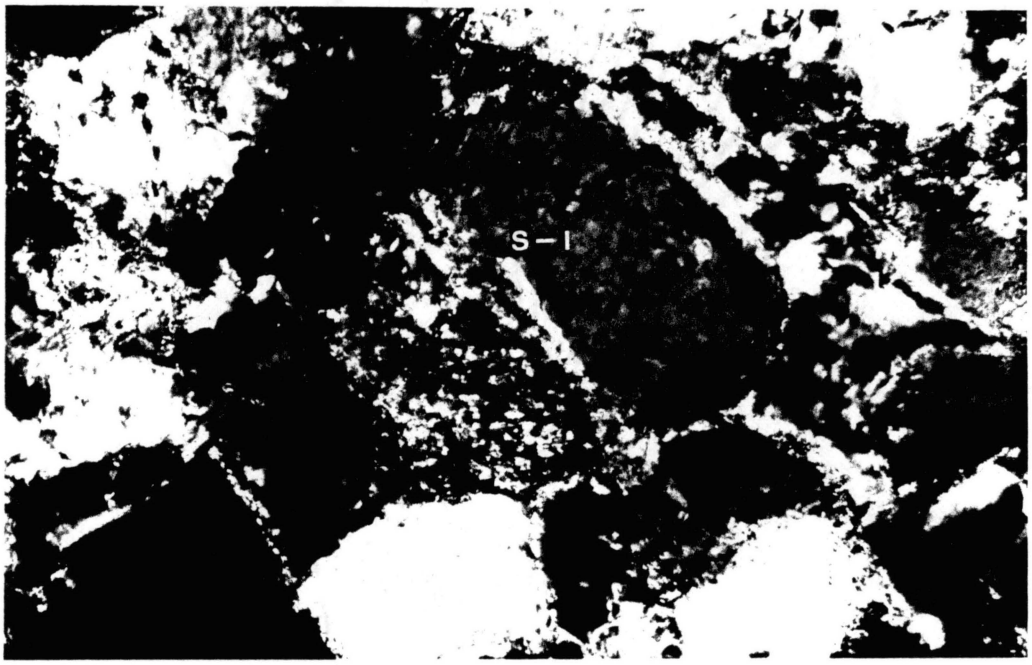

Figure 42.--Photomicrograph of smectite-illite mixed layered clay (400X, PP).

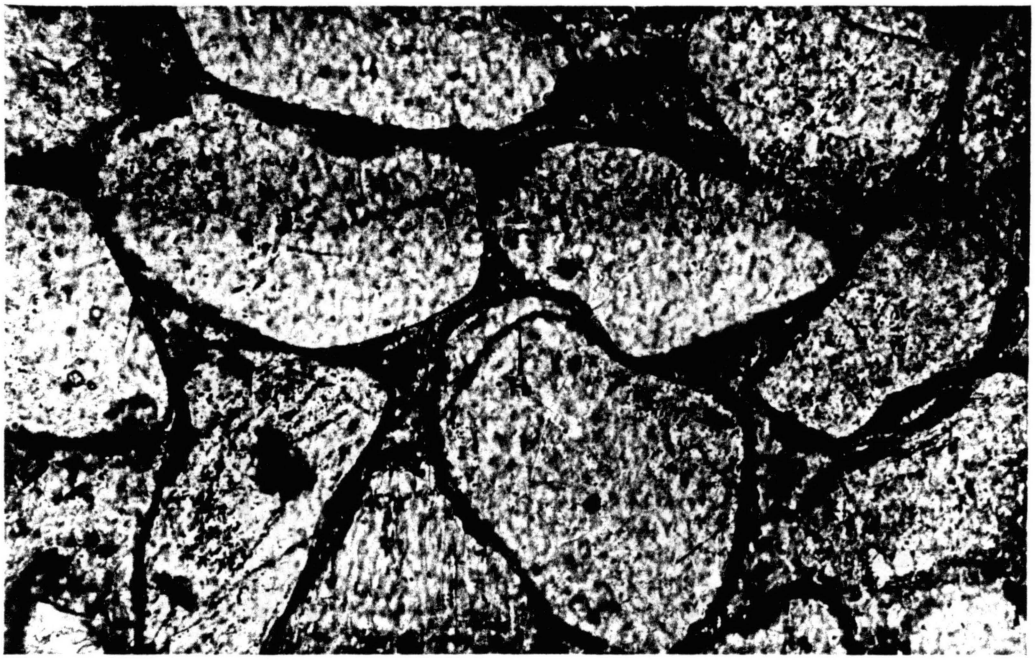

Figure 43.--Photomicrograph showing a quartz overgrowth and hematite dust rim (400X, PP).

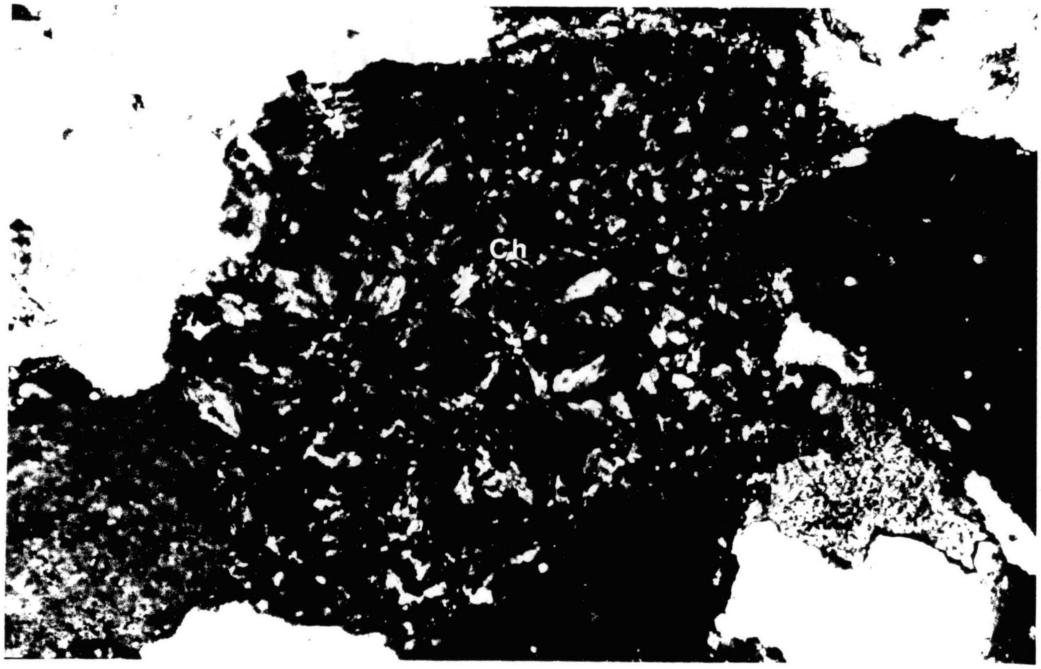

Figure 44.--Photomicrograph of chalcedony (400X, CN).

cement also account for intracement porosity (Figure 45). Intracement porosity is by far the most prominent in the samples. Minor amounts of intragranular porosity formed by partial dissolution of feldspar grains. Microporosity occurs between the booklets of kaolinite.

Porosity in the samples ranges from a trace to 30%. The porosity in the carbonate cemented samples averages 6% while the porosity in the other samples averages 15% to 18%. Carbonate precipitation and dissolution are definite factors in the presence of secondary porosity. Extensive carbonate precipitation destroys the porosity and permeability. The relationship between carbonate cemente and porosity is shown in Figure 46. Generally, an increase in carbonate cement results in a decrease in porosity.

Paragenesis of the Diagenetic Events

The diagenetic history for the samples is complex due to the constant changing of the geochemistry of pore fluids. Figure 47 is the paragenetic history of the sandstones studied. The precipitation of hematite cement initiated the diagenesis of the redbeds. Subsequent dissolution of the cement resulted in the formation of intergranular and intracement porosity evidenced by the successive precipitation of silica overgrowths, silica cement, and chalcedony.

The introduction of hydrocarbon products drastically changed the geochemical environment. This change was

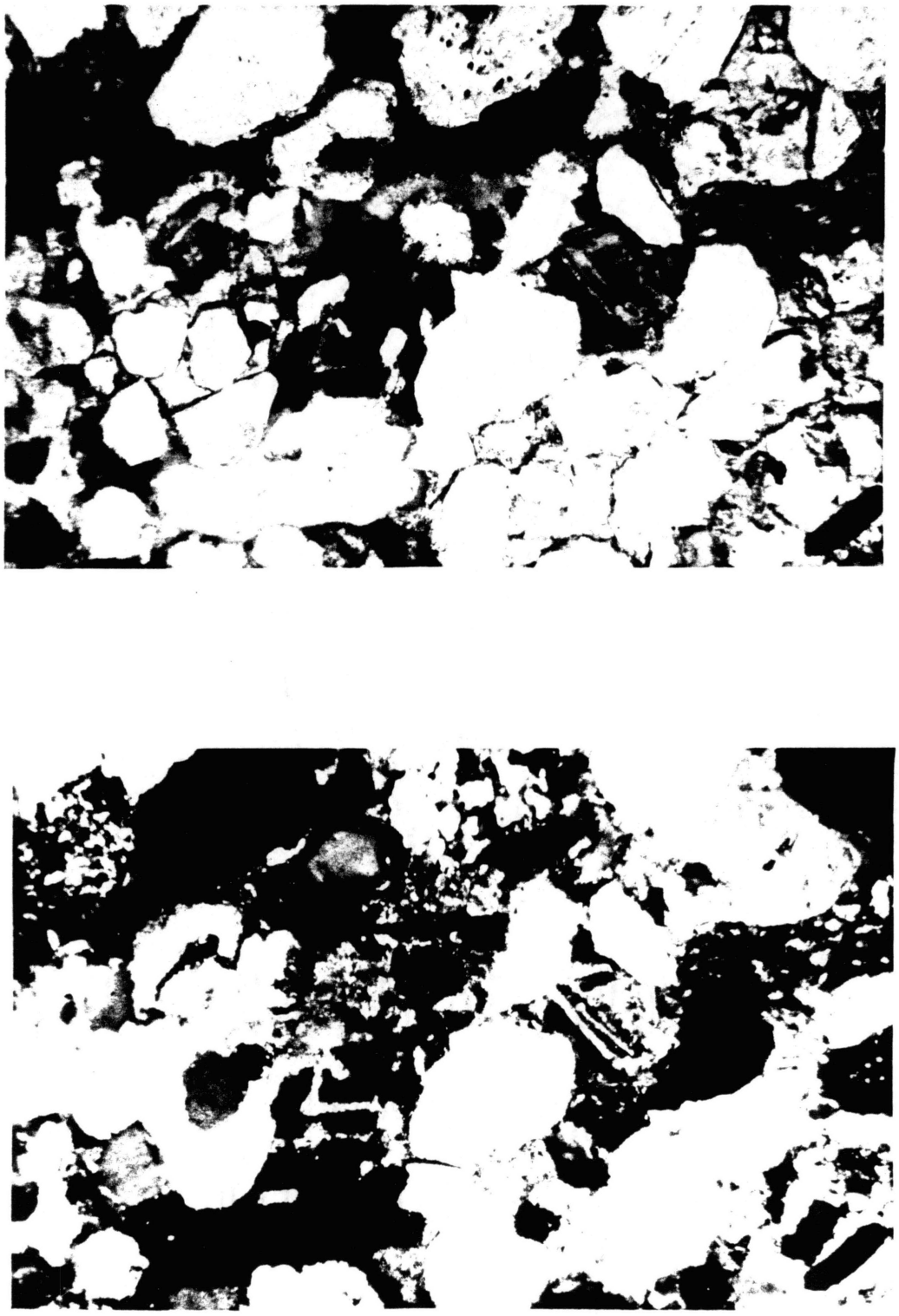

Figure 45.--Photomicrographs of dissolution of hematite in the dolomite rhombs (200X, upper-PP, lower-CN).

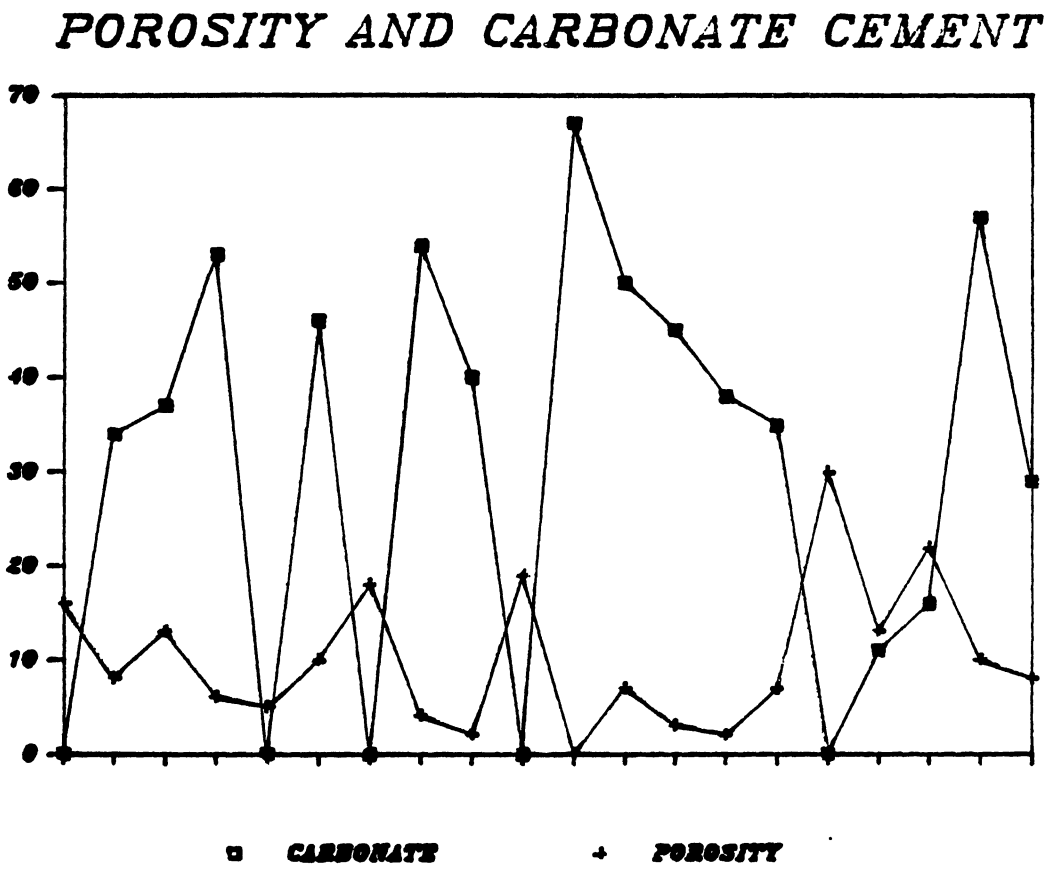

Figure 46.—Graph of porosity and carbonate percentages determined from thin section.

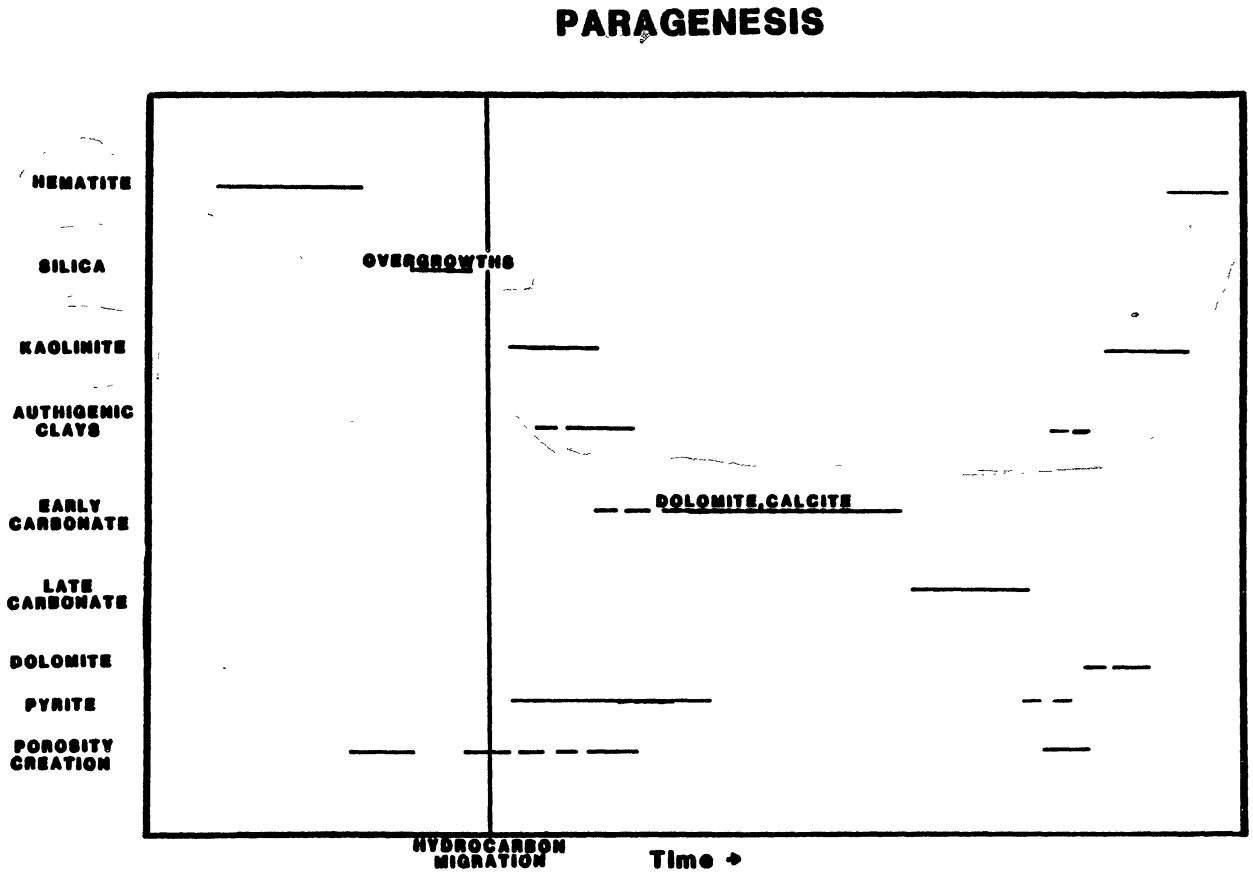

Figure 47.--Paragenetic sequence.

responsible for the onset of the new diagenetic products. Reduction of the hematite by associated hydrocarbon products provided iron to precipitate as pyrite. Pyrite formation was early in the paragenesis evidenced by pyrite lining grain boundaries and by the presence of pyrite in slightly altered redbeds. Authigenic clays such as kaolinite and mixed-layered smectite/illite are also associated with the alteration of the redbeds. These clays are found in both the slightly altered, red sandstones and in the altered, bleached sandstones.

Carbonate cementation replaced and displaced the diagenetic and the detrital constituents. Figure 48 is a photomicrograph illustrating the displacement of pyrite by dolomite cement. The earliest carbonates that were observed in the samples were rhodocrosite, found as the initial carbonate in a bleached sample, and manganese-rich dolomite, observed in the early stages of carbonate mineralization. Most likely, varieties of ferroan calcite and ferroan dolomites were formed as early carbonate cements. The source of the iron was probably iron released during reduction of hematite. Often, rhombohedral carbonates have impurities such as overgrowths of hematite or pyrite enclosed in the crystal. The incorporation of hematite indicates different rates of crystal growth. Zones containing hematite indicate a faster rate of crystal growth than those rhombs void of hematite (Figures 48 and 49).

Figure 48.--Photomicrograph showing dolomite displacement of pyrite (400X, CN).

Figure 49.--Photomicrograph of dolomite rhombs enclosing oxidized pyrite, hematite (200X, CN).

Carbonate cementation continued to occur resulting in a later, more extensive stage of carbonate mineralization. This stage resulted in the purification the early carbonate minerals and further replacement of quartz and rock fragments until the remaining constituents were stable detrital quartz grains. The preferential replacement of metastable rock fragments and feldspars by carbonate produces a diagenetic limestone. As a result, the quartz to feldspar and rock fragment ratio is very large; this sample resulting from diagenetic processes is classified as a quartzarenite in the Folk classification. Quartz grains appeared to be etched much more dramatically than in the earlier stage of mineralization.

The final generation of secondary porosity occurred with the dissolution of carbonate cement. Traces of the cement were left in pore spaces that were being filled by a late stage of kaolinite. The last stage of carbonate precipitation was the initiation of dolomitization evidenced by the appearance of small rhombs in the calcite cement.

Finally, the paragenetic episode went full circle in the last stage of diagenesis with the oxidation of pyrite to hematite which changed the rocks to their original color. Figure 49 represents dolomite rhombs containing the red alteration product of pyrite.

CHAPTER V

GEOCHEMICAL MECHANISMS IN THE FORMATION OF THE HYDROCARBON-INDUCED AUREOLES

Diagenetically altered Permian redbeds show distinct signs of underlying hydrocarbon accumulations. The redbeds overlying the reservoirs have undergone obvious diagenetic and geochemical alterations. Although many diagenetic processes are associated with the formation of the aureoles, the most common products of hydrocarbon inducement are carbonates and sulfides. Carbonate minerals that are associated with the HIDA are calcite, dolomite, ferroan and/or manganese dolomite, and rhodocrosite. Sulfide minerals such as marcasite, pyrite, pyrrhotite, galena, and sphalerite are found in the altered redbeds. The diagenetic aureoles were formed in a complex chemical regime involving organic-inorganic reactions due to the migration of vast amounts of the hydrocarbons, gases, and associated products.

Pore water chemistry is affected by both the maturation and the migration of hydrocarbons. Petroleum is generated from organic matter that has undergone thermal or biological alteration. Maturation of organic matter is a function of time and temperature.

Generally, the transformation of petroleum is viewed as a continual process where the initial organic matter is composed of high-molecular weight compounds such as aromatics and naphthenes. As the transformation progresses, the hydrocarbon product becomes more saturated in low-molecular weight substances (paraffins). During the transformation, methane, carbon dioxide, and hydrogen sulfide gases are liberated (Andreev, et al, 1968). The gases may then migrate upward or lateraly through porous conduits or fault systems to act as catalysts in the diagenesis of new environments producing products not likely to have formed without their presence.

Migration of the oil and gas can produce similar reactions as the transformation of organic matter. Transformation continues to change the composition of the hydrocarbons even during migration. Eventually, migration of the fluids through the permeable reservoir will lead to separation of the oil and gas in certain parts of these rocks. These processes are described in Hunt (1979) and Silverman (1964). Lighter hydrocarbon fractions more easily removed than the heavier fractions. The removal or leakage of the lighter petroleum fraction was mentioned by Donovan (1974) in reference to the Marchand reservoir sand of the Cement field. He noticed that the API gravity of oil over the anticline was 10-18° units heavier than that of other oils in the area. Donovan suggested that partial evaporation of the lighter crude fraction (high API values)

resulted in an enrichment of heavy hydrocarbon fractions (low API values) in the entrapped oil. Donovan's idea can be applied to the Healdton field. The average range of normal API gravity values for the oil of the Healdton reservoir is 32° to 40°. Anomalous areas of concentrated heavy hydrocarbon fractions occur over the Healdton field (Figure 50). The anomalies occur within the aureole limits of the field.

Carbonate System

Methaneand carbon dioxide are liberated from petroleum separation. Decarboxylation results in the release of CO_2 during transformation (Andreev,et al., p.303, 1968):

$$C_nH_{2n+1}\text{----}1\text{--}COOH \rightarrow C_nH_{2n+2} + CO_2.$$

Carbon dioxide is not only liberated during maturation, but the gas is also produced by the oxidation of methane gas:

$$CH_4 + 2O_2 \rightarrow CO_2 + 2H_2O.$$

Carbon dioxide is essential in the formation and dissolution of carbonates. Therefore, carbonate equilibrium is the major system affecting the chemistry of natural waters. In absence of a buffering system, the pH (hydrogen-ion concentration) of the water is generally controlled by carbonate equilibrium. Introduction and removal of carbon dioxide (CO_2) from solutions determines the carbonate species present as shown by the following reactions.

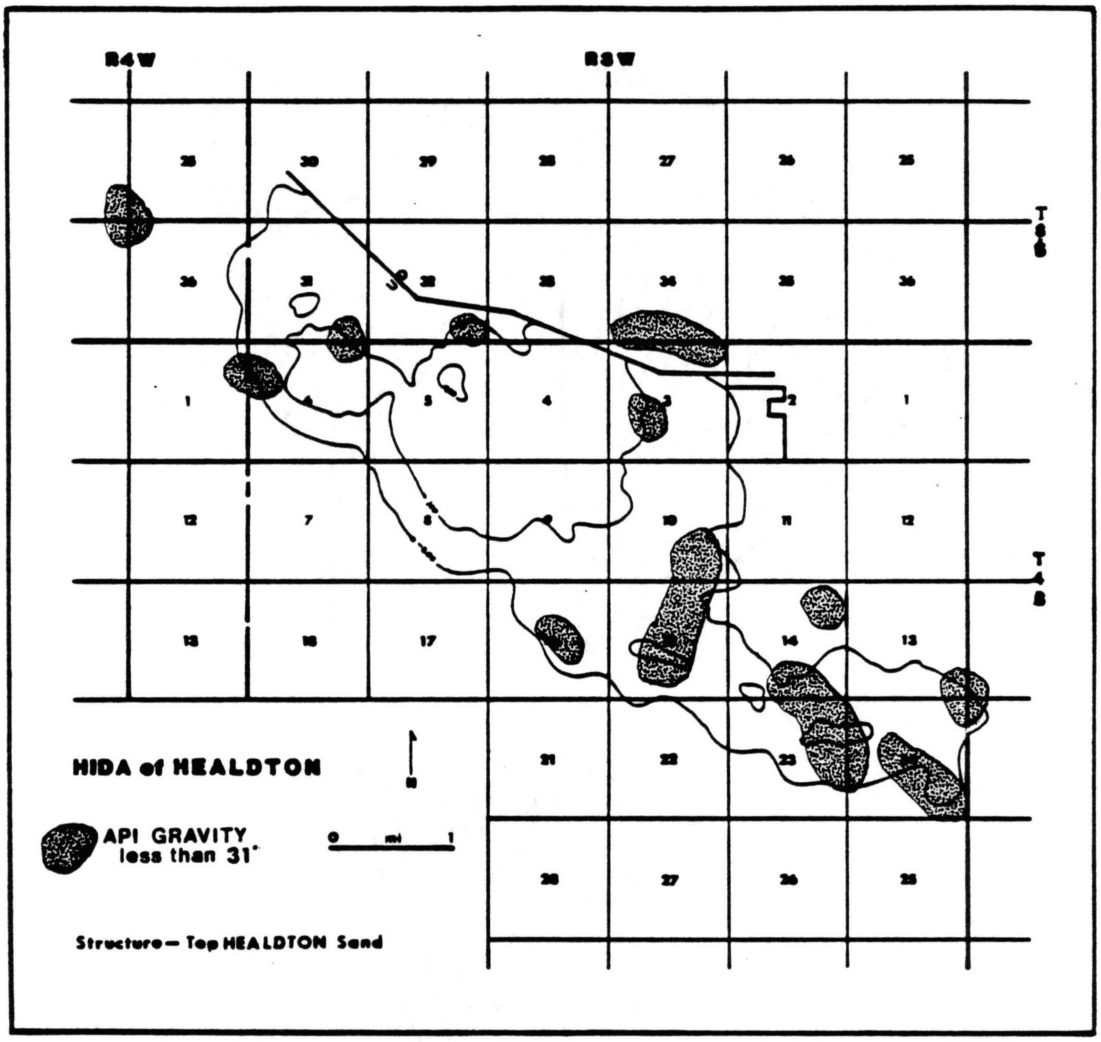

Figure 50.--Anomalous API gravity values of crude oil for the Healdton field.

M represents the available cation:

$$CO_2 + H_2O$$

$$\updownarrow$$

$$MCO_3 + H_2CO_3 \rightleftharpoons M^{++} + 2HCO_3^-.$$

Carbonic acid (H_2CO_3) is produced by the dissolution of carbon dioxide and water. Therefore, if CO_2 is added to the system, carbonic acid will be formed very readily resulting in the dissolution of carbonate. However, if CO_2 is removed, carbonate will precipitate. If CO_2 is introduced in the presence of a buffer such as acetic acid, then the solubility of calcium will decrease (Surdam, et al., 1985).

In areas of the HIDA, ferroan, manganesian, and magnesium-rich carbonates are also observed. Calcium carbonates rich in manganese and iron have been identified. These form according to the following reactions:

$$CaCO_3 + xMn^{++} + yFe^{++} \rightleftharpoons (Ca_{1-x-y}, xMN_x, yFe_y)CO_3 + (x+y)Ca^{++}.$$

Manganese carbonate, rhodocrosite, is observed as early stages of mineralization. Manganese is associated with the iron in the redbeds. Figure 51 shows that the manganese is closely related to the iron in the samples. The Eh-pH diagram of manganese minerals (Figure 52) shows stability fields for the divalent state (Mn^{2+}) and manganese carbonate (Krauskopf, 1979), while the Eh-pH diagram of iron minerals shows the stability fields for ferrous iron (Fe^{2+}) and hematite. Comparison of the Eh-pH diagrams of manganese and iron minerals indicate that the stability

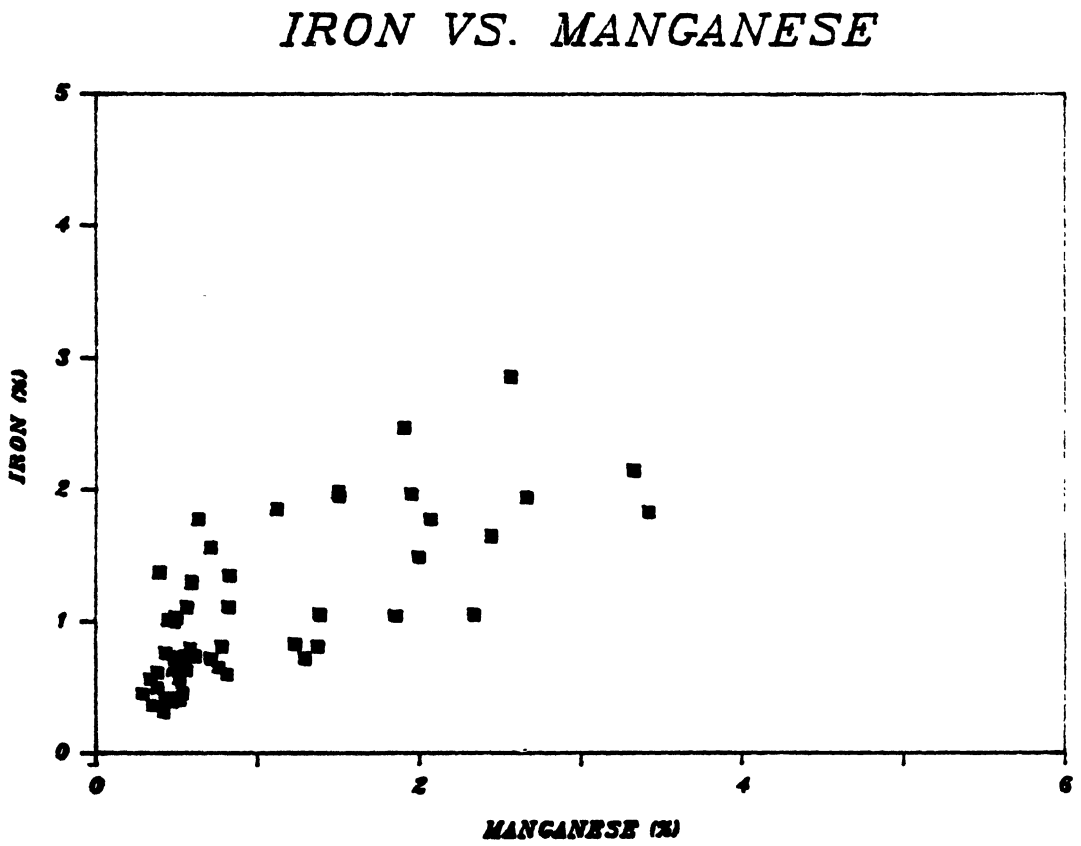

Figure 51.--Graph of manganese versus iron concentration.

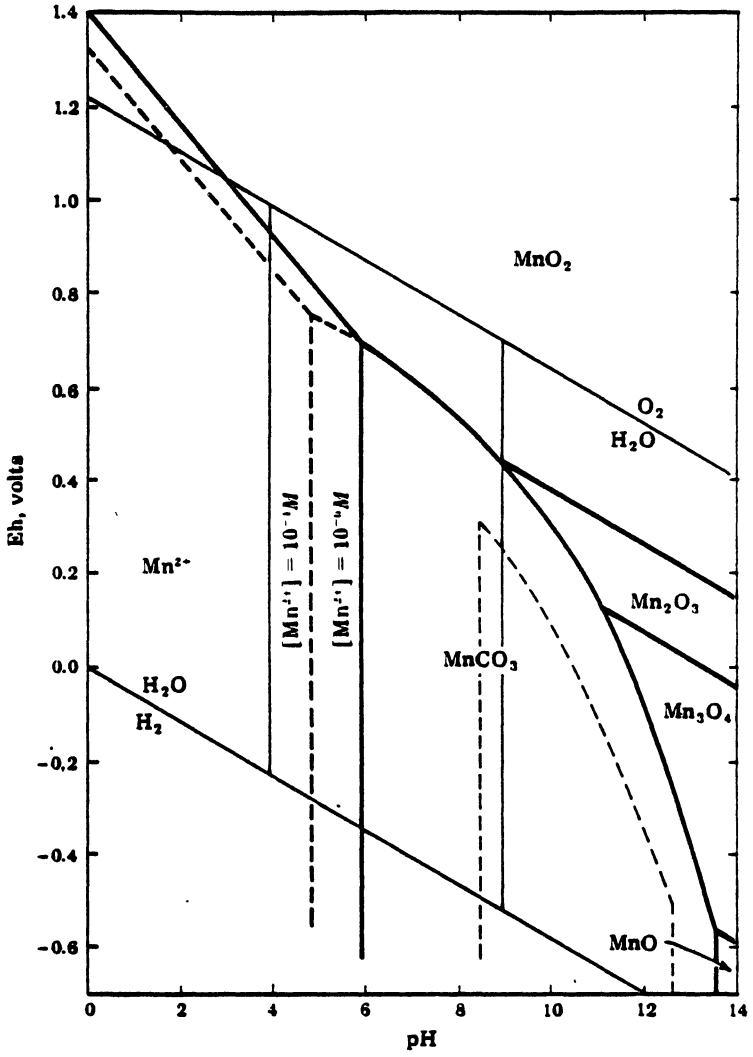

Figure 52.--Eh-pH stability diagram of common manganese minerals (Krauskopf, 1979).

fields of Mn^{2+} and Fe^{2+} ions are very similar. Therefore, the Mn^{2+} ion will be released to the formation water during the chemical reactions involved in HIDA. The Mn^{2+} ion will be incorporated in the dolomite as seen by the above reaction or form rhodocrosite according to the following reaction (Hem, p. A19, 1963):

$$MnCO_3 + H_2CO_3 \leftrightharpoons Mn^{2+} + 2HCO_3^-.$$

Ferroan dolomite, ankerite, is defined by the following reaction (Lilburn and Al-Shaieb, p. 49, 1983):

$$4CaCO_3 + Fe^{++} + Mg^{++} \leftrightharpoons 2CaFe_{.5}Mg_{.5}(CO_3)_2 + 2Ca^{2+}.$$

The types of carbonate cementation are determined by the pressure of CO_2 and the cation availability.

Iron System

Iron (ferric oxide) is the most discernable component of the redbeds. Ferric oxides in the red Permian sediments occur usually as hematite cement. Several modes of hematite formation have been suggested (Krynine, 1949; Walker, 1967; Van Houten, 1968; Chukhrov, 1973). Hematite may be detrital or may form in situ, but, nevertheless, ferric oxide is an indication of an oxidizing environment.

Iron occurs in two oxidation states, divalent (ferrous) form, and trivalent (ferric) form. Both states form hydroxides in aqueous solutions. These hydroxides, especially the ferric form, have low solubilities. Eh-pH of the formation water is the major variable in determining the stability of a particular iron species. Reduction-

oxidation potentials are measured by their Eh values expressed volts. Increasing oxidizing potentials are represented by increasing Eh. For a solution containing ferric and ferrous iron, under equilibrium conditions, the relative activities of the oxidized and reduced forms of iron present in a solution is a function of the redox potential. Figure 53 is a stability-field diagram for an aqueous ferric-ferrous system where the abscissa represents the pH of the solution and the ordinate represents the Eh of the solution. For a solution containing iron with a pH approximately 10 and Eh ranging from -0.2 to 0.6 volts, the dominant iron species in the solution would be ferric hydroxide. Likewise, if the iron-bearing solution had an Eh range of 0.0 to 0.76 volts and a pH less than 8.5, the ferrous ion would be the predominant iron species in solution. Ground water in an anaerobic environment where carbon dioxide is present in excess amounts commonly has a relatively low pH value (less than 6) and an Eh value of 2.0 volts or less (Hem and Cropper, 1959). Collins (1975) recognized that the Eh of oil-productive waters is generally reducing. He (1969) indicated that the redox potential of Anadarko basin oil field brines range from -.27 to -.30 volts. Under these conditions, ferrous ions would be very stable. As oxygen is dissolved, however, ferrous ions become unstable and precipitate as ferric-hydroxides. The formation of iron minerals can be predicted using an Eh-pH diagram (Figure 54).

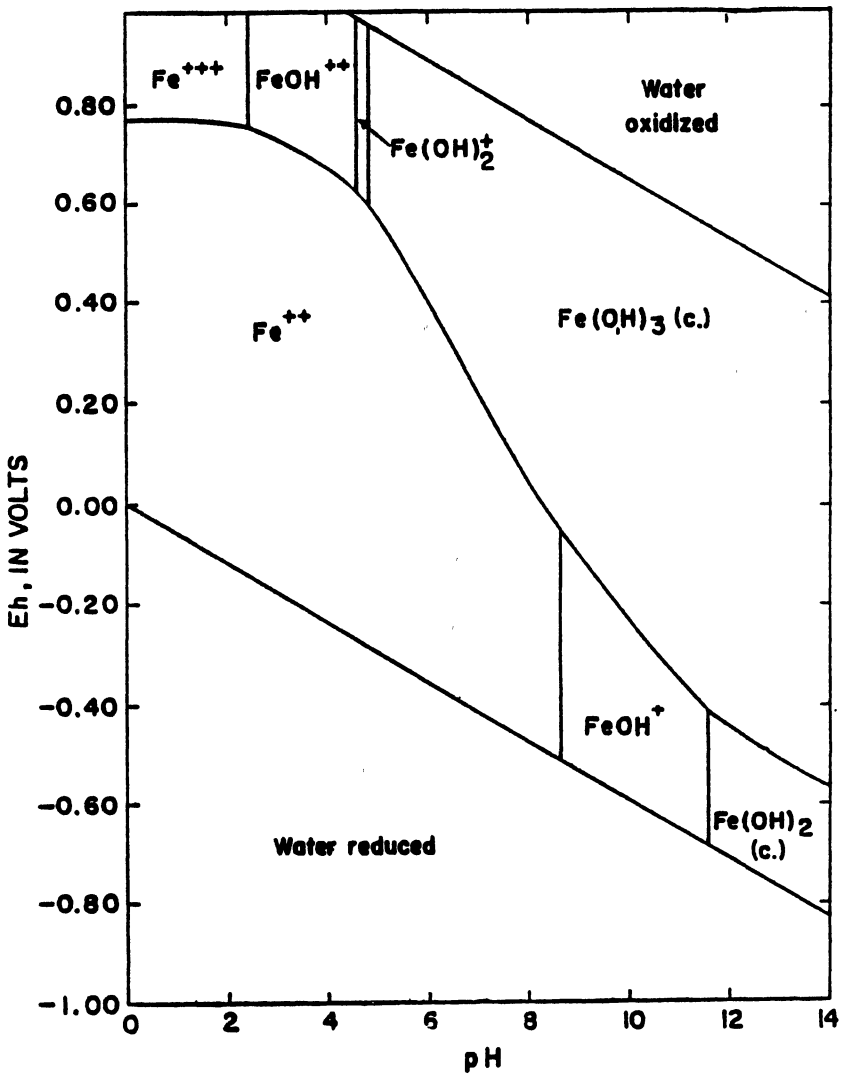

Figure 53.--Eh-pH stability diagram for the aqueous ferric-ferrous system (Hem and Cropper, 1959).

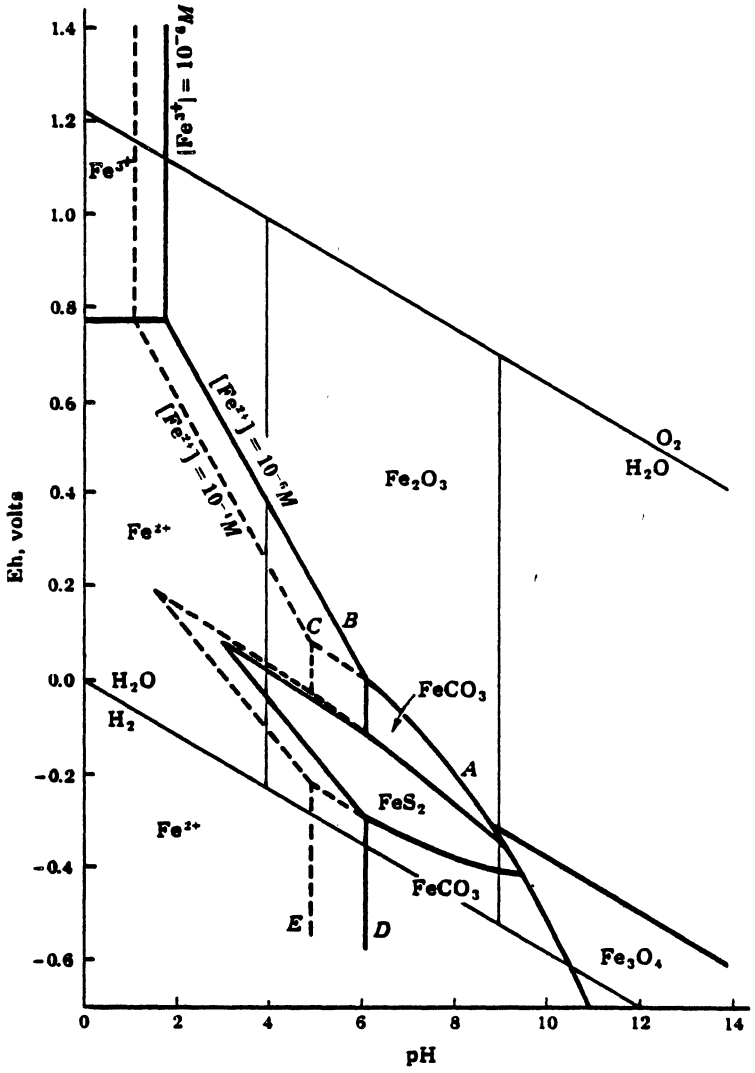

Figure 54.--Eh-pH stability diagram of iron minerals (Garrels and Christ, 1965).

Formation of iron minerals is not only based on the concentration of the iron in the solution but, also, iron mineral precipitation is a dependent on the anions in the system such as sulfide and carbonate. The sulfur species present in a solution, like iron, is pH and Eh dependent. Figure 55 is a stability field diagram of sulfur species likely to occur in natural waters (Hem, 1960). For a solution with low pH, reduced sulfur in the form of hydrogen sulfide (H_2S) may be present. In the pH range of natural waters, the sulfate ion, $SO_4^=$, is the most prevalent. The combination of Figures 54 and 55 can result in a composite stability diagram to predict the common iron minerals that are likely to form under the constant ion activities (Figure 56). In solutions where both ferrous ions and aqueous sulfides are present, pyrite (iron disulfide) would be the precipitate. Conversely, under the same Eh and pH, where aqueous sulfide is absent and bicarbonate is present, siderite will dominate (Curtis, 1967).

Sulfur System

Hydrogen sulfide gas plays an important role sulfide mineralization in HIDA. The major sources of H_2S are (1) gas liberated from hydrocarbons through petroleum transformation, (2) the reduction of sulfate by bacterial reaction during methane migration through formation water (Krauskopf, p. 266, 1965):

$$2H^+ + SO_4^= + CH_4 \rightleftharpoons H_2S + CO_2 + 2H_2O.$$

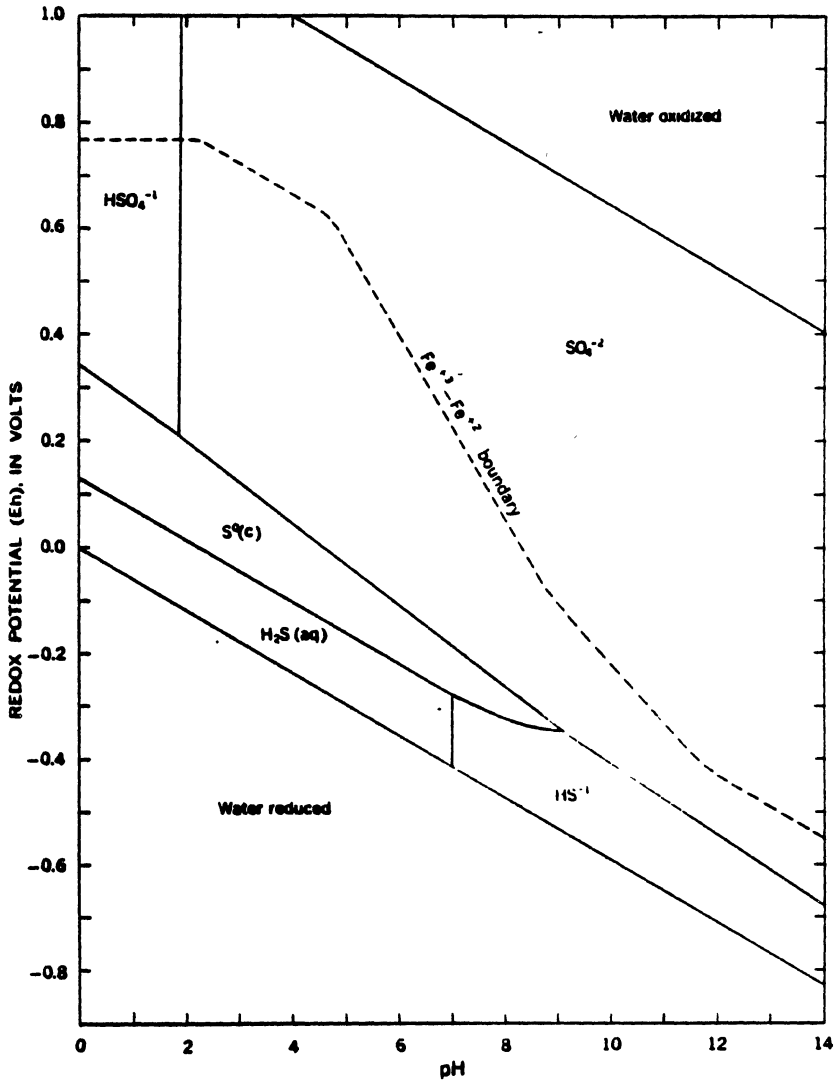

Figure 55.--Eh-pH stability diagram for aqueous sulfur species (Hem, 1960).

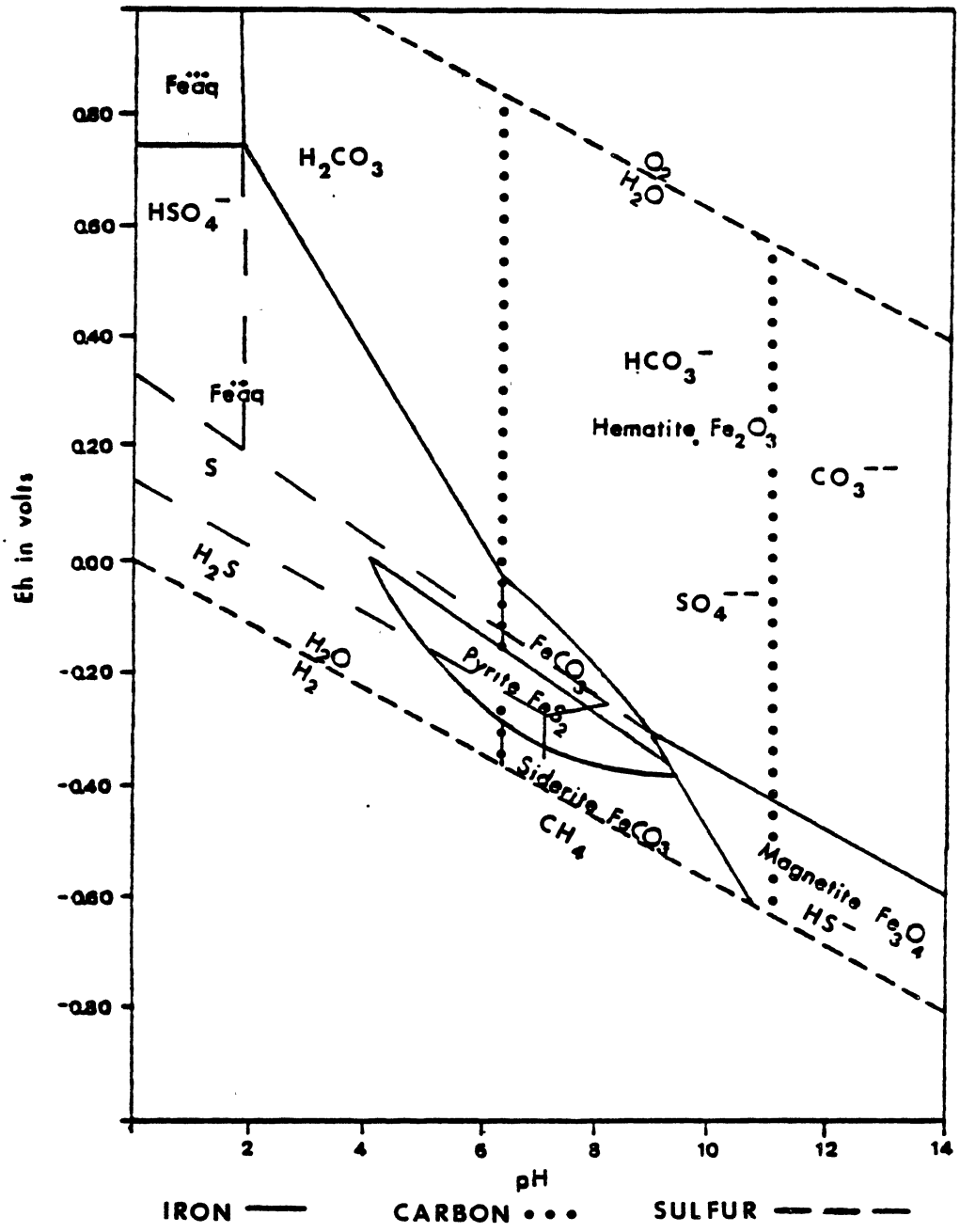

Figure 56.--Eh-pH stability diagram combining the iron, sulfur, and carbonate systems (after Garrels and Christ, 1965).

Sulfides form readily by the reaction of dissolved hydrogen sulfide with divalent metals such as Fe^{++}, Pb^{++}, and Zn^{++}. These minerals are pyrite, pyrrhotite, marcasite, galena, and sphalerite. The dominant sulfide in HIDA is pyrite.

Garrels and Christ (1965) proposed the following reaction for the formation of pyrite (p. 219):

$$Fe_2O3 + 4H_2S_{aq} \leftrightharpoons 2FeS_2 + 3H_2O + 2H^+ + 2e^-.$$

Pyrrhotite, $(Fe_{1-x})S$, is usually thought of as a hydrothermal mineral, however, the sulfide has been reported from some low-temperature occurrences (Berner, 1964). Parameters of the environment are limited to the Eh and pH specified on the stability diagram (Figure 57). The reaction between pyrrhotite and pyrite is independent of pH and the partial pressure of CO_2 (Berner, p. 829, 1964):

$$FeS_{hex} + S_{aq}^{=} \leftrightharpoons FeS_{2pyr} + 2e^-.$$

The diagram shows that the reduction of hematite does not produce pyrrhotite. Therefore, the pyrrhotite was most likely a product of the diagenetic alteration of pyrite.

Magnetite is also a possible precursor of pyrrhotite. Donovan et al. reported magnetite occurrences over the Cement field, however, magnetite has not been identified in the samples analyzed in the study area. Samples with strong magnetic properties were analyzed for their mineralogy. The samples possessed identical properties to analyzed samples of the Cement field (Reynolds, 1985). Reynolds and others (1984) have identified ferromagnetic pyrrhotite (Figure 58) in the Cement area.

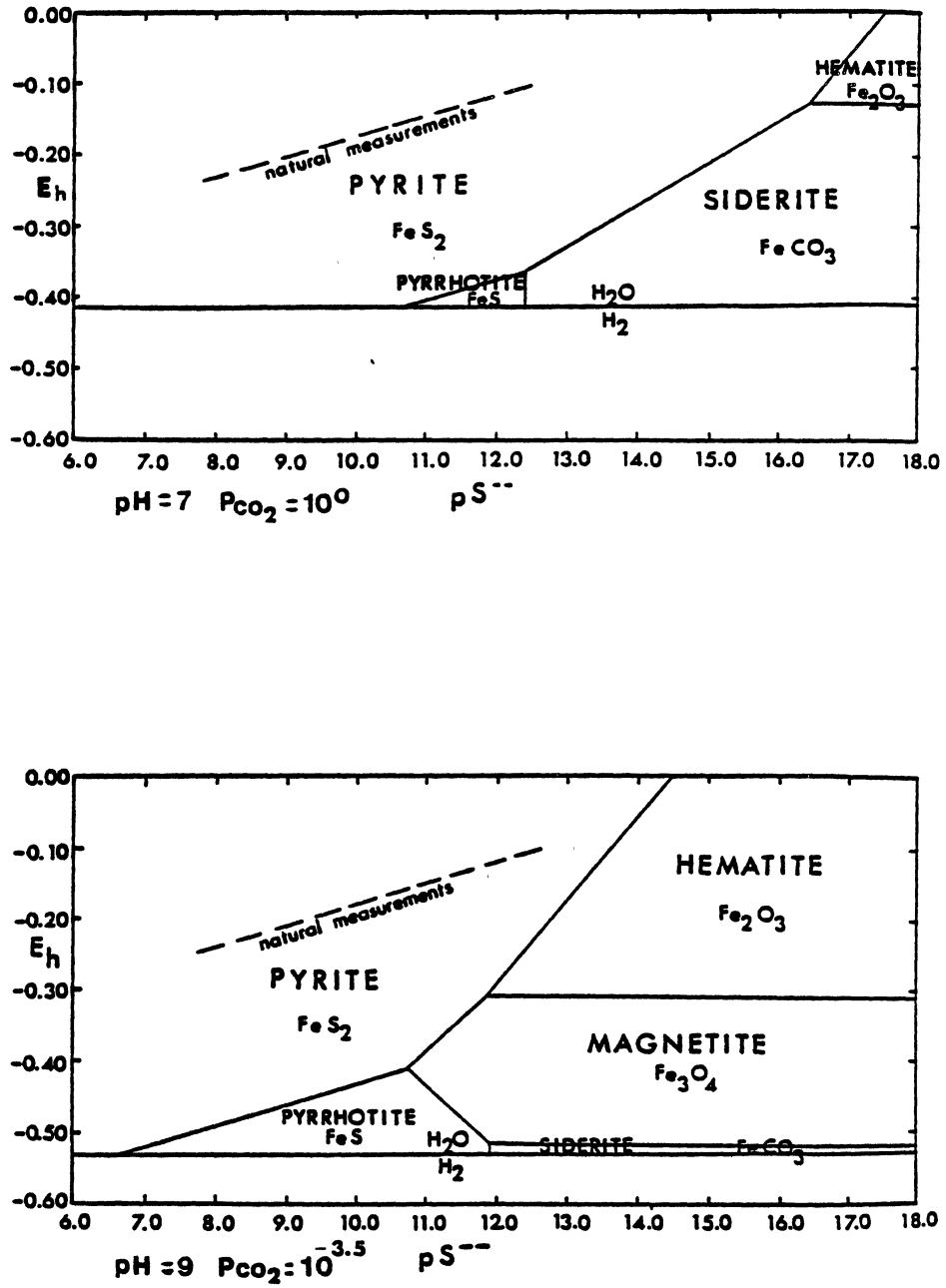

Figure 57.--Stability field diagrams of iron minerals (Berner, 1964).

Figure 58.--Photomicrograph of pyrrhotite blades (photo by Reynolds, 1985).

Sulfur is found in well cutting and on the surface of the altered redbeds. Sulfur results from the oxidation of H_2S gas and oxygen (Davis and Kirkland, 1970):

$$2H_2S + O_2 \leftrightharpoons 2S^o + 2H_2O.$$

Authigenic Clays

Smectite-illite mixed-layered clays are present in the altered sandstones. The formation of the mixed-layered clay and early precipitation of kaolinite is probably due to the alteration of detrital illite. Hydrolysis of illite results in the formation of kaolinite by the following reaction (Krauskopf, p. 150, 1979):

$$2KAl_3Si_3O_{10}(OH)_2 + 2H^+ + 3H_2O \leftrightharpoons 3Al_2Si_2O_5(OH)_4 + 2K^+.$$

Equilibrium of this equation is dependent upon the ratio of the K^+ concentration to the H^+ concentration. Systems involving Na^+ and Ca^{2+} rather than K^+ react similarly to the kaolinite. However, an input of Na^+ and Ca^{2+} ions decreases the stability of illite and increases the stability of smectite (montmorillonite). Smectite would be stable in systems where the ratio of metal ions to hydrogen ions is large (Krauskopf, 1979; Drever, 1982). With the exception of the K^+ in the illite structure, the K^+ content in the sandstone is probably small due to the minor amount of potassium feldspars. Although plagioclase feldspars are relatively low in concentration, the dissolution of these minerals may provide the calcium and sodium necessary for smectite formation.

The late stage of kaolinite precipitation is associated with carbonate dissolution. Kaolinite solubility increases at high and low pH as shown on Figure 59. Acidic waters commonly carry metal ions such as Mg^{2+}, K^{2+}, and Al^{3+}. The introduction of an acidic solution supersaturated with respect to kaolinite to a carbonate environment would result in the dissolution of the carbonate cement. Upon dissolution of the carbonate, H^{+} ions are consumed raising the pH from levels of 3 to 6. In this range, carbonate dissolves but kaolinite precipitates (Curtis, 1983).

Mechanisms of Formation

Carbonate and sulfide mineralization in the sandstone are usually more prominent along bedding planes due relatively to their higher porosity and permeability. Figure 60 is a photograph that shows the alteration along the cross-bedding. The initial mineralization occurs as carbonate and sulfide seeds. The growth and enlargement of the seeds form a continuous network, replacing and displacing the original framework constituents. Figure 61 is an illustration to show the stages of mineralization. Figure 62 is a series of photographs that illustrate the evolution of carbonate cementation. The mineralization shows increasing intensity from the upper to the lower photograph, while figure 63 are photographs that exemplify the accumulation of carbonate on an initial seed to form a

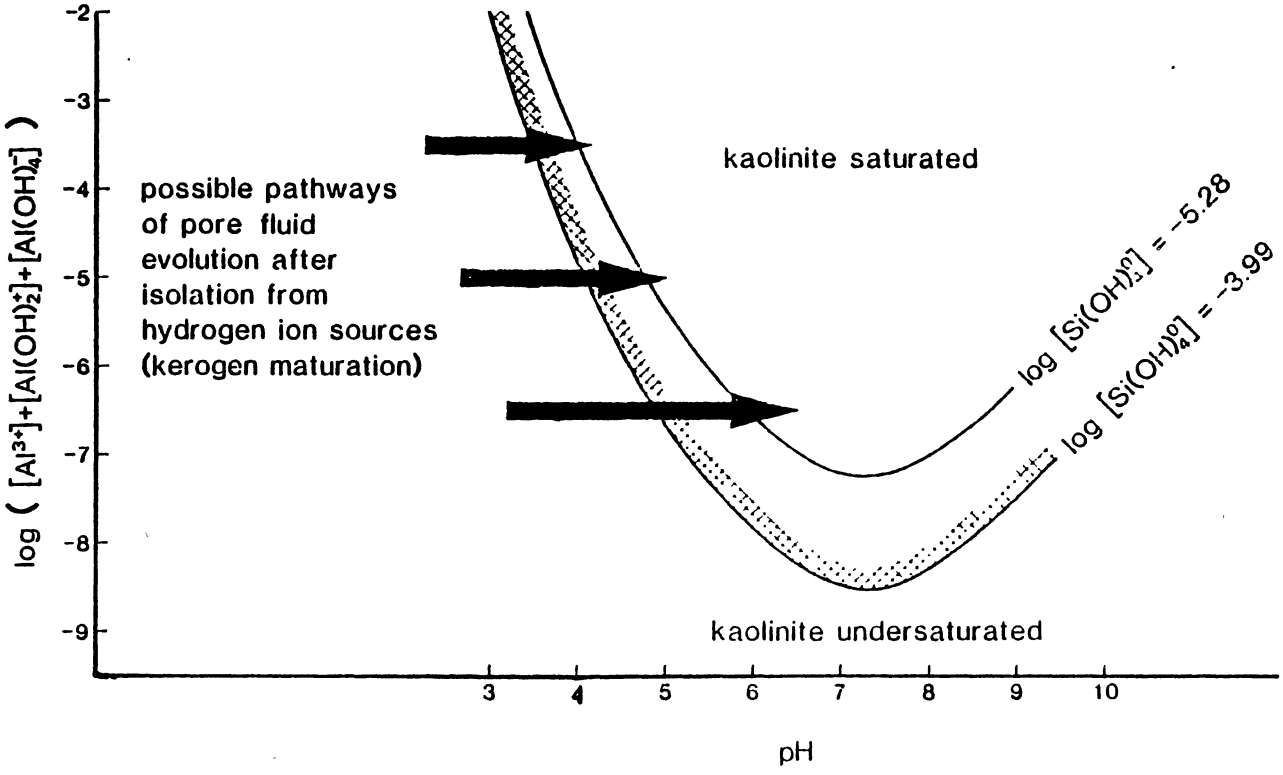

Figure 59.--Stability diagram for kaolinite (Curtis, 1983).

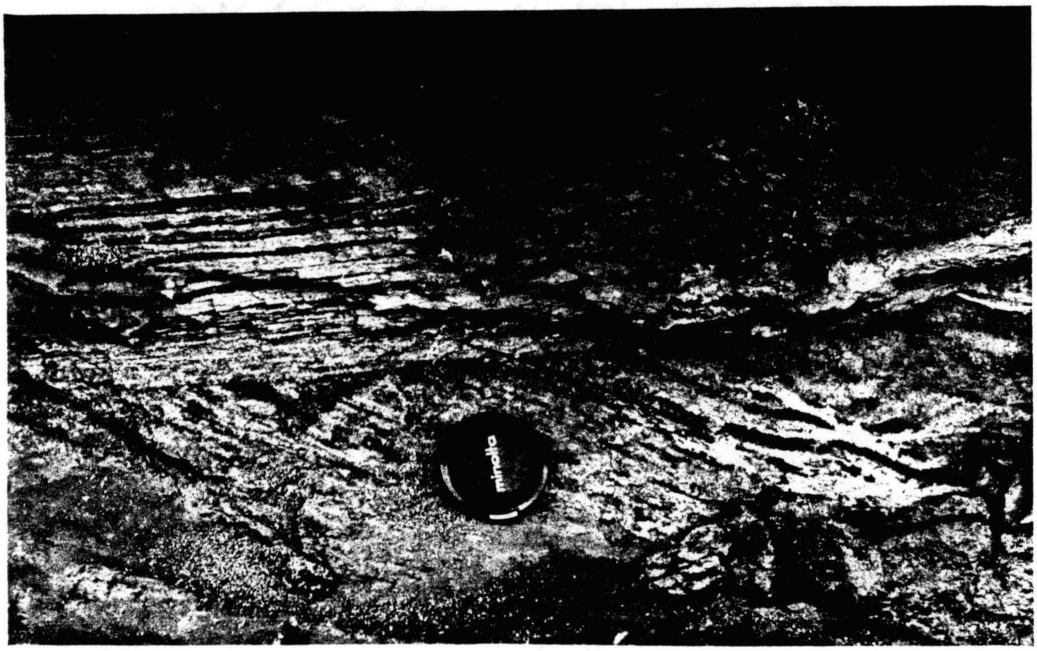

Figure 60.--Outcrop photograph showing alteration along the crossbedding.

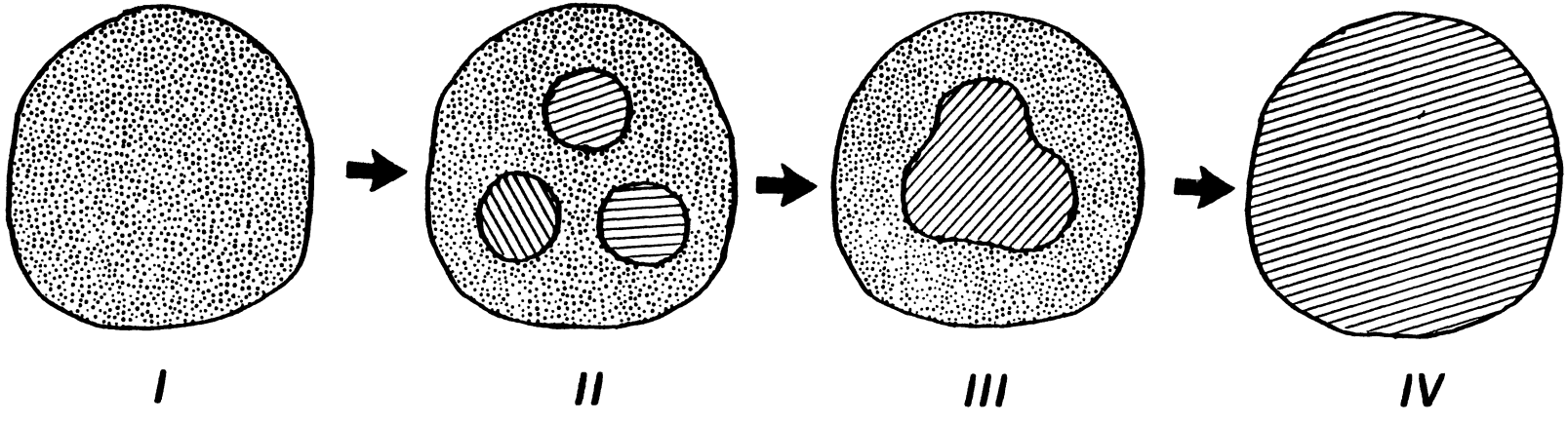

Figure 61.--Illustration of the stages of carbonate and sulfide mineralization.

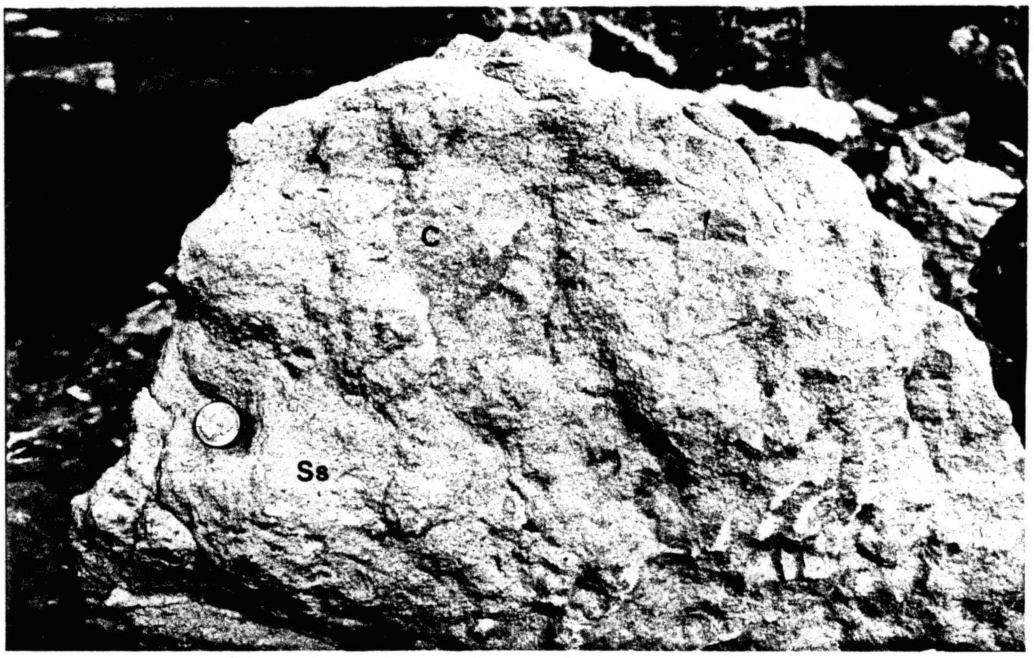

Figure 62.--Outcrop photographs showing the mineralization of carbonate.

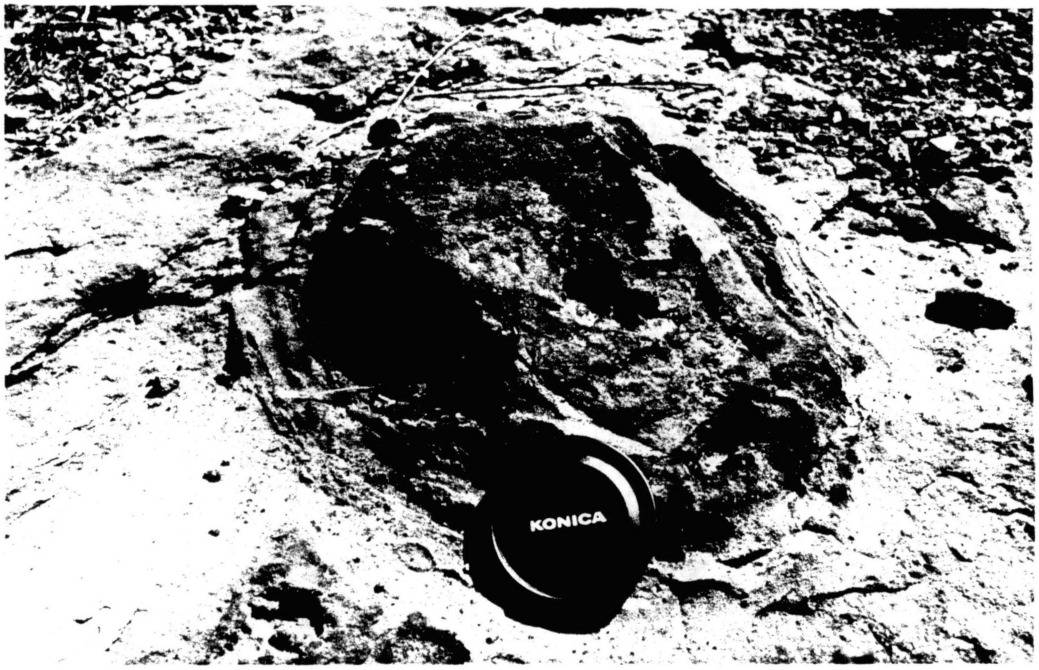

Figure 63.--Outcrop photographs showing concretions of carbonate.

prominent concretion.

An important observation is that the type of carbonate minerals observed on surface outcrops show slight variation between different oil fields. Calcite is the major carbonate present in both the Velma and Healdton fields with minor amounts of ankerite, manganesian carbonate, ferroan calcite and dolomite. On the other hand, dolomite is the dominant mineral in the Carter-Knox oil field. The variation of carbonate between Carter-Knox and the other oil fields may be due to the presence of relatively higher activities of iron and magnesium ions in the formation water. This geochemical environment, therefore, is conducive to the formation of dolomite.

Figure 64 is a summation of the HIDA diagenetic model in cross sectional view. Extensive carbonate cementation (zone 1) occurs over the crest of the anticline and is dominated by the carbonate-related reactions (A). The bleached sandstone (zone 2) occurs on the outer edges of the aureole. Zone 2 is characterized by the reduction of hematite and the removal of the ferrous ion. Zone 3 which represents the presence of sulfides is characterized by the iron and sulfur reactions (B). The bacterial-induced reactions (C) produce some of the carbon dioxide and hydrogen sulfide used in reactions A and B.

HIDA DIAGENETIC MODEL

A. *CARBONATE REACTIONS*

$$CaCO_3 + H_2CO \rightleftharpoons 2HCO_3^- + Ca^{2+}$$

$$\| \quad + H_2O$$

$$CO_2$$

$$2CaCO_3 + xMn^{2+} + yFe^{2+} + zMg^{2+} \rightleftharpoons \quad (x+y+z=1)$$

$$CaMn_xFe_yMg_z(CO_3)_2 + Ca^{2+}$$

Ma-DOLOMITE

B. *IRON AND SULFUR REACTIONS*

$$Fe_2O_3 + 4HS^- + 2H^+ \rightleftharpoons 2FeS_2 + 3H_2O + 2e^-$$

HEMATITE — PYRITE or MARCASITE

$$H_2S + \tfrac{1}{2}O_2 \rightleftharpoons S^\circ + H_2O$$

C. *BACTERIAL-INDUCED REACTIONS*

$$CH_4 + 2O_2 \rightleftharpoons CO_2 + 2H_2O$$

$$SO_4^{=} + H^+ + CH_4 \rightleftharpoons H_2S + CO_2 + 2H_2O$$

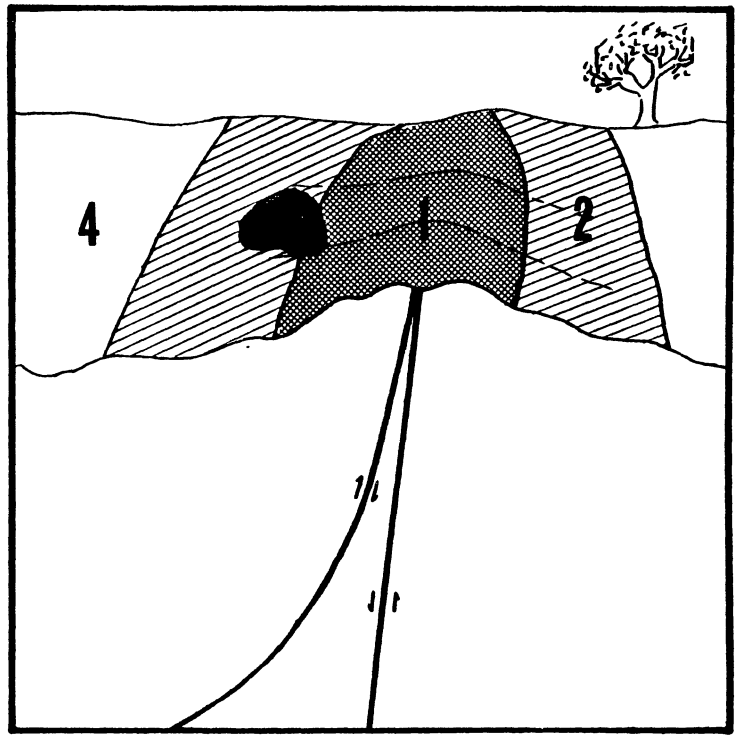

Figure 64.--Illustration of the cross sectional view of the HIDA diagenetic model.

CHAPTER VI

ISOTOPE GEOCHEMISTY

Basic Isotope Theory

Isotopes are variations of an element that have an identical number of protons but differ in the number of neutrons in the nuclei. Therefore, isotopes have the same atomic number but differ in atomic weight. As a result, isotopes vary slightly in physical and chemical properties. The process that alters the relative abundance of stable isotopes is known as fractionation. The separation of isotopes regardless of the mechanism, can be expressed in terms of a ratio called fractionation factor:

$$\alpha = \frac{R_A}{R_B} \qquad 6\text{-}1$$

where R_A is a ratio of the heavy to light isotopic composition of phase A and R_B is the same ratio for phase B. Ratios of heavy (I_H) to light (I_L) isotopes for elements are expressed in another kind of symbolism where the sample is compared to a standard:

$$\delta R_H = \frac{(I_H/I_L)_{sample} - (I_H/I_L)_{SMOW}}{(I_H/I_L)_{SMOW}} \times 1000 \text{ ‰} . \qquad 6\text{-}2$$

A positive δR_H represents an enrichment in the heavy isotope whereas a negative δR_H signifies a depletion in the heavy

isotope. The relationship between and is given:

$$\alpha = \frac{R_A}{R_B} = \frac{R_{HA} + 1000}{R_{HB} + 1000} \qquad 6\text{-}3$$

Three processes of stable isotope fractionation are recognized:

1. Physical Fractionation - i.e., evaporation or diffusion.

2. Equilibrium Fractionation - this results in an exchange reaction between the isotopes until equilibrium of the isotopic phases is reached. However, the concentration of an isotope in an element may differ due to the difference in the bonding energy of the element in the two phases. The lighter isotope, which forms a weaker bond will be preferentially concentrated in the more weakly bonded site. The amount of fractionation is a function of temperature and is independent of pressure.

3. Kinetic Fractionation - isotopic separation occurs due to the different rates of reaction. The lighter isotope tends to faster react than the heavier isotope. Consequently, the initial product will be slightly enriched in the light isotopic phase. If the reaction goes to completion, the isotopic ratio of the product will be the same as the reactant (Figure 65). In order to observe kinetic fractionation, the reaction must be incomplete or the products must be successively removed so that the product is not allowed to homogenise.

Fractionation of isotopes occurs differently for each

element. Isotopic separation may be influenced by a particular environment.

Carbon Isotopes

Theory

Carbon has two stable isotopes, C^{12} and C^{13}. The fractionation and the ratios of the carbon isotopes are expressed in terms of alpha (α) as in equation 6-1 and delta (δ) C^{13} shown in equation 6-2. Relative isotopic ratios are obtained by comparison of the sample ratios to the ratio of the common standard, PDB (Belemnite of the Peedee formation, Cretaceous, South Carolina) of the University of Chicago.

Carbon isotopic values of gases, cements, and waters are useful in determining their sources of formation and their relationships to hydrocarbon migration. C^{13} values of crude oils range from -18 to -34 per mil. (‰). In other words, the oils contain heavy carbon (δC^{13}) in 18 to 34 parts per thousand less than the PDB. The lighter fractions of the oils such as the paraffins are depleted in δC^{13} while heavier fractions, the aromatics and NSO compounds, are enriched in δC^{13}. The reservoir crude oil becomes increasingly heavy and enriched in δC^{13} upon degredation (Hunt, 1979; Stahl, 1977).

Isotopic values of methane gas are dependent on the mode of formation. Biogeneic gas usually forms at low temperatures from the degredation of organic matter by

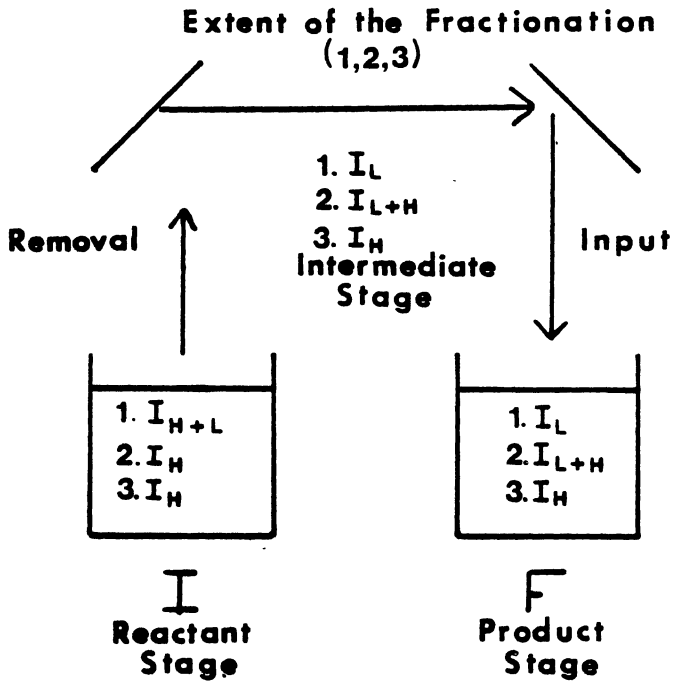

Figure 65.--Illustration of the extent the of fractionation (after Coleman, 1977).

anaerobic microorganisms (Rice and Claypool, 1981). The range of biogenic gas at temperatures less than 75°C range from -50 to -90‰. Thermal methane gas usually results from kinetic isotope fractionation in which the C^{12}-C^{12} bonds are more easily broken than the C^{12}-C^{13} bonds. At temperatures greater than 75°C, δC^{13} values range from -25 to -60‰. Maturity affects the δC^{13} values in that the initial gas produced will be the most highly depleted in C^{13}. During maturation, the δC^{13} values of the produced gas will approach the δC^{13} range of the organic carbon source (Fuex, 1977; Schoell, 1983).

Carbonate cements from several oil fields have been analyzed for their isotopic compositions. Meteoric or fresh water carbonates have an average δC^{13} value of -4.9 +/- 2.8 per mil. while the average value for marine carbonates is +0.6 +/- 2.8 per mil. (Keith and Weber, 1964, reported by Lilburn and Al-Shaieb, 1984). Diagenetic carbonates over the petroleum producing areas of the Cement field had a range of C^{13} values for the carbonates from -5.47 to -35.3 ‰ (Lilburn, 1981). Lilburn and Al-Shaieb (1984) suggested that the carbon in the carbonate was derived from two major source, hydrocarbon-derived and meteoric-derived. Figure 66 displays the C^{13} data of the Cement field. Al-Shaieb (1981; reported by Lilburn, 1981) proposed a model to represent the contribution based on two end members (Lilburn and Al-Shaieb, p. 61, 1984):

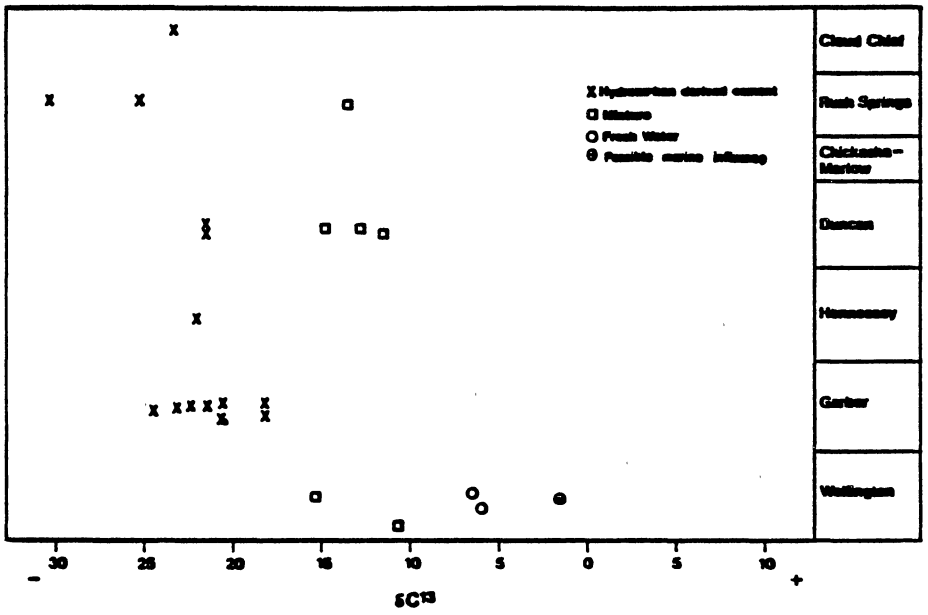

Figure 66.-- C^{13} isotopes for the Cement field (Lilburn and Al-Shaieb, 1984).

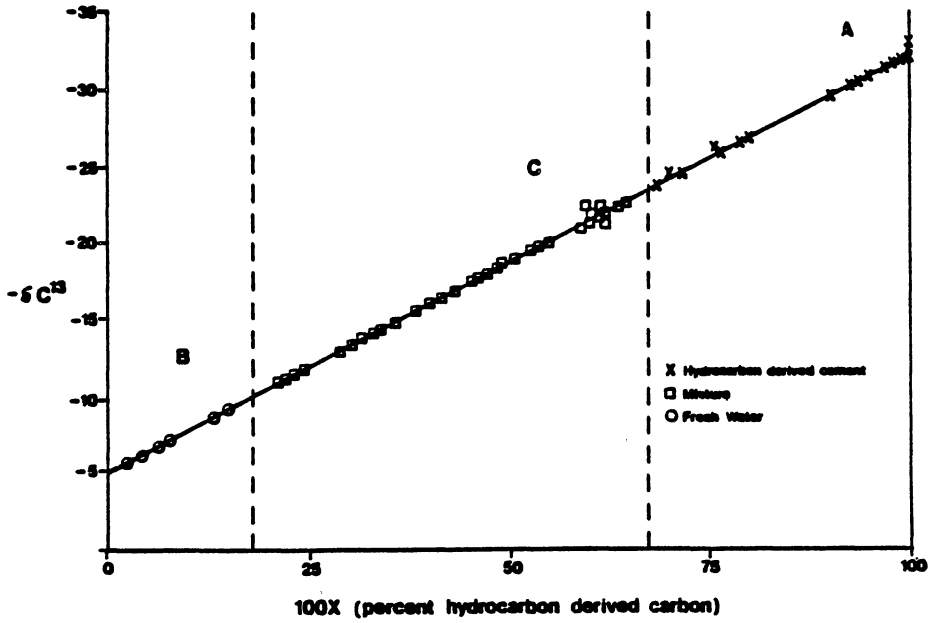

Figure 67.--Model for the hydrocarbon contribution of the Cement data (Al-Shaieb, 1981).

$$-32 * X + -4.9 * (1-X) = Z$$

where X represents the fraction of hydrocarbon contribution and Z represents the measured δC^{13} value (Figure 67).

Results and Interpretation

Diagenetic carbonate samples were analyzed from the Velma, Carter-Knox, and Healdton fields. The samples were collected both from surface outcrops and subsurface well cuttings. Table I is a list of the analyzed samples. Figure 68 represents the δC^{13} data collected from the three fields. The δC^{13} isotopic composition of Velma and Carter-Knox falls in the range of hydrocarbon-derived carbon with an average δC^{13} values of -21.5 ‰ ranging from -7.7 to -35.8 ‰ . The average of these values is in the range of δC^{13} from crude oils. The lighter values suggest an influx of δC^{13} from meteoric water as documented in the Cement study by Lilburn and Al-Shaieb (1984).

Healdton carbonates are heavier and suggest three sources of carbon. These sources of δC^{13} are hydrocarbon, meteoric, and marine. The Pennsylvanian Hoxbar that underlies the Permian strata is characterized by a thin fossiliferous limestone. This limestone has δC^{13} values approximating +1.8 ‰ . The marine limestone was probably the source of the enrichment of δC^{13}. Diagenetic carbonate was observed in a core of Pennsylvanian Healdton sandstones that lies above the thin marine limestone. The diagenetic carbonate was located at depths of 300 (752'

TABLE I

ISOTOPE DATA ON CARBONATES, SULFIDES, OIL, AND WATER SAMPLES

Sample Name	Location	Depth	C	O	S	
HEALDTON FIELD						
JK	31-3S-3W	SUR	-10.1	23.7		
JK2	"	"	-3.3	32.3		
NU	34-3S-3W	"			24.9	PYR
NU	"	"			-37.9	PYR
MQ	4-4S-3W	"	-2.1	25.8	16.2	PYR
MT	22-4S-3W	"			30.2	PYR
UE	24-4S-3W	"	-3.9	24.4		
MO	11-3S-4W	"	-8.5	21.6		
NV	28-3S-4W	"	-14.0	27.6		
NW	36-3S-4W	"			-9.7	BIT
SIN. HUXIE FEE	31-3S-3W	300'	-17.7	19.3		
"	"	360'			28.0	PYR
MAG. 11 WOODWORT	32-3S-3W	120'	-5.4	26.0		
"	"	110'			-13.2	PYR
"	"	110'			5.2	BIT
MAG. 8 WOODWORTH	"	337'			21.9	PYR
SP MULLENS	4-4S-3W	120'	-2.4	25.6		
"	"	240'	-6.7	24.7		
FRANKLIN	8-4S-3W	510'	-17.3	16.0		
SIN. RICHARDS	9-4S-3W	190'	-8.7	23.3		
"	"	320'			26.5	PYR
MAG. SMALLEY	10-4S-3W	170'	-24.7	23.5	36.9	PYR
RAIS. SMALLEY	16-4S-3W	475'	2.0	25.2		
AMERADA MARGO	17-4S-3W	720'	1.3	25.9		
AMERADA BOYLES	28-4S-3W	640'	-9.9	32.8	13.2	GAL
"	"	710'			14.7	SPH
SHELL	5-4S-3W	HEALDTON			10.6	OIL
UNION	23-4S-3W	"			12.1	OIL
SHELL	5-4S-3W	"	-11.7	-3.3		METEORIC
"	"	"		-3.1		BRINE
MOBILE	31-3S-3W	"		-2.6		"
UNION	24-4S-3W			-3.2		"

TABLE I

(CONTINUED)

Sample Name	Location	Depth	C	O	S
CARTER-KNOX FIELD					
LA	5-2N-5W	SUR	-7.7	34.6	
AK	21-3N-5W	"			10.6 PYR
NI	34-3N-5W	"	-35.8	26.2	
LE	35-3N-5W	"			-21.1 PYR
SKELLY 1 SADLER	11-2N-5W	360'			-0.5 PYR
"	"	640'	-16.8	32.4	4.9 PYR
"	"	1160'	-33.1	31.3	6.9 PYR
TEXAS 1 CLARK	8-3N-5W	410'	-10.2	29.9	
"	"	710'	-11.3	30.8	4.1 PYR
CARTER KERN 6	21-3N-5W	150'	-20.7	32.7	
"	"	790'			6.0 PYR
"	"	1160'	-24.4	35.8	
VELMA FIELD					
MBB	27-1S-5W	SUR	-16.2	32.6	
UC	35-1S-5W	"	-32.6	25.3	
McCAS. 1 RIVIERE	9-1S-5W	140'	-20.5	26.6	16.0 PYR
SKELLY 1 CROSBY	25-1S-5W	1260'	-28.1	28.5	2.3 PYR
HASSELL #35	35-1S-5W	<1000'			16.3 PYR
" #37	2-2S-5W	"			20.6 PYR
" #38	"	"			3.7 PYR
" #39	"	"			12.0 PYR
" #40	"	"			14.1 PYR
LOCO FIELD					
MG	10-3S-5W	SUR			13.1 PYR

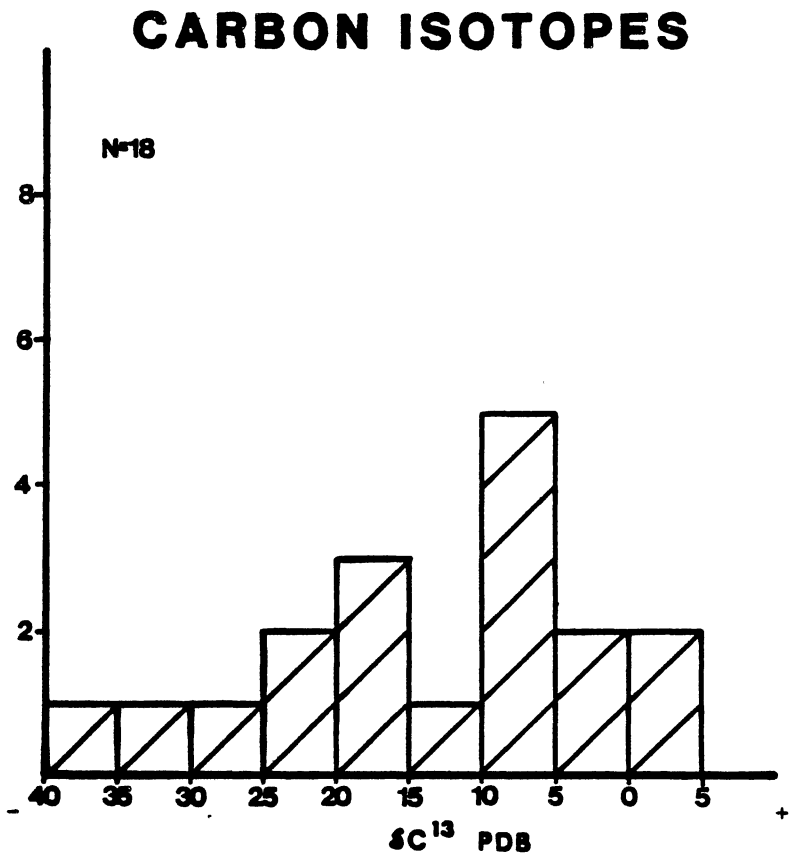

Figure 68.--Frequency distribution of C^{13} values for the Velma, Healdton, and Carter-Knox fields.

core depth) and 100 (908' core depth) feet above the producing sands. Analysis of the carbonate at 752 feet recorded a δC^{13} value of -7.0 per mil. while the carbonate at 908' had a δC^{13} value of -4.0 ‰. Undoubtly, the heavy marine carbon influenced the composition of the pore fluids which induced the precipitation of this diagenetic carbonate. Figure 69 is a graph of the δC^{13} values for analyzed carbonates of the three fields and the hydrocarbon contribution of carbon to the δC^{13} values. The data on the three fields indicate that hydrocarbons influenced the δC^{13} values of the carbonates.

Oxygen Isotopes

Theory

Oxygen fractionation is expressed in terms of equation 6-1 where O^{18} translates to R_A and O^{16} replaces R_B. The oxygen ratio is represented by δO^{18} relative to the standard ratio, SMOW (standard mean ocean water) in per mil. (‰). The fractionation of oxygen is dependent on temperature. At elevated temperatures, evaporation of ocean water causes preferential removal of the O^{16} and subsequent enrichment in δO^{18} of the sea water. This is due to the higher vapor pressure of H_2O^{16} than H_2O^{18}. This type of oxygen isotope enrichment is extensively discussed by Lloyd (1966).

Seawater has a constant δO^{18} value ranging from -1 to +1 per mil. relative to SMOW (Epstein and Mayeda, 1953).

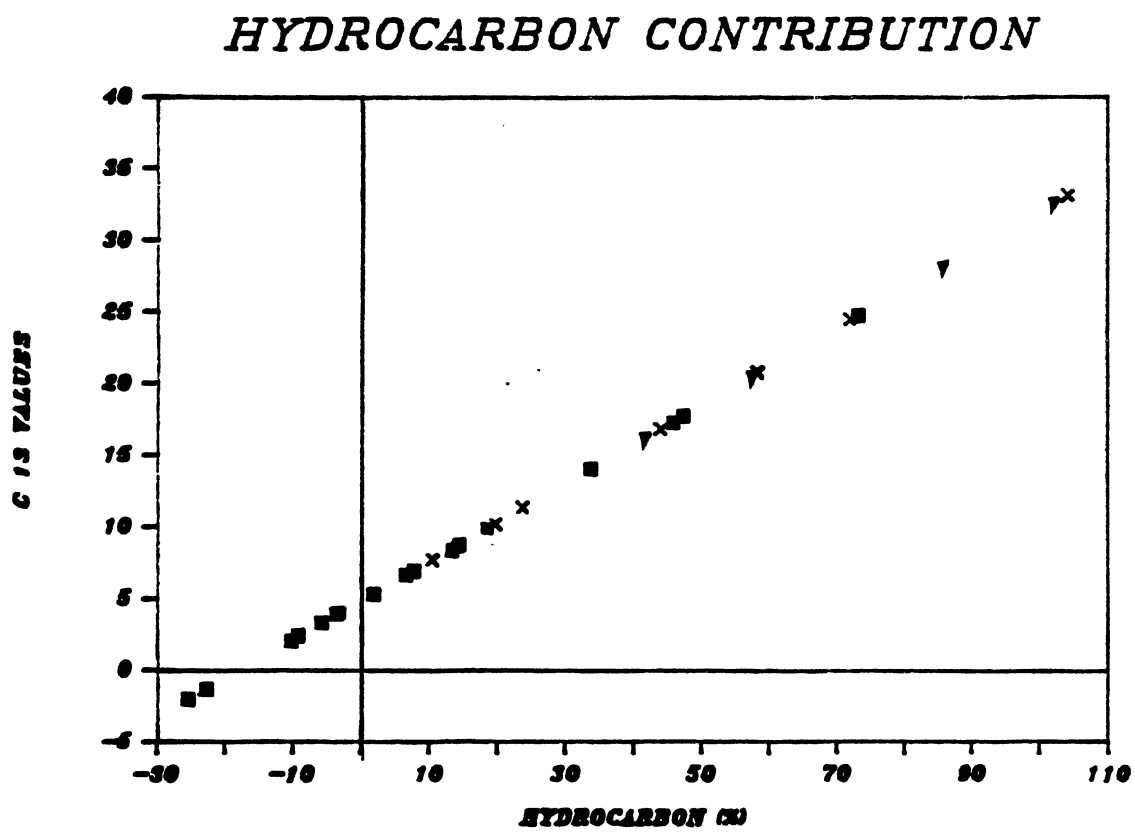

Figure 69.--Model for the hydrocarbon contribution of the Velma, Healdton, and Carter-Knox fields.

Meteoric waters are depleted in O^{18}; these waters range from 0 to -60 ‰ (Faure, 1977). Saline formation waters (brines) are often enriched in O^{18}. Clayton et al. (1966) suggests that the water of oil-field brines is meteoric in origin and that the heavy isotope is enriched in the waters of greatest salinities. Craig et al. (1956) proposed that the enrichment was due to isotopic exchange between water and rock at elevated temperatures. Recent studies by Clayton et al. (1966) show that the previously mentioned reaction might be expected to the dominant factor in determining the oxygen in oil-field brines.

The δO^{18} of diagenetic carbonate is dependent on the isotopic composition of the waters. Donovan et al. (1981) suggest two fractionation mechanisms of the δO^{18} isotopes of diagenetic carbonate over the Velma oil field. They reported values significantly less and greater than the expected values. The light values were explained by micropore filtration where the light water fractions are passed through shales while the heavier water is retained (Coplen and Hanshaw, 1973). The mechanism proposed responsible for the heavy δO^{18} values of the carbonates is related to the gas induced evaporation process which results in an enrichment of O^{18} in the formation waters. This is due to the expansion of depressurized gas in the waters leading to an evaporation of the H_2O^{16} (Mills and Wells, 1919; Nisle, 1941).

Results and Interpretation

Oxygen isotopic values of carbonates analyzed for the Velma, Carter-Knox, and Healdton fields range from +16 to +34.6 ‰ SMOW (Table I, Figure 70). These values are similar to the values of the Cement field reported by Lilburn and Al-Shaieb (1984). The δO^{18} values for the above three fields and the Cement field have little variation (Figure 71). The very light oxygen (+16.0 ‰) values may be a result of micropore filtration as suggest by Donovan et al. (1981) while the extremely heavy values (+34.6 ‰) may indicate an influx of brine waters. The O^{18} data indicates that the carbonates were deposited from waters of fixed temperature and isotopic composition.

The isotopic composition of water in equilibrium with the diagenetic carbonate can be predicted by using an isotopic separation curve and the mean annual temperature (Figure 72). Lilburn and Al-Shaieb (1981) predicted the δO^{18} value of water in equilibrium with the calcite of δO^{18} is equal to 27.1 per mil. at a temperature of 16.4°C to be approximately -3.4 ‰ . This value was supported by analyses of water samples from Healdton. Three brine water samples and one meteoric water sample were analyzed for their δO^{18} composition. The δO^{18} values of the brine water samples ranged from -2.6 to -3.2 ‰ while the value for the meteoric sample was -3.3 ‰ .

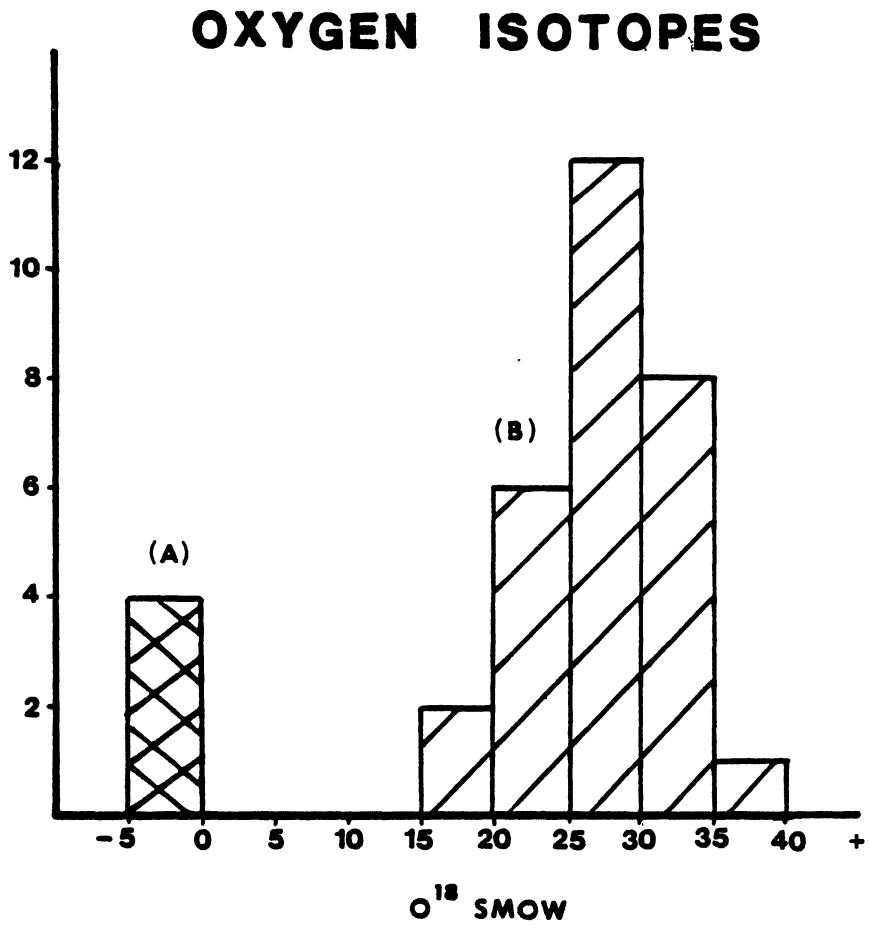

Figure 70.--Frequency distribution of O^{18} isotopes for the Velma, Healdton, and Carter-Knox fields: (a) oxygen isotopes of water, (b) oxygen isotopes of carbonate.

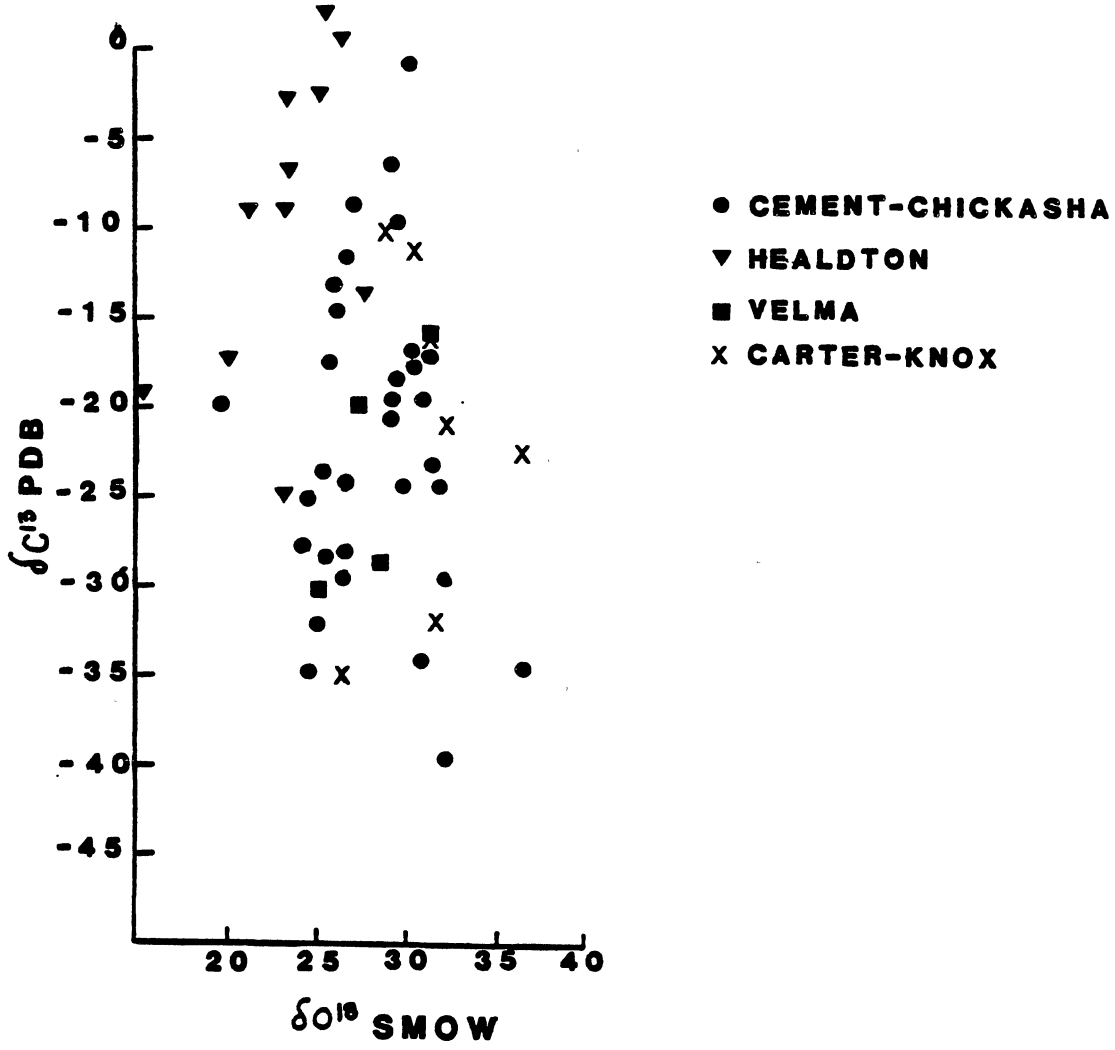

Figure 71.--Graph of δC^{13} and δO^{18} values for the various fields.

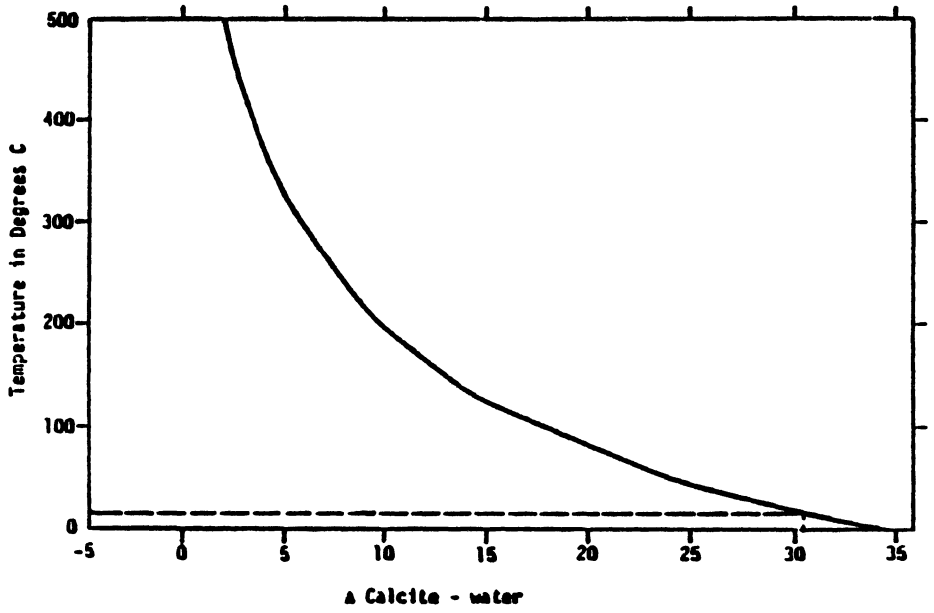

Figure 72.--Isotopic separation of O^{18} isotopes for calcite and water as a function of temperature (Goldhaber, Reynolds, Rye, and Grauch, 1979).

Sulfur Isotopes

Theory

Sulfur isotopes are influenced by the source of the sulfur. They are expressed in terms of the quantity of S^{34} per mil. defined by the S^{34}/S^{32} abundance ratio in the sample. This is compared to the standard ratio in troilite of the Canon Diablo meteorite as in equation 6-3.

Two kinds of processes control the fractionation in the sulfur isotopic composition:

1. reduction of sulfate ions to sulfide ions
2. various isotopic exchange reactions between sulfur bearing ions, molecules, and solids.

Initial H_2S produced by fractionation will be enriched in the light S^{32} isotope relative to the source. However, the isotopic composition depends on the size of the sulfur source. If the sulfur source is infinite, then the $\int S^{34}$ values of H_2S will remain constant. Conversely, if the sulfur reservoir is limited, the isotopic composition of the H_2S will gradually increase in $\int S^{34}$ due to the preferential removal of the light sulfur as H_2S (Faure, 1977).

The S^{34} values of petroleum range from -8 to +32 per mil. (Faure, 1977). H_2S may be incorporated into the petroleum during maturation when the organic matter is in contact with sulfates and sulfides (Orr, 1974). Thode and Monster (1970) suggested that generally petroleum is

depleted in δS^{34} by approximately 15 ‰ relative to ancient seawater; therefore, marine sulfate is most likely the source of sulfur in petroleum.

Results and Interpretations

Pyrite, sulfate, and oil samples from the Carter-Knox, Velma, and Healdton fields were analyzed for their isotopic composition. Table I lists the δS^{34} values for the fields studied. A frequency distribution of the δS^{34} values in pyrite (Figure 73) indicates various types of of S^{34} values. The δS^{34} values enriched in S^{32} are indicative of sulfur derived from a bacterial source (Kaplan, 1983). Values ranging from -9.7 to +16.2 ‰ indicate hydrocarbon-derived sulfur. Figure 74 shows the percent cumulative frequency of the δS^{34} of pyrite from the three fields and the δS^{34} of the H_2S gas associated with petroleum as reported by Goldhaber, Reynolds, and Rye (1978). The similarity between the two trends is remarkable.

The isotopic compositions show similarities as well as differences between the oil fields. The mean δS^{34} value of pyrite for the Carter-Knox field is 4.3 per mil., very similar to the δS^{34} values of the pyrite and oil samples reported by Lilburn and Al-Shaieb (1984) for the the Cement field. δS^{34} values of pyrite analyzed from the Velma field average 12.2 ‰. These values are slightly heavier than Carter-Knox and Cement, but in general, they resemble those of hydrocarbon-derived sulfides. Krouse

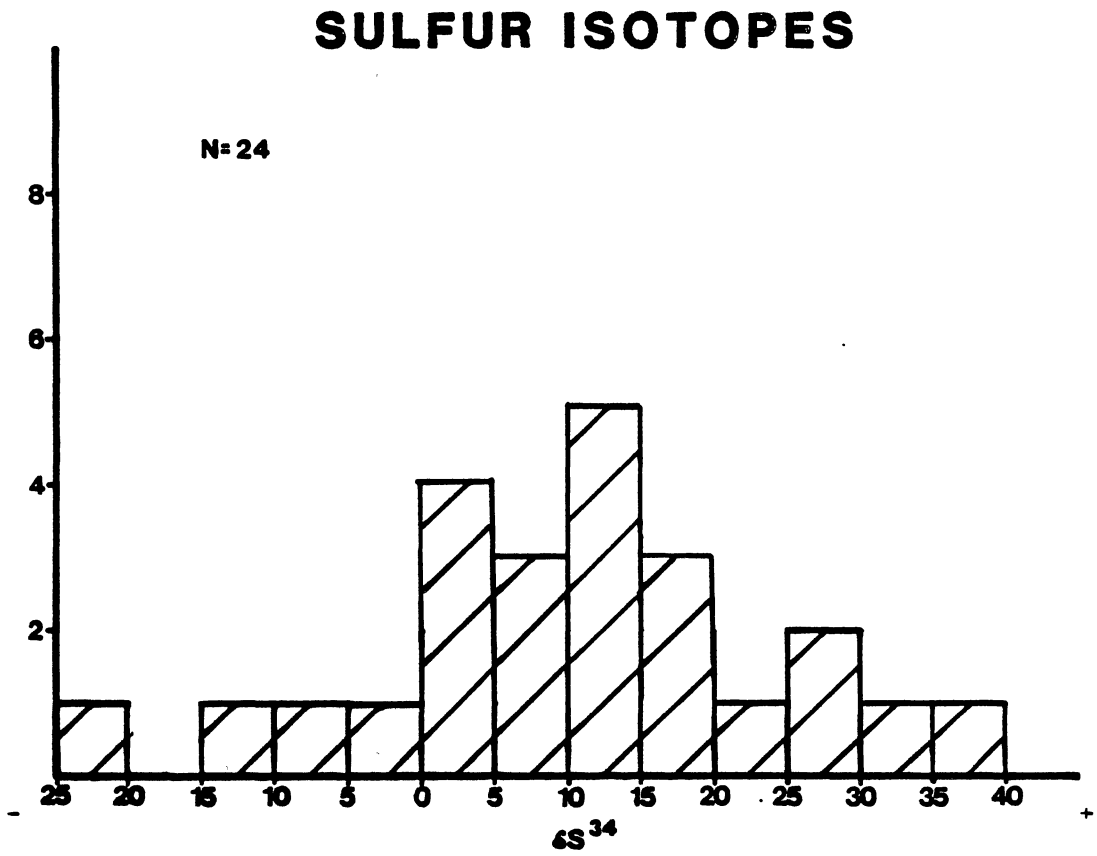

Figure 73.--Frequency distribution of δS^{34} isotopes for the Velma, Healdton, and Carter-Knox fields.

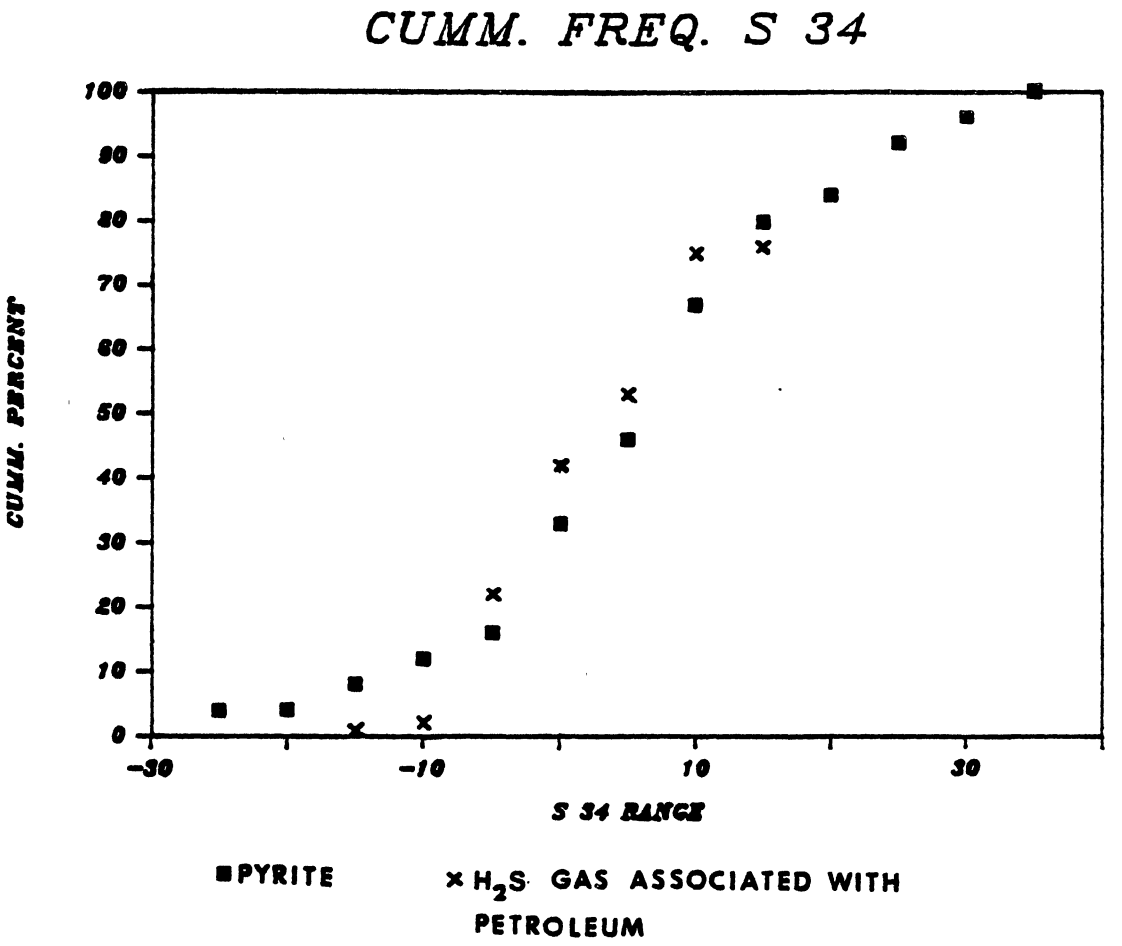

Figure 74.--Cummulative frequency of the S^{34} values for the pyrite and H_2S gas associated with petroleum (Goldhaber, Reynolds, and Rye, 1978).

(1977) suggested that H_2S gas associated with petroleum has the same or slightly heavier sulfur isotope ratios than the hydrocarbon. Pyrite, inorganically synthesized during a reaction H_2S and goethite, has the same isotopic value as the H_2S (Price and Shieh, 1970). Therefore, because the δS^{34} values of the pyrite are similar to those of the oils, assumptions can be made that the petroleum is the source of the sulfur in the pyrite.

The sulfur isotopic composition pyrites and other sulfides from the Healdton oil field show a bimodal distribution (Figure 75). Type A includes values similar to those associated with hydrocarbon-derived sulfur. The δS^{34} values of oil from this field is 12.1 ‰. Type B exhibits anomalously and unusually heavy values. The δS^{34} enriched samples may be the result of a local sulfate source that became enriched early in S^{34} as S^{32} was removed by bacteriogenic processes that produced hydrogen sulfide. Without an additional input of sulfate-rich waters, the residual sulfate became heavier as the escape of H_2S gas continued. Therefore, the subsequent pyrite mineralization of this localized δS^{34} enriched sulfate produced values observed in population B. This explanation was provided by Goldhaber (1985).

An alternative explanation for this occurrence is suggested by Vredenburgh and Cheney (1971) in their isotopic investigation of petroleum in the Wind River Basin, Wyoming. The hydrogen sulfide gas of the Tensleep

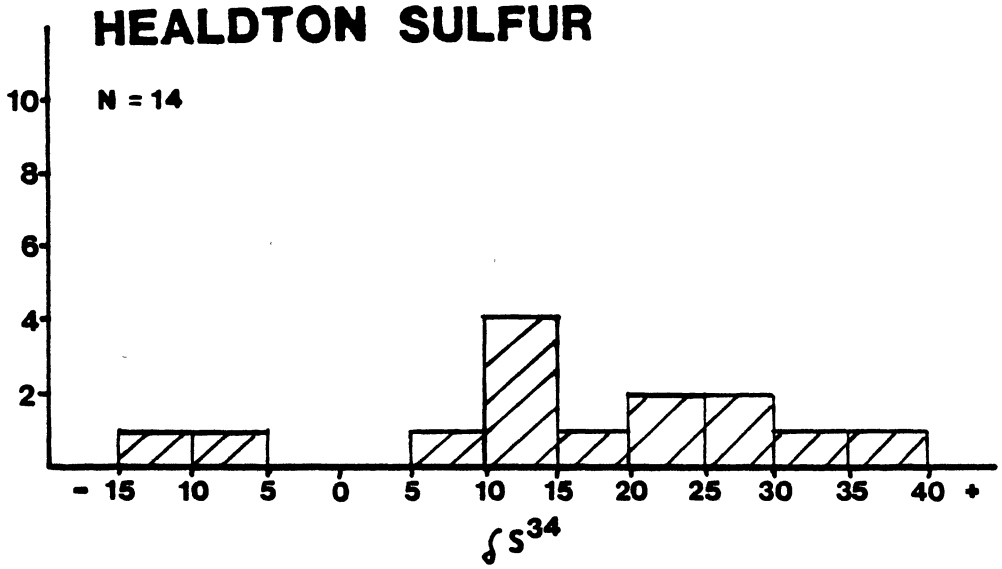

Figure 75.—Frequency distribution of S^{34} isotopes for the Healdton field.

formation has δS^{34} values greater than those of the petroleum. They suggested several hypotheses. One of these is that during the nonbiological desulfurization of the petroleum, a gaseous sulfur-bearing compound might have been generated in addition to H_2S. If this gas were sufficiently abundant and were sufficiently depleted in δS^{34}, it would cause the observed net enrichment of δS^{34} in the oils. Furthermore, if the bonding in this gas were weaker than the hydrogen bonding in hydrogen sulfide, the H_2S gas would be more enriched in δS^{34} than this hypothetical gas, and the H_2S might become more enriched in δS^{34} than the petroleum from which it was generated. Krouse (1977) reported a possible mechanism for δS^{34} enrichment of sulfate in formation waters by water-washing (degredation) of petroleum. Water-washing involves the removal of the lighter hydrocarbons by fresh water. This results in an increase in the sulfur content of the oil. He reported that Bailey et al. (1973) found depletions in heavier paraffins accompanied by an increase in δS^{34} of $SO_4^=$ in the formation water. Subsequent reduction of the sulfate could result in an enrichment of the heavy sulfur in pyrite.

CHAPTER VII

SUMMARY AND CONCLUSIONS

Specific criteria are necessary for the development of HIDA and can be used to identify hydrocarbon-induced alterations. Formation of the aureole is not restricted to the surface. If the extent of the migration of hydrocarbon products is short or blocked by an impermeable barrier, the alteration may only be observed in the subsurface Permian strata. The criteria that must be met in order for the aureoles to form are listed below.

1. The trapping and seepage of hydrocarbon products in the Healdton, Cement, Chickasha, Carter-Knox, and Velma fields are controlled by faulted anticlines. These faults are normal and high-angle reverse faults. In order for the aureole to form, vertical migration of the hydrocarbon products is very essential. Although faults in these areas act as the major conduits for fluids, they are not a prerequisite in the development of seepage-induced anomalies over all fields. Oehler and Sternberg (1984) identified anomalies in the shallow subsurface of the Ashland field in Oklahoma where the vertical seepage of hydrocarbons was not controlled by faults but most likely by the buoyancy of the seeping methane.

2. Iron-bearing strata may play a major role in the formation of sulfides within the aureoles. Hydrogen sulfide gas reduces the ferric ions in the hematite to ferrous ions necessary for precipitation of pyrite.

3. An abundant source of calcium must be present in formation waters for precipitation of the carbonate. The calcium concentration in waters associated with the redbed evaporites is probably much greater than normal formation waters. This may be the reason that the extent of carbonate mineralization is very extensive. The formation of the iron- and manganese-rich dolomites and calcites require a source of manganese, ferrous, and magnesium ions.

4. The composition of the hydrocarbon reservoir is an important control in the species or types of alterations that will form. In order for sulfides to form in abundance, a substantial source of sulfur must be present. Presumably, the source of sulfur is a sulfur-rich crude oil. These type oils are typically low in gravity, low gasoline-content, naphthenic oils containing high concentrations of sulfur-, nitrogen-, and oxygen-bearing compounds (Silverman, 1964). It is also speculated that the migration of hydrocarbons is rather limited to the site of the aureole.

Alteration of redbeds overlying the Velma, Healdton, and Carter-Knox oil fields is directly related to hydrocarbon seepage. The extent of the diagenesis is controlled by the underlying structure; areas proximal to major fault

zones and structural axes are likely to be affected more than areas away from these features.

The mineralogical and geochemical hydrocarbon induced diagenetic products form prominent features that can be mapped as an aureole consisting of four distinct concentric zones. Extensive carbonate-cemented sandstone, often called diagenetic limestone (zone 1), occurs in immediate vicinities to faults and structural axes. Zone 2 represents bleached sandstone (buff to yellow) with slight carbonate cementation. This sandstone is observed outward from the diagenetic limestone. Zone 2 is considered a gradation between the limestone and the unaltered redbeds (zone 4). Pyrite cement (zone 3) occurs in both the bleached sandstone and the diagenetic limestone.

Throughout hydrocarbon migration and transformation, the light fraction that is enriched in methane, carbon dioxide, hydrogen sulfide, and possibly carboxylic acids, are preferentially removed. Changes in the pore water chemistry due to the introduction of these products initializes the formation of diagenetic minerals that are atypical to the redbeds. Calcite is the most common carbonate mineral to form; however, other carbonate minerals such as dolomite, rhodochrosite, ferroan and/or manganesian dolomite, and ferroan calcite are observed within the limits of the aureole. Sulfides are direct products of the reaction between dissolved hydrogen sulfide and various divalent cations. Pyrite is the most

abundant sulfide while galena, sphalerite, marcasite, and pyrrhotite are occasionaly present in trace quantities.

Isotopic evidence in carbonate and sulfide minerals clearly suggests their relationship to a hydrocarbon source. The δC^{13} values of diagenetic carbonates indicate three major sources of carbon. These include hydrocarbon, meteoric water, and a hybrid mixture of the two. In addition, the isotopic composition of the carbonates in the Healdton field suggests an influx by carbon derived from underlying marine carbonates.

The isotopic composition of the sulfides in the three fields indicates conclusively that the source of the sulfur is from hydrogen sulfide gas associated with petroleum. δS^{34} values that are extremely light indicate bacteriogenic sulfur whereas anamolous heavy values that are explained by an early depletion of S^{32} in the source.

Without a doubt, the formation of the diagenetic features is related to petroleum products. Therefore, the hydrocarbon-induced diagenetic aureole (HIDA) can be used as a general model for oil and gas exploration in areas with similiar criteria.

BIBLIOGRAPHY

Allen, R. F., 1980, Uranium potential of the Cement District, southwestern Oklahoma: Unpublished M.S. thesis, Oklahoma State University, 84 p.

Al-Shaieb, Z., 1985, Personal Communication.

Al-Shaieb, Z., Shelton, J. W., et al., 1977, Evaluation of uranium potential in selected Pennsylvanian and Permain units and igneous rocks in southwestern and southern Oklahoma: Bendix Field Engineering Corporation, Subcontract #76-024-E, Open-File Report, 248 p.

Andreev, P. F., et al., 1968, Transformation of Petroleum In Nature: New York, Pergamon Press, 466 p.

Ault, W. U., and Kulp, J. L., 1959, Isotopic geochemistry of sulfur: Geochim. et Cos. Acta, vol. 16, p. 201-235.

Bailey, N. J. L., Krouse, H. R., Evans, C. R., and Rogers, M.A., 1973, Alteration of crude oil by waters and bacteria--evidence from geochemical and isotope studies: Am. Assoc. Petro. Geol. Bull., vol. 57, n. 7, p. 1276-1290.

Berner, R. A., 1962, Iron sulfides formed from aqueous solution at low temperatures and atmospheric pressure: J. of Geology, vol. 72, p. 293-306.

--------, 1964, Stability fields of iron minerals in anaerobic marine sediments: J. of Geology, vol. 72, p. 826-834.

--------, 1967, Comparative dissolution characteristics of carbonate minerals in the presence and absence of aqueous magnesium ion: Am. J. of Science, vol. 265, p. 45-70.

--------, 1970, Sedimentary pyrite formation: Am. J. of Sci., vol. 268, p. 1-23.

Carothers, W. W., and Kharaka, Y. K., 1978, Aliphatic acid in oil-field waters--implications for origin of natural gas: Am. Assoc. Petro. Geol. Bull., vol. 62, n. 12, p. 2441-2449.

--------, and --------, 1980, Stable carbon isotopes of HCO^-_3 in oil-field waters--implications for the origin of CO_2: Geochim. et Cos. Acta, vol. 44, p. 323-332.

Chukhrov, F. V., 1973, On mineralogical and geochemical criteria in the genesis of red beds: Chem. Geol., vol. 12, p.67-75.

Clayton, R. N., and Degens, E. T., 1959, Use of carbon isotope analysis of carbonates for differentiating fresh-water and marine sediments: Am. Assoc. Petro. Geol. Bull., vol. 43, n. 4, p. 890-897.

--------, et al., 1966, The origin of saline formation waters: J. of Geophysical Res., vol. 71, n. 16, p. 3869-3882.

Coleman, M.L., 1977, The application of sulphur isotope geochemistry to oil, gas and ore studies, a review: Proceedings of Forum on Oil and Ore in Sediments, Imperial College, March 1975, p. 53-92.

Collins, A. G., 1969, Chemistry of some Anadarko Basin brines containing high concentrations of iodine: Chem. Geol., vol. 4, p. 169-187.

--------, 1975, Geochemistry of Oilfield Waters-Developments in Petroleum Science 1: New York, Elsevier, p. 193-252.

Coplen, T. B., and Hanshaw, B. B., 1973, Ultrafiltration by a compacted clay- I. oxygen and hydrogen isotopic fractionation: Geochim. et Cos. Acta, vol. 37, p. 2295-2310.

Curtis, C. D., 1967, Diagenetic iron minerals in some British Carboniferous sediments: Geochim. et Cos. Acta, vol. 31, p. 2109-2123.

--------, 1983, Link between aluminum mobility and destruction of secondary porosity: Am. Assoc. Petro. Geol. Bull., vol. 67, no. 3, p.380-384.

Davis, L. V., 1955, Geology and groundwater resources of Grady and northern Stephens Counties, Oklahoma: Oklahoma Geol. Survey Bull. 73, p. 184.

Davis, L. V., and Kirkland, D. W., 1970, Native sulfur deposition in Castille Formation, Culberson County, Texas: Econ. Geol., vol. 65, p. 107-121.

DeSitter, L. U., 1947, Diagenesis of oil-field brines: Am. Assoc. Petro. Geol. Bull., vol. 31, n. 11, p. 2030-2040.

Deuser, W. G., and Degens, E. T., 1967, Carbon isotope fractionation in the system CO_2(gas)-CO_2(aqueous)-HCO_3^- (aqueous): Nature, vol. 215, p. 1033-1035.

Dickey, P. A., 1966, Patterns of chemical composition in deep subsurface waters: Am. Assoc. Petro. Geol. Bull., vol. 50, n. 11, p. 2472-2478.

Donovan, T. J., 1974, Petroleum microseepage at Cement, Oklahoma--evidence and mechanism: Am. Assoc. Petro. Geol. Bull., vol. 58, p. 429-446.

--------, Forgey, R. L., and Roberts, A. A., 1979, Aeromagnetic detection of diagenetic magnetite over oil fields: Am. Assoc. Petro. Geol. Bull., vol. 63, n. 4, p. 245-248.

--------, and Dalziel, M. C., 1977, Late diagenetic indicators of buried oil and gas: U.S. Geol. Survey Open-File Report 77-817, 44p.

--------, et al., 1981, Epigenetic zoning in surface and near-surface rocks resulting from seepage-induced redox gradients, Velma oil field, Oklahoma: a synopsis: Shale Shaker, vol. 32, n. 3, p. 1-7.

Drever, J. I., 1982, The Geochemistry of Natural Waters: New Jersey, Prentice-Hall, p. 35-115.

Emery, K. O., and Rittenberg, S. C., 1952, Early diagenesis of California basin sediments in relation to origin of oil: Am. Assoc. Petro. Geol. Bull., vol. 36, n. 5, p. 735-806.

Eslinger, E., et al., 1979, Role of iron reduction in the conversion of smectite to illite in bentonites in the disturbed belt, Montana: Clay and Clay Minerals, vol. 27, n. 5, p. 327-338.

Faure, G., 1977, Prinicples of Isotope Geology: New York, John Wiley & Sons, p. 323-423.

Fay, R. O., 1968, The geology of region II, in the Appraisal of water and related land resources in Oklahoma: Oklahoma Water Resources Board Publ. 24, p. 21-24.

Ferguson, J. D., 1977, The subsurface alteration and mineralization of Permian red beds overlying several oil fields in southern Oklahoma: Unpublished M.S. thesis, Oklahoma State University, 95 p.

Flood, J. R., Areal geology of western Jefferson County, Oklahoma: Unpublished M.S. thesis, University of Oklahoma, 61 p.

Frank, J. R., Carpenter, A. B., and Oglesby, T. W., 1982, Cathodluminescence and composition of calcite cement in the Taum Sauk Limestone (Upper Cambrian), southeast Missouri: J. of Sed. Pet., vol. 52, n. 2, p. 631-638.

Frondel, C., and Bauer, L. H., 1955, Kutnahorite: a manganese dolomite: Am. Mineralogist, vol. 40, p. 749-759.

Fuex, A. N., 1977, The use of stable carbon isotopes in hydrocarbon exploration: J. of Geochem. Exploration, vol. 7, p. 155-188.

Garrels, R. M., and Christ, C. L., 1965, Minerals, solutions, and equilibria: New York, Harper and Row, p. 224.

Gautier, D. L., 1985, Interpretation of early diagenesis in ancient marine sediments in Relationship of Organic Matter and Mineral Diagenesis: SEPM Short Course No. 17, p. 6-79.

Goldhaber, M. B., 1985, Personal Communication.

--------, Reynolds, R. L., and Rye, R. O., 1978, Origin of a south Texas rolltype uranium deposit: II. sulfide petrology and sulfur isotope studies: Econ. Geol., vol. 73, p. 16901705.

--------, --------, Rye, R. O., and Grauch, R. I., 1979, Petrology and isotope geochemistry of calcite in a South Texas roll-type uranium deposit: U.S. Geol. Survey Open-File Report 79-828, 21 p.

Gouin, F., 1956, Surface criteria of southern Oklahoma oil fields in Petroleum Geology of Southern Oklahoma: Am. Assoc. Petro. Geol., vol. 1, p. 14-35.

Habicht, J. K. A., 1979, Paleoclimate, paleomagnetism, and continental drift: Am. Assoc. Petro. Geol. Studies in Geology no. 9, 31 p.

Ham, W. E., 1960, Middle Permian evaporites in southwestern Oklahoma, in Report of the Twenty-First session Norden: Part 12, International Geologic Congress, Copenhagen, p. 138-151.

--------, Denison, R. E., and Merritt, C., 1964, Basement rocks and structural evolution of southern Oklahoma: Okla. Geol. Survey Bull., n. 95, 302 p.

--------, 1969, Regional geology of the Arbuckle Mountains, Oklahoma: Okla. Geol. Survey Guidebook XVII.

Harlton, B. H., 1960, Stratigraphy of Cement pool and adjacent area, Caddo and Grady Counties, Oklahoma: Am. Assoc. Petro. Geol. Bull., vol. 44, p.210-226.

Harrison, A. G., and Thode, H. G., 1958, Sulphur isotope abundances in hydrocarbons and source rocks of Uinta Basin, Utah: Am. Assoc. Petro. Geol. Bull., vol. 42, n. 11, p. 2642-2649.

Hem, J. D., 1960, Some Chemical relationships among sulfur species and dissolved ferrous iron in Chemistry of Iron in Natural Waters: U.S. Geol. Survey Water-Supply Paper 1459-C, p. 57-73.

--------, 1963, Chemical equilibria and rates of manganese oxidation in Chemistry of Manganese in Natural Water: U.S. Geol. Survey Water-Supply Paper 1667-A, 64 p.

--------, 1972, Chemical factors that influence the availability of iron and manganese in aqueous systems: Geol. Soc. Am. Bull., vol. 83, p. 443-450.

--------, and Cropper, W. H., 1959, Survey of ferrous-ferric chemical equilibria and redox potentials in Chemistry of Iron in Natural Waters: U.S. Geol. Survey Water-Supply Paper 1459-A, p. 1-31

Hicks, I. C., 1971, Southern Oklahoma folded belt: Am. Assoc. Petro. Geol. Mem. 15, vol. 2, p. 1070-1077.

Ho, T. Y., Rogers, M. A., Drushel, H. V., and Koons, C. B., 1974, Evolution of sulfur compounds in crude oils: Am. Assoc. Petro. Geol. Bull., vol. 58, n. 11, p. 2338-2348.

Holster, W. T., and Kaplan, I. R., 1966, Isotope goechemistry of sedimentary sulfates: Chem. Geol., vol. 1, p. 93-135.

Hunt, J. M., 1979, Petroleum Geochemistry and Geology: San Francisco, W. H. Freeman and Company, p. 1-258.

Irwin, H., Curtis, C., and Coleman, M., 1977, Isotopic evidence for source of diagenetic carbonates formed during burial of organic-rich sediments: Nature, vol. 269, p. 209-213.

Kaplan, I. R., 1983, Stable isotopes of sulfur, nitrogen and deuterium in recent marine environments in Stable Isotopes in Sedimentary Geology: SEPM Short Course No. 10, p. 2-4 - 2-61.

Katz, A., 1971, Zoned dolomite crystals: J. of Geology, vol. 79, p. 38-51.

Keith, M. L., and Weber, J. N., 1964, Carbon and oxygen isotopic composition of selected limestones and fossils: Geochim.et Cos. Acta, V. 28, p. 1787-1816.

Kharaka, Y. K., Berry, F. A. F., and Friedman, I., 1973, Isotopic composition of oil-field brines from Kettleman North Dome, California, and their geologic implications: Geochim. Cos. Acta, vol. 37, p. 1899-1908.

--------, Hull, R. W., and Carothers, W. W., 1985, Water-rock interactions in sedimentary basins in Relationship of Organic Matter in Mineral Diagenesis: SEPM Short Course No. 17, p. 79-176.

Krauskopf, K. B., 1979, Introduction to Geochemistry: New York, McGraw-Hill Book Company, 617 p.

Krouse, H. R., 1977, Sulfur isotope studies and their role in petroleum exploration: J. Geochem. Exploration, vol. 7, p. 189-211.

Krynine, P. D., 1949, The origin of red beds: N.Y. Acad. Sci. Trans., ser. 2, vol. 11, p. 60-68.

Latham, J. W., 1970, Petroleum geology of Healdton field, Carter County, Oklahoma, in Geology of Giant Petroleum Fields: Am. Assoc. Petro. Geol. Mem. 14, p. 255-276.

Lilburn, R. A., 1981, Mineralogical, geochemical, and isotopic evidence of diagenetic alteration, attributable to hydrocarbon migration, Cement-Chickasha field, Oklahoma: Unpublished M.S. thesis, Oklahoma State University, 88p.

--------, and Al-Shaieb, Z., 1983, Geochemistry and isotopic composition of hydrocarbon-induced diagenetic aureole(HIDA), Cement, Oklahoma: Shale Shaker, part I, vol. 34, n. 4, p. 40-56.

--------, and --------, 1984, Geochemistry and isotopic composition of hydrocarbon-induced diagenetic aureole (HIDA), Cement, Oklahoma: Shale Shaker, part II, vol. 34, n. 5, p. 57-67.

Lloyd, R. M., 1966, Oxygen isotope enrichment of sea water by evaporation: Geochim. et Cos. Acta, vol. 30, p. 801-814.

MacLachlan, M. E., 1967, Oklahoma, in Paleotectonic investigations of the Permian system in the United States: U.S. Geol. Survey Prof. Paper 515-E, p. 85-92.

Mamchur, G. P., 1969, Isotopic composition of carbon in calcite paragenetic with sulfur: Geochem. International, vol. 6, p. 660-670.

Miser, H. D., 1954, Geologic Map of Oklahoma: U.S. Geol. Survey and Oklahoma Geol. Survey.

Mills, R. V. A., and Wells, R. C., 1919, The evaporation and concentration of waters associated with petroleum and natural gas: U.S. Geol. Survol. Bull. 693, 104 p.

Monster, J., 1972, Homogeneity of sulfur and carbon isotope ratios S^{34}/S^{32} and C^{13}/C^{12} in petroleum: Am. Assoc. Petro. Geol. Bull., vol. 56, n. 5, p. 941-949.

Nisle, R. G., 1941, Considerations on the vertical migration of gases: Geophysics, vol. 6, p. 449-454.

Olmstead, R. W., 1975, Geochemical studies of uranium in south-central Oklahoma: Unpublished M.S. thesis, Oklahoma State University, 116 p.

Orr, W. L., 1974, Changes in sulfur content and isotopic ratios of sulfur during petroleum maturation--study of Big Horn Basin Paleozoic oils: Am. Assoc. Petro. Geol. Bull., vol. 58, n. 11, p. 2295-2318.

Pedersen, T. F., and Price, N. B., 1982, The geochemistry of manganese carbonate in Panama Basin sediments: Geochim. et Cos. Acta, vol. 46, p. 59-68.

Price, F. T., and Shieh, Y. N., 1979, Fractionation of sulfur isotopes during laboratory synthesis of pyrite at low temperatures: Chem. Geol., vol. 27, p. 245-253.

Pruatt, M. A., 1975, The southern Oklahoma aulacogen: A geophysical and geological investigation: Unpublished M.S. thesis, University of Oklahoma, 59 p.

Rascoe, B., and Adler, F. J., 1983, Permo-Carboniferous hydrocarbon accumulations, mid-continent, U.S.A.: Am. Assoc. Petro. Geol. Bull., vol. 67, n. 6, p. 979-1001.

Reedy, H. J., and Sykes, H. A., 1959, Carter-Knox oil field, Grady and Stephens Counties, Oklahoma in Petroleum Geology of Southern Oklahoma: Am. Assoc. Petro. Geol., vol.2, p. 198-219.

Reeves, F., 1921, Geology of the Cement oil field, Caddo County, Oklahoma: U.S. Geol. Survey Bull. 726, p. 41-85.

Reynolds, R. L., 1985, Personal Communication.

--------, et al., 1984, Thermomagnetic behavior and composition of Pyrrhotite in lower Permian strata, Cement oil field, Oklahoma: EOS Trans. Am. Geophysical Union, vol. 65, n. 45, p. 866.

--------, and Goldhaber, M. B., 1978, Recognition of oxidized sulfide minerals as an exploration guide for uranium: J. Research U.S. Geol. Survey, vol. 6, n. 4, p. 483-488.

Rice, D. D., and Claypool, G. E., 1981, Generation, accumulation, and resource potential of biogenic gas: Am. Assoc. Petro. Geol. Bull., vol. 65, n. 1, p. 5-25.

Rutledge, R. B., 1956, The Velma oil field, Stephens County, Oklahoma, in Petroleum Geology of Southern Oklahoma: Am. Assoc. Petro. Geol., vol. 1, p. 260-281.

Sackett, W. M., 1968, Carbon isotopic composition of natural methane occurrences: Am. Assoc. Petro. Geol. Bull., vol. 52, n. 5, p. 853-857.

Schoell, M., 1980, The hydrogen and carbon isotopic composition of methane from natural gases of various origins: Geochim. et Cos. Acta, vol. 44, p. 649-661.

--------, 1983, Genetic characterization of natural gases: Am. Assoc. Petro. Geol. Bull., vol. 67, n. 12, p.2225-2238.

Silverman, S. R., 1964, Migration and segregation of oil and gas, in Fluids in Subsurface Environments: Am. Assoc. Petro. Geol. Mem. 4, p. 53-65.

Stahl, 1977, Carbon and nitrogen isotopes in hydrocarbon research and exploration: Chem. Geol., vol. 20, p. 121-149.

Surdam, R. C., and Crossey, L. J., 1985, Mechanisms of organic/inorganic interactions in sandstone/shale sequences in Relationship of Organic Matter and Mineral Diagenesis: SEPM Short Course No. 17, p. 177-231.

Tasse, N., and Hesse, R., 1984, Origin and significance of complex authigenic carbonates in Cretaceous black shales of the Western Alps: J. of Sed. Pet., vol. 54, n. 3, p.1012-1027.

Thode, H. G., Monster, J., and Dunford, H. B., 1958, Sulphur isotope abundances in petroleum and associated materials: Am. Assoc. Petro. Geol. Bull., vol.42, n.11, p.2619-2641.

--------, and Monster, J., 1965, Sulfur isotope geochemistry of petroleum, evaporites, and ancient seas in Fluids in Subsurface Environments: Am. Assoc. Petro. Geol. Mem. 4, p. 367-377.

--------, and Monster, J., 1970, Sulfur isotope abundances and genetic relations of oil accumulations in Middle East Basin: Am. Assoc. Petro. Geol. Bull., vol. 54, p. 627-637.

Topographic Map of Velma, Oklahoma, 1974: U.S. Geol. Survey.

Turner, P., 1980, Continental Redbeds in Developments in Sedimentology #29: New York, Elsevier, p. 265-322.

Van Houten, F. B., 1961, Climatic significance of red beds, in Nairn, A.E.M., Descriptive paleoclimatology: New York, Interscience Pub., Inc., p. 89-139.

--------, 1964, Origin of red beds--some unresolved problems in Nairn, A.E.M., Proceedings of NATO Paleoclimates Conference 1963: New York, Interscience Pub., Inc., p. 647-661.

--------, 1968, Iron oxides in red beds: Geol. Soc. Am. Bull., vol. 79, p. 399-416.

Vredenburgh, L. D., and Cheney, E. S., 1971, Sulfur and carbon isotopic investigation of petroleum, Wind River Basin, Wyoming: Am. Assoc. Petro. Geol. Bull., vol. 55, n. 11, p. 1954-1975.

Walker, T. R., 1967, Formation of red beds in modern and ancient deserts, Geol. Soc. Am. Bull., vol. 78, p. 353-368.

--------, 1974, Formation of red beds in moist tropical climates: a hypothesis: Geol. Soc. Am. Bull., vol. 85, p. 623-638.

Webster, R. E., 1980, Evolution of s. Oklahoma aulacogen: Oil and Gas J., vol. 78, p. 150-172.

Wegemann, C. H., 1915, The Loco gas field, Stephens and Jefferson Counties, Oklahoma: U.S. Geol. Survey Bull. 621C, p. 31-41.

Wegemann, C. H., and Heald, K. C., 1915, The Healdton oil field, Carter County, Oklahoma: U.S. Geol. Survey Bull. 621B, p. 13-25.

White, D. E., 1964, Saline waters of sedimentary rocks, in Fluids in Subsurface Environments: Am. Assoc. Petro. Geol. Mem. 4, p. 342-366.

Wilkinson, T. A., 1955, The subsurface geology of the northwestern Healdton area, Carter, Stephens and Jefferson Counties, Oklahoma: Unpublished M.S. thesis, University of Oklahoma.

APPENDIX

WELL LOG RESPONSES TO DIAGENETIC MINERALIZATION

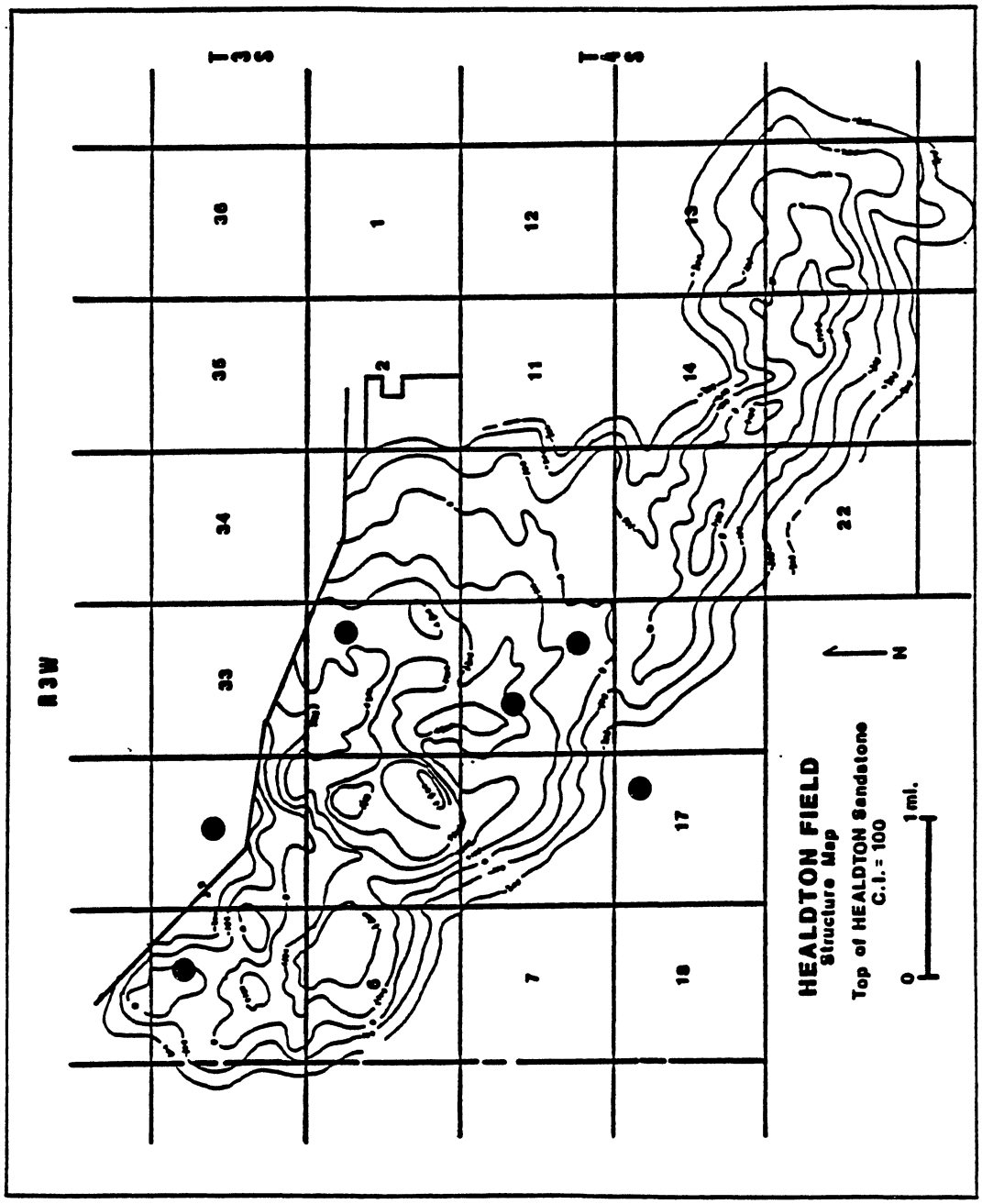
T 3 S
T 4 S
R 3 W
36
1
12
13
35
2
11
14
34
22
33
17
7
18
HEALDTON FIELD
Structure Map
Top of HEALDTON Sandstone
C.I. = 100
N
0
1 mi.

Sinclair
Haxie Fee * 17
31 – 3S – 3W

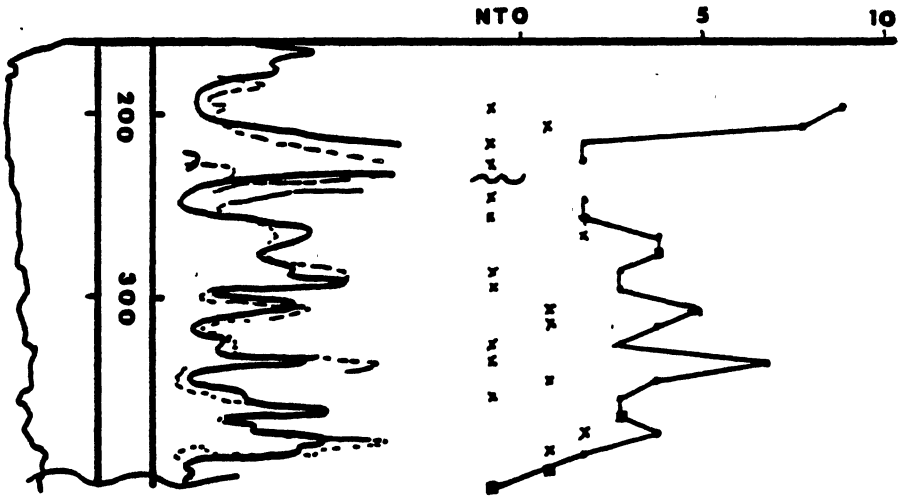

Magnolia
Woodworth # 11
32 – 3S – 3W

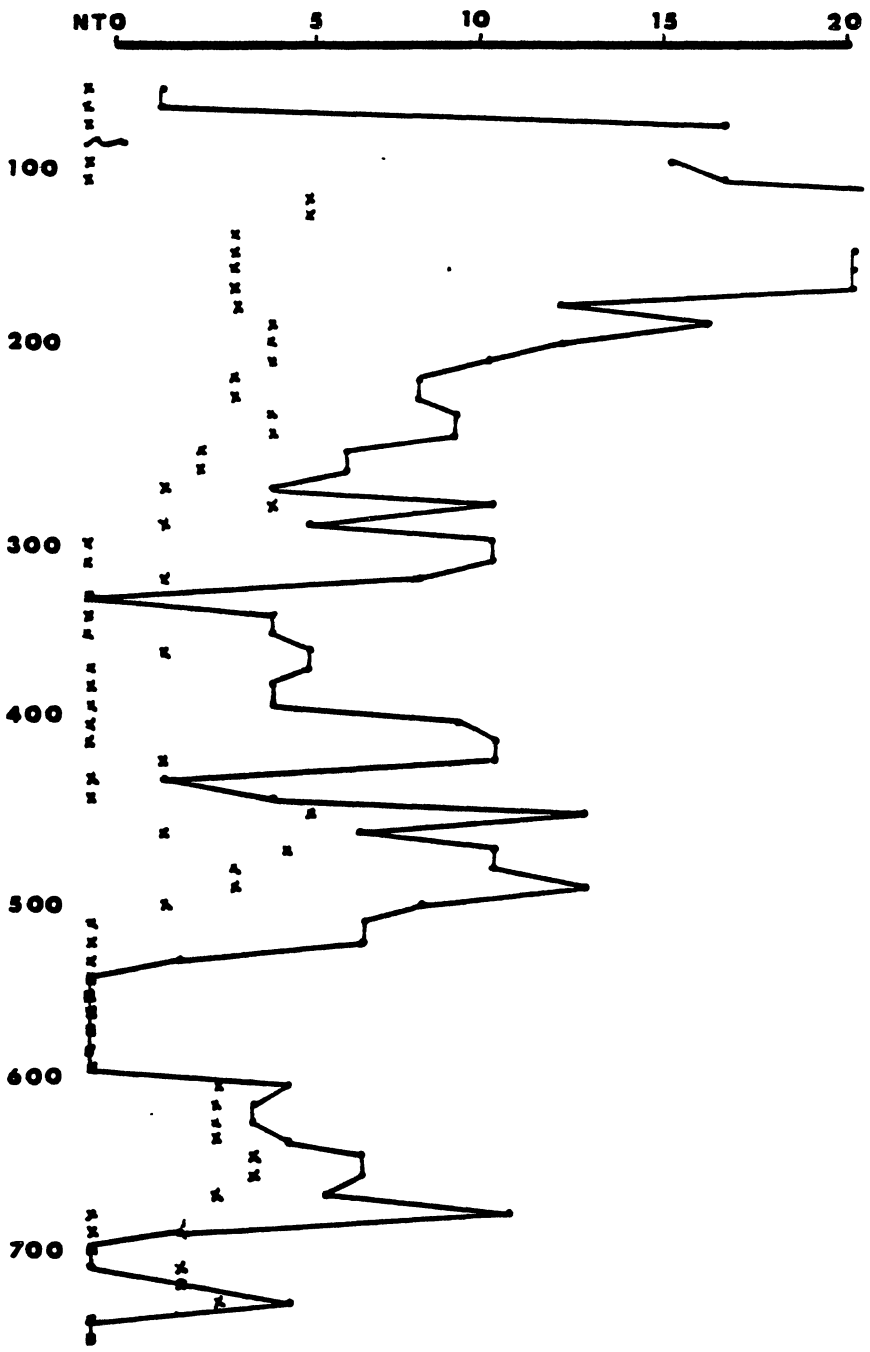

Sinclair - Prairie
Mullens #24
4 - 4S - 3W

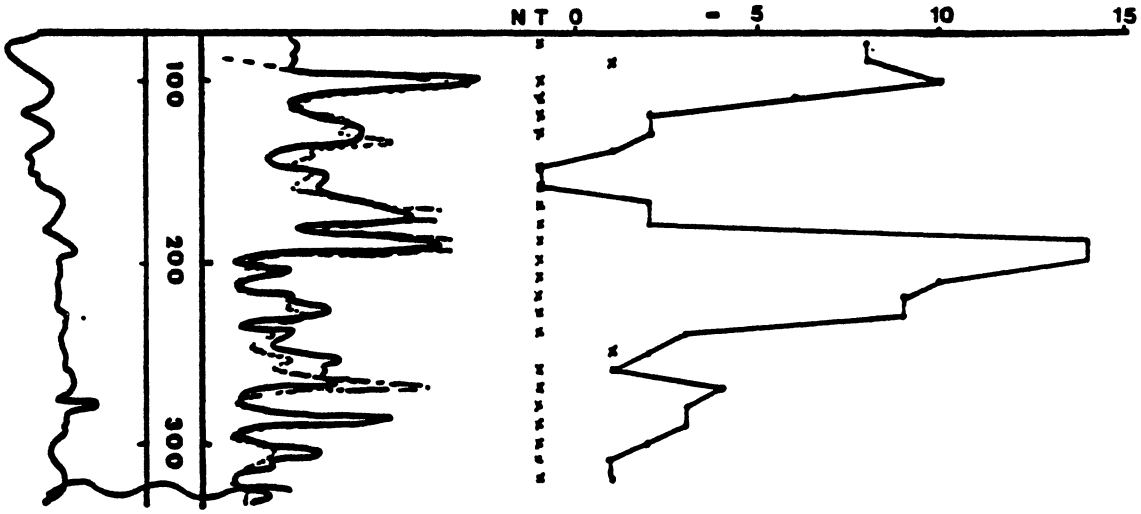

Schermerhorn
Williams #5
9-4S-3W

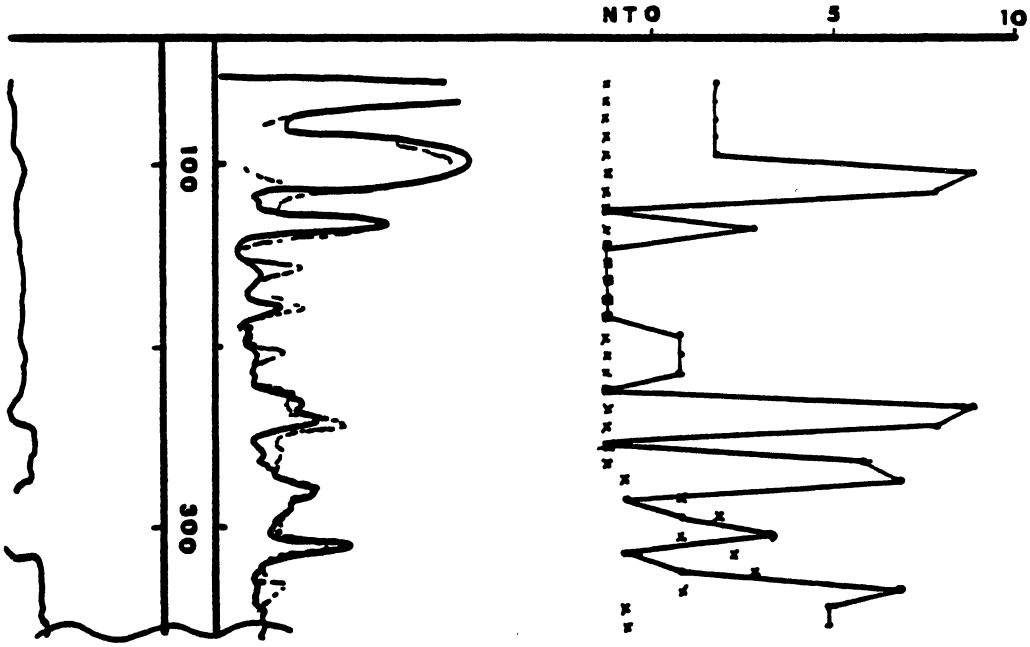

Sinclair
Richards # 21
9 – 4S – 3W

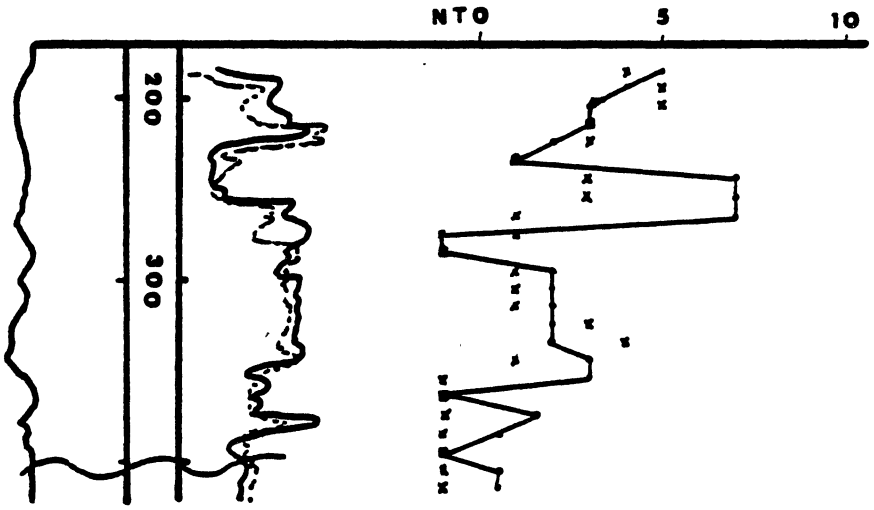

Amerada
Mago ※1
17-4S-3W

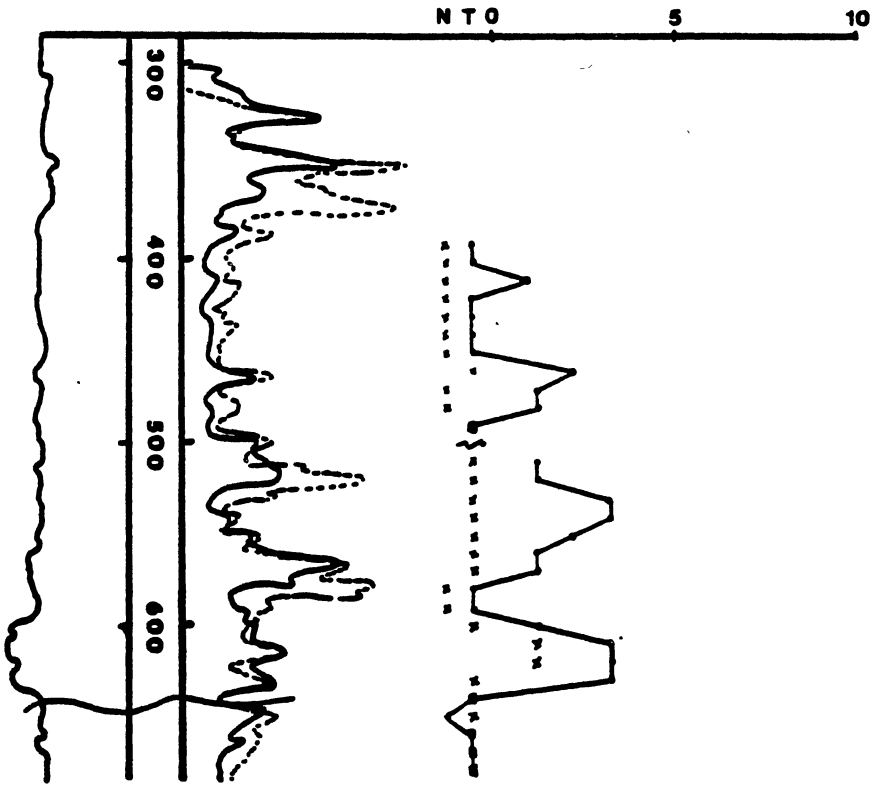

Amerada
Smalley #1
19-4S-3W

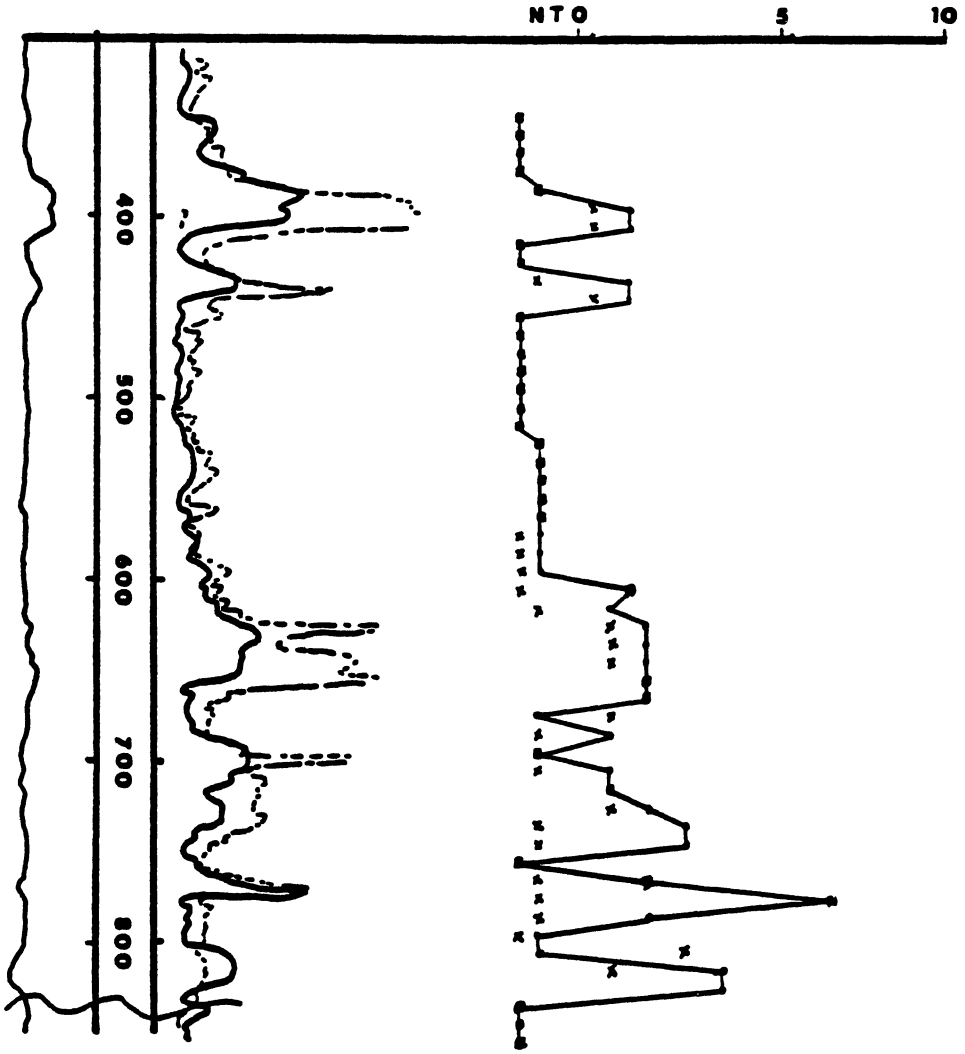

Sinclair – Prairie
Ingram # 1
21 – 4S – 3W

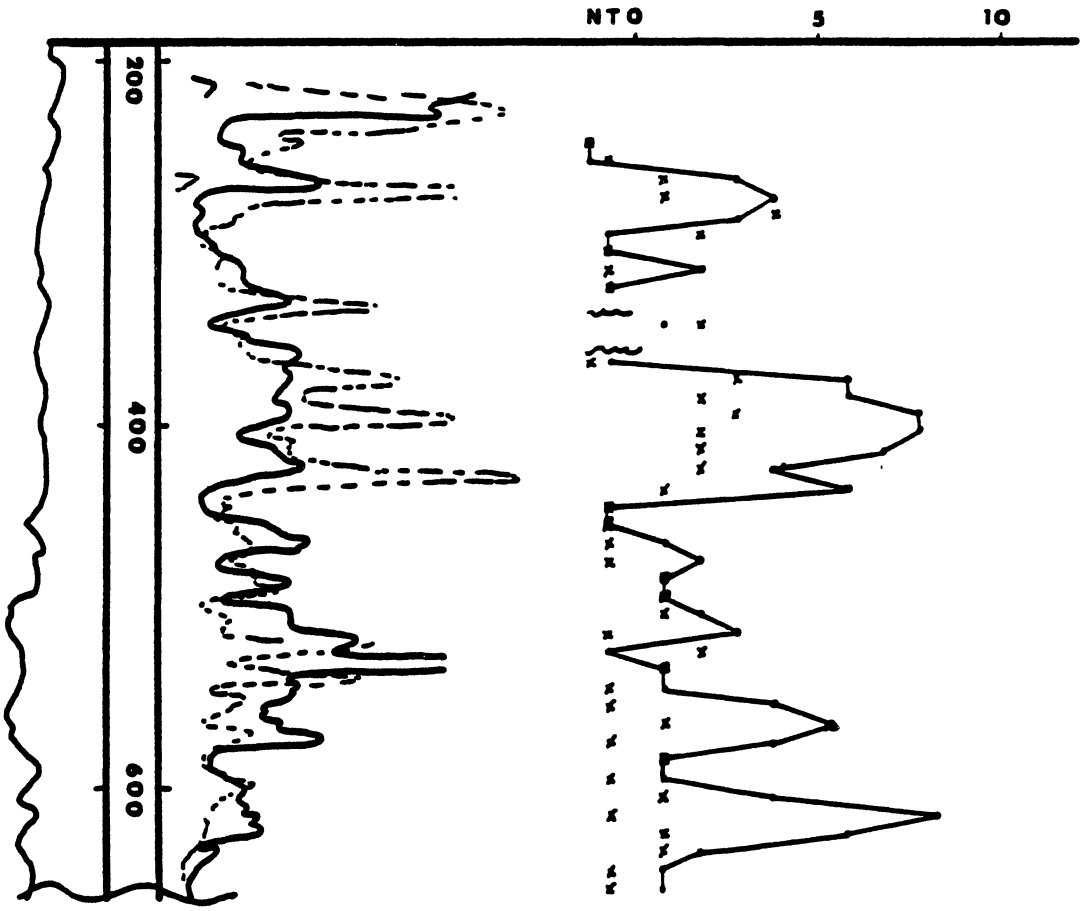

Amerada
Boyles #1
28-4S-3W

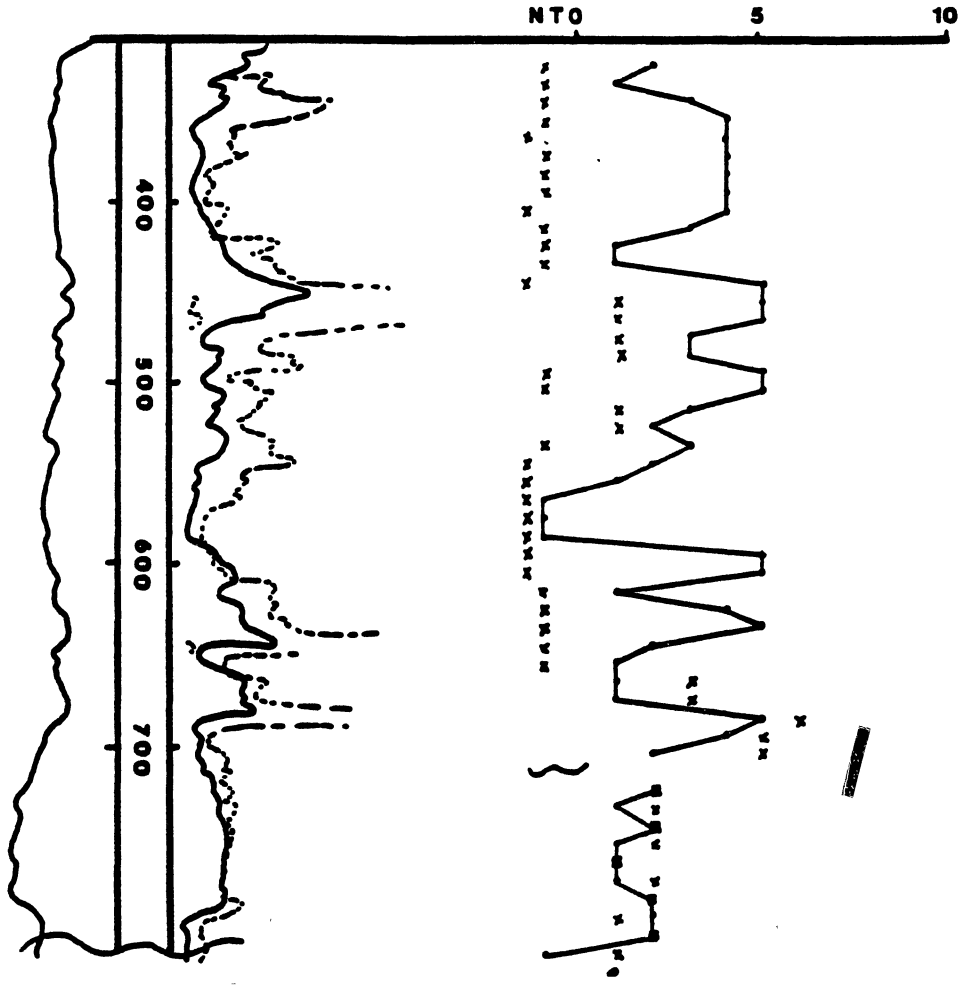

VITA

Janet Lorraine Cairns

Candidate for the Degree of

Master of Science

Thesis: DIAGENETIC AUREOLES INDUCED BY HYDROCARBON MIGRATION IN THE PERMIAN REDBEDS OF SOUTH-CENTRAL OKLAHOMA

Major Field: Geology

Biographical:

Personal Data: Born in Tulsa, Oklahoma, October 31, 1961, the daughter of Thomas W. and Sharon L. Cairns.

Education: Graduated from East Central High School, Tulsa, Oklahoma, in May, 1979; received Bachelor of Science Degree in Geology from Oklahoma State University in May, 1983; completed requirements for the Master of Science degree at Oklahoma State University in July, 1985.

Professional Experience: Speaker AAPG National Convention, New Orleans, March 1985, "Hydrocarbon-Induced Diagenetic Aureole (HIDA) - Mineralogic and Isotopic Models"; Research Assistant and Teaching Assistant, Department of Geology, Oklahoma State University, August, 1983, to July, 1985.